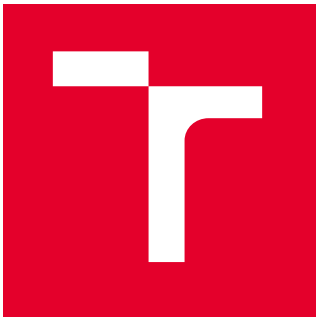

BRNO UNIVERSITY OF TECHNOLOGY

VYSOKÉ UČENÍ TECHNICKÉ V BRNĚ

FACULTY OF ELECTRICAL ENGINEERING AND COMMUNICATION

FAKULTA ELEKTROTECHNIKY
A KOMUNIKAČNÍCH TECHNOLOGIÍ

DEPARTMENT OF MICROELECTRONICS

ÚSTAV MIKROELEKTRONIKY

ELECTRICAL CHARACTERIZATION OF GRAPHENE-BASED CHEMICAL SENSORS

ELEKTRICKÁ CHARAKTERIZACE CHEMICKÝCH SENZORŮ NA BÁZI GRAFENU

MASTER'S THESIS
DIPLOMOVÁ PRÁCE

AUTHOR — **Bc. Patrik Staroň**
AUTOR PRÁCE

SUPERVISOR — **doc. Mgr. Dinara Sobola, Ph.D.**
VEDOUCÍ PRÁCE

BRNO 2025

BRNO UNIVERSITY OF TECHNOLOGY
FACULTY OF ELECTRICAL ENGINEERING AND COMMUNICATION

Master's Thesis

Master's study program **Microelectronics**

Department of Microelectronics

Student: Bc. Patrik Staroň ***ID:*** 213213

Year of study: 2 ***Academic year:*** 2024/25

TITLE OF THESIS:

Electrical characterization of graphene-based chemical sensors

INSTRUCTION:

The goal of the project is to study the mechanism of operation of graphene-based sensors, as well as measure their electrical characteristics.

• Study the literature about chemical sensors based on 2D materials. Explain the choice of material and describe the mechanism of sensoring.

• Study the changes in the conductive channel resistance and detection of specific noise signals in the spectral region (introduction of gas selectivity).

• Summarize the results, propose a sensor geometry modification and definition of conditions for reliability testing

RECOMMENDED LITERATURE:

Yasaei, P. et al. Chemical sensing with switchable transport channels in graphene grain boundaries. Nat. Commun. 5:4911 doi: 10.1038/ncomms5911 (2014).

Hwang, Y.J., Yu, H., Lee, G. et al. Multiplexed DNA-functionalized graphene sensor with artificial intelligence-based discrimination performance for analyzing chemical vapor compositions. Microsyst Nanoeng 9, 28 (2023). https://doi.org/10.1038/s41378-023-00499-y.

Date of project specification: 10.2.2025 ***Deadline for submission:*** 26.5.2025

Supervisor: doc. Mgr. Dinara Sobola, Ph.D.

doc. Ing. Lukáš Fujcik, Ph.D.
Chair of study program board

ABSTRACT

Graphene sensors show promising capabilities in detecting various gases, thanks to the unique properties of graphene, such as its electrical conductivity, high surface area to volume ratio and chemical configurability. Their practical use in the current state of development is difficult. Although graphene sensors can detect various molecules with great resolution, the electrical characteristics of graphene under certain environments is not well understood. This thesis provides an in-depth research of gas sensing theory, 2D materials used in gas sensing applications and it elaborates on graphene physics, to introduce the root mechanisms that allow graphene to sense gases. Theoretical text includes noise sources in graphene and it does not omit several discoveries and methods very relevant to practical 2D material gas sensor testing. Graphene samples prepared by chemical vapor deposition were tested under the effects of isopropylalcohol, acetone, exhaled gas, temperature, humidity, visible and UV light. These experiments were performed independently, some in DC and some in spectral domain and conclusion is derived for each separately. This thesis provides a solid introduction to the theory of gas sensing based on 2D materials and a starting point for good quality graphene gas sensors testing.

KEYWORDS

noise, sensor, graphene, carbon, nano, molecules, detection, 2D-material, surface

ABSTRAKT

Grafénové senzory vykazujú subné schopnosti detekcie rôznych plynov, vaka jedineným vlastnostiam grafénu, ako sú jeho elektrická vodivos, vysoký pomer povrchu k objemu a chemická prispôsobitenos. Ich praktické vyuitie v súasnom tádiu vývoja je vak nároné. Aj ke grafénové senzory dokáu detegova rôzne molekuly s vysokým rozlíením, elektrické charakteristiky grafénu v uritých prostrediach nie sú dobre pochopené. Táto práca poskytuje hbkovo spracovanú teóriu detekcie plynov, 2D materiálov vyuívaných v senzorických aplikáciách a predkladá fyzikálny základ pre grafén, z ktorého sú odvodené princípy ktoré umoujú grafénu detegova plyny. Teoretická as tie obsahuje zdroje umu v graféne a nevynecháva viaceré objavy a metódy, ktoré sú vemi relevantné pre praktické testovanie senzorov plynov zaloených na 2D materiáloch. Grafénové vzorky pripravené metódou chemickej depozície z plynnej fázy boli testované pod vplyvom izopropylalkoholu, acetónu, vydychovaného plynu, teploty, vlhkosti, viditeného a UV svetla. Tieto experimenty boli vykonané nezávisle, niektoré v jednosmernej doméne a niektoré v spektrálnej oblasti a pre kadý experiment je odvodený samostatný záver. Táto práca poskytuje solídny úvod do teórie detekcie plynov na báze 2D materiálov a poiatoný bod pre kvalitné testovanie grafénových senzorov.

KĽÚČOVÉ SLOVÁ

šum, senzor, grafén, uhlík, nano, molekuly, detekce, 2D-materiál, povrch

ROZŠIRENÝ ABSTRAKT

Senzory na báze grafénu sú populárnym predmetom štúdií vo vedeckej komunite. Grafén patrí do skupiny 2D materiálov a jeho vlastnosti sú unikátne v porovnaní s inými materiálmi. Jeho elektronická štruktúra obsahuje lineárny prechod medzi vodivostným a valenčným pásmom v oblasti Dirakových bodov. Vďaka tomu sa dokážu elektróny v graféne správať ako nehmotné Dirakové fermióny. Koncentrácia voľných nosičov môže byť menená dopovaním pomocou elektrického poľa smerujúceho na plochu grafénu. Grafén má pevnosť 325x vyššiu ako A36 oceľ a dokáže absorbovať relatívne vysoké množstvo svetla. Tieto a ďalšie vlastnosti sú priblížené v texte v sekcii o fyzikálnych a chemických vlastnostiach grafénu. Tieto vlastnosti majú priamy dopad na merané javy v laboratóriu a ponúkajú vysvetlenie v preskúmaných oblastiach grafénu. Práca však začína úvodom o senzoroch. Oblasť senzorov je potom zúžená na oblasť chemických senzorov a tá je zúžená na oblasť plynových senzorov, ktorá bola relevantná v období rozšíreného ručného ťaženia uhlia. V práci sú spomenuté vlastnosti týchto senzorov, akými sú napríklad selektivitya a doba zotavenia. Tiež sú spomenuté mechanizmy, na základe ktorých tieto senzory pracujú. Práca sa po fyzike grafénu sústreďuje na 2D materiály používané pri detekcii plynov. Je spomenutých niekoľko ďalších 2D materiálov, ktoré sú popri graféne aktívne skúmané. Táto teoretická časť práce dobre uvedie čitateľa do problematiky grafénových senzorov. Praktická časť práce má niekoľko celkov. Prvým je analýza vzorkov použitých v meraniach, po nej nasleduje celok s fyzikálnou analýzou meraného modelu relality so senzorom, od čoho je odvinutý ideálny merací aparát, ktorý izoluje množstvo nežiadúcich javov, ktoré ovplyvujú cieľový meraný jav a tým je vplyv konkrétneho plynu na elektronickú reakciu grafénu. Tento ideálny aparát je možné vyrobiť, no nie je pre rozsah tejto práce relevantný. Práca pokračuje prípravou vzorkov, experimentálnou sekciou a záverom. Pri príprave vzorkov je rozobratá problematika ich rezania a čistenia. Na meranie bol obdržaný kremíkoý plátok na ktorom sa nachádza 36 senzorov. Tieto senzory boli ochránené povrchovým polymerom a lasérovo rezané. Lasér však tento polymer poškodil a to ovplyvuje následné merania, napriek tomu že sa senzory javia ako funkčné. Vlastná doska plošného spoja bola navrhnutá pre čo najpohodlnejšie využívanie vzorku v laboratórnom prostredí. Pre samotné merania boli použité 3 rezané vzorky s polymerom a 2 pôvodné bez polymeru. Ramanová spektroskopia bola prevedená nad jedným vzorkom, ktorý bol poškodený a ďalej sa nepoužíval. Na vzorkoch s polymerom bola prevedená volt-ampérová charakteristika. Bolo zistené, že vzorky nejavili veľmi presnú koreláciu s veľkosťou ich grafénového kanálu. Volt-ampérová charakteristika pod vplyvom acetónu, izopropylalkoholu a svetla ukázala očakávaný smer rozdielov, aj keď rozdiely boli malé. Vzorka s grafénom bola podrobená zmietanému sínusu od 3 do 50kHz a bolo zistené, že amplitúda vo frekvenčnom spektre môže mať

výpovednú hodnotu pre identifikáciu konkrétnych meraných javov, aj keď primárna odozva bola odporová, než spektrálna. Meranie rezistivity vzorku v čase odhalilo veľký rozsah zmeny odporu v závislosti na množstve vystavenia izopropylalkoholu. Senzor sa po meraní zotavoval na pôvodnú hodnotu vyše hodiny. Vydychovaný vzduch mal efekt znižovania odporu a senzor sa z neho zotavoval veľmi rýchlo, zatiaľ čo izopropylalkohol zvýšil odpor grafénu a senzor sa zotavoval pomaly. Na záver boli prevedené unikátne spektrálne merania, kde bol zistený derivačný efekt voči sledovanému javu. Senzor reagoval na zmeny v koncentrácií acetónu, izopropylalkoholu a tiež boli sledované reakcie na svetlo vo viditeľnej, UV aj IR oblasti. čím bola zmena rýchlejšia, tým boli efekty pozorovateľné vo vyšších frekvenciách spektra. Efekty svetla na frekvenčné pásmo sú však priradené reakcií samotného substrátu, než grafénu. Tieto merania ponúkajú základ pre ďalšie experimenty s kvalitnejším meracím aparátom.

STAROŇ, Patrik. *Electrical characterization of graphene-based chemical sensors*. Master's Thesis. Brno: Brno University of Technology, Faculty of Electrical Engineering and Communication, Department of Microelectronics, 2025. Advised by Mgr. Dinara Sobola, PhD.

Author's Declaration

Author:	Bc. Patrik Staroň
Author's ID:	213213
Paper type:	Master's Thesis
Academic year:	2024/25
Topic:	Electrical characterization of graphene-based chemical sensors

I declare that I have written this paper independently, under the guidance of the advisor and using exclusively the technical references and other sources of information cited in the paper and listed in the comprehensive bibliography at the end of the paper.

As the author, I furthermore declare that, with respect to the creation of this paper, I have not infringed any copyright or violated anyone's personal and/or ownership rights. In this context, I am fully aware of the consequences of breaking Regulation § 11 of the Copyright Act No. 121/2000 Coll. of the Czech Republic, as amended, and of any breach of rights related to intellectual property or introduced within amendments to relevant Acts such as the Intellectual Property Act or the Criminal Code, Act No. 40/2009 Coll. of the Czech Republic, Section 2, Head VI, Part 4.

Brno *May 24, 2025*
. . . . . .

The author signs only in the printed version.

ACKNOWLEDGEMENT

First of all, I thank Lord Most High for creating such an interasting universe that we study until now and humbly still don't understand a lot, and I thank Him for giving me the ability to gain wisdom, learn and understand concepts Iwrite about in this thesis. I thank to my great supervisor doc. Mgr. Dinara Sobola PhD. for her help in overcoming obstacles that occured while progressing in research for this thesis. Special thanks to prof. Dr. Ing. Pavel Zemík. dr. h. c. and Ing. Jakub Lojda. Ph.D. for support during tense times. Thanks to Brno Universtity of Technology for providing the necessary equipment for the research.

Contents

List of Figures

Introduction

Sensing of substances in an environment is demanding in many areas. Gas sensing market in 2024 reached USD 1.621 and is estimated to grow. These sensors allow for the measurement of humidity, manufacturing conditions in many areas, detection of hazardous chemicals in working environments and in the atmosphere. They are used in research environments and in storage facilities to allow for safe and monitored conditions for people, products, devices and materials. These sensors can operate on many principles and this thesis addresses some of them. Physics allows for the creation of devices that can reliably monitor concentrations of desired gases in many types of environments. These sensors however tend to degrade over time or they reach their limitations in resolution, minimum concentrations, selectivity only to the desired chemicals and more. Every major framework for currently available commercial sensors was firstly researched in a laboratory. Sensors based on 2D materials show very promising abilities to reliably sense gases and if they are configured properly, they may surpass other frameworks for gas sensing, because of their unique physical abilities. One of the mostly researched 2D materials is graphene. It has been proven that even though sensors based on 2D materials are very configurable, there are big problems in mass production and out-of-the-lab ability to perform sustainable and reliable measurements, while using their actual superior properties. That's why research on graphene and other 2D materials continues. Currently, a solid understanding of physical phenomena relevant to gas sensing is available and many experiments were already performed since these materials were first synthesized. Due to the wide sea of possibilities, some experiments have not even been tried, or widely adopted. In this thesis the main points of gas sensing research are presented in a deeper way. Resources cited span the field of research on 2D materials and namely on graphene very well, although several interesting findings were not included in this thesis because of its limited scope. Sources of noise and overview of the graphene physical framework are also elaborated here. Experimental section provides details on several measurements of phenomena that graphene samples react to and it gives the reader a good starting point for their own graphene research. The goal of this work is to inform the reader about the field of graphene gas sensing and inspire them to perform higher-quality measurements and analysis that would bring the scientific community closer to creation of a commercially viable graphene-based chemical sensor.

1 State of The Art

As industry was evolving in the early 19th century, manual coal mining was spread around the world and many people were mining coal. In some coal mines, people were fainting and the cause was traced to a lack of oxygen. Probably one of the very first gas sensors was a flaming light. This light was brought into the mine and when the flame was fainting or was extinguished [2], it was an alerting signal that the level of oxygen is below the safe level for human operation and miners had to go out of the mine. In coal mines, people could be exposed to dangerous gases, such as carbon monoxide (CO), hydrogen sulfide (H_2S) and methane. These gases have neither color, taste, nor smell [2]. Because of this, the workers themselves were oblivious to the concentration of these gases in their working environment. Without proper detection of these gases, these miners were exposed to deadly poisoning and explosions. It was later figured out, that canary birds have smaller lungs and much higher blood circulation, which makes them more sensitive to carbon monoxide [3]. When a canary started to have problems, it was a sign that miners would have a problem too. As technology advanced, more areas where gas sensing was required arose. This is why research of major technologies that were promising for potential of gas sensing (such as field-effect transistors), were also researched for this purpose. Among the early more sophisticated chemical sensors was a sensor developed in the year 1970 by Johannessen and it was based on an Open Gate Field Effect Transistor (OGFET), which was able to detect polar gases, such as water vapor (H_2O) and methanol (CH_3OH) [1]. The architecture of this sensor is shown in Figure 1.1.

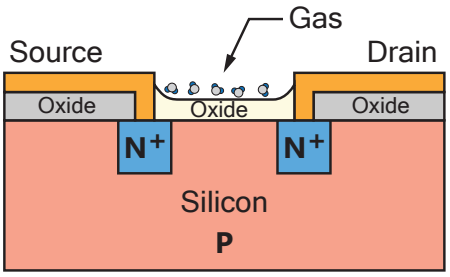

Fig. 1.1: Diagram of an Open Gate Field Effect Transistor (Inspired from [1])

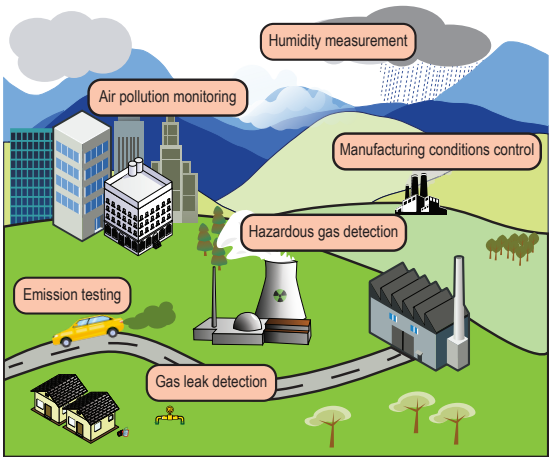

Fig. 1.2: Example of gas sensing applications in our daily lives.

Today, the society has developed many industries, which require some form of gas sensing (Figure 1.2). For example, if a factory solders components onto a printed

circuit board, innertness of the atmosphere must be monitored, in order to prevent oxidation and pass the product quality tests. In the working environment and in cities, where people spend most of their lives, gas sensing is necessary to prevent harm from dangerous gases. From an understanding of the chemical composition in the air, it is possible to properly identify the root causes of pollution, and steps can be taken to improving the air quality. CO_2 detection in the atmosphere can be used to monitor the greenhouse effect and ozone detectors enable periodical checking of the protective layer, which was for many years degrading, possibly because of freons [4].

This chapter lays down what a sensor is and since there are many kinds of sensors, the focus is then drawn to the chemical ones. It their working principle, properties, methods of the signal analysis and it ends with graphene physics and an introduction to 2D materials in gas sensing.

1.1 Chemical sensor

In general, a sensor is a device, which allows to sense something in its surroundings. It provides an insight into what is happening at a point in space. Just like a human body has many sensors, such as eyes, ears or touch, which provide an insight to a person about what is happening around them, sensor devices enable systems to have an insight into what is happening in the environment they are sensing [5] [6]. There are many ways how sensors can be classified, and the classification given here is just one of them. The term sensor can be applied to a wide variety of systems, such as biologically based receptors, photon detectors, particle sensors, or reactive elements, which as a result of the reaction, sense the presence of a chemical. Some of these systems are visualized in Figure 1.3. All sensors work under a common principle, and that is a reaction to some physical phenomena, which produces some action at the output of the sensor. Sensors can be further classified as physical sensors and chemical sensors.

Physical sensors

Physical sensors are sensors which react to physical phenomena through physical or chemical process. Physical sensors are for example hall sensors, which measure electric field orientation and their output can be interpreted as a rotor position, an optical sensor, which can measure proximity, or spectral light intensity, which is in some form used in cameras, which produce pictures. These sensors are visualized in Figure 1.4. The other category of sensors is chemical sensors, and they are a primary focus of this thesis.

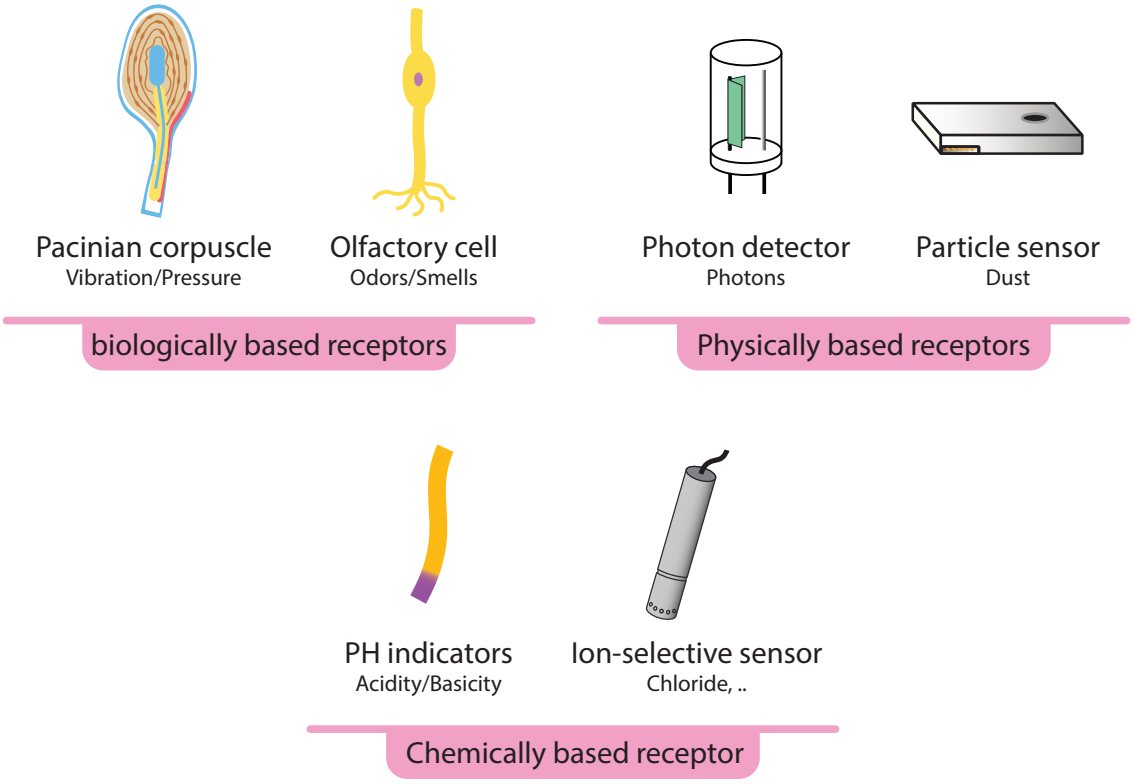

Fig. 1.3: An illustration of different kinds of sensors that operate on different principles. Biological sensors are grown structures that through a chemical or physical process detect something and send the response usually as a neural impuls. Physical sensors receive something physical and react usually in an electrical manner and chemical sensors react to the environment in a chemical way and the response may be produced visually or electrically.

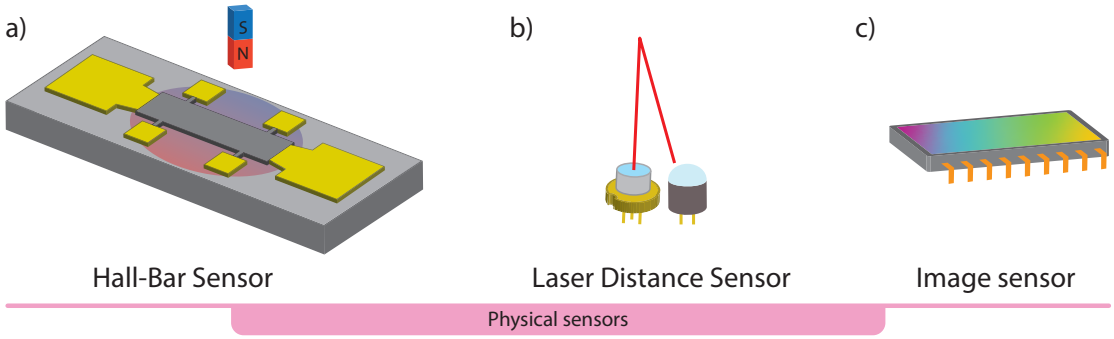

Fig. 1.4: Physical sensors measure some physical quantity, such as **a)** magnetic field intensity or direction, **b)** distance, **c)** color intensity at various places, weight and others. They can measure the physical quantity in physical or chemical way.

Chemical sensors

Based on the classification style of physical sensors above, chemical sensors are sensors which react to chemical phenomena through physical or chemical process. Chemical sensors are for example dopamine receptors, PH sensors, or gas and humidity sensors. Chemical sensors work under a general architecture that is found in the literature [5] [6]. This architecture defines a receptor and a transducer. Receptor and transducer are often combined into one block that is called 'sensing layer', 'active layer' or 'sensing material'. Examples of sensing materials include metal oxides, polymers, catalytic metals, semiconductors and graphene [7] [8]. This architecture is visualized in Figure 1.5 along with a simple explanation of a receptor and a transducer and the role of a receptor and a transducer is explained further down.

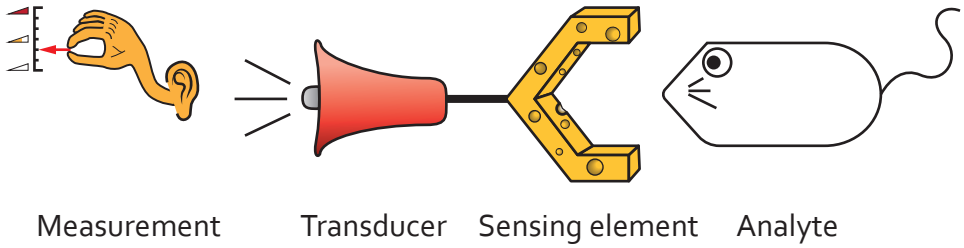

Fig. 1.5: Visualization of a general sensor architecture. Analyte is an atom, molecule or a chemical structure of interest (structure such as protein), sensing element is the material the analyte attaches to, and transducer is a material that changes its properties, which are directly measurable.

1.1.1 Ways of detection in chemical sensors

Here is a non-exhaustive list of how chemical sensors detect the analyte. The detection methods are split into groups of recognition and transduction, to better illustrate the function of the two blocks. Goal of section is to introduce the complexity of chemical sensing. As the thesis is focused on 2D structures, chemical sensors discussed in this thesis mainly revolves around gas and vapor sorption. To avoid confusion, it is important to note that many chemical sensors contain 2 primary electrodes that interface the sensing (recognition and transduction element in one) element and these electrodes do not contribute to the sensing process and their function is to electrically interface with the sensing element. These electrodes must be chemically stable. Chemical sensors that measure the analyte in an aquenous solution contain usually two or three electrodes where two or all of them perform

some sensing function by themselves and this function concerns interaction with ions in the solution.

Recognigion (sensing):

- *Ion recognition*: The sensing element contains charged ions with charge opposite to the analyte.
- *Affinity interaction*: An interface of two chemicals is made, where the binding between atoms is possible due to opposite atomic affinities. This attracts the atoms together and two structures are bound. These bonds are either ionic, hydrogen, metallic, or van der Waals.
- *Nucleic acid (or other bio-receptor)*: Configuration of nucleic acid that forms the sensor provides specific spatial electrostatic configuration, which allows only certain molecular structures to bind to them. With other biosensors the process of detection may include an enzyme and the detection is performed in a series of several steps where the enzyme reacts with the analyte, performs its recognition action and then reverts to its original state.
- *Gas and vapor sorption*: Gas and vapor molecules are detected by either being adsorbed (attached to the surface of a sensing material), or absorbed (attached into the sensing material). This sorption can be either entirely physical or accompanied by a chemical reaction that modifies the sensing element, or the analyte, if it is composed of multiple molecules [5].

Transduction:

- *Thermometric*: When the analyte interacts with the sensing element, it generates heat, which is then measured. Example of this is detection of flamable gases that burn on the surface of the sensing element.
- *Mechanically based transduction*: This method measures the change of mass of a sensing element. Mass change is proportional to the amount of detected analyte. This change is usually measured by resonance.
- *Resistive*: As the analyte reacts with the recognition element, the element changes its resistance. This is usually a function of the analyte concentration.
- *Electrochemical*: The sensor contains two electrodes. These two electrodes interact with an aquenous solution. It may be for example water-like substance, or drops of sweat. Reference electrode is exposed to reference concentration of analyte ions. When a detection electrode is in contact with the analyte solution, ion transportation takes place. The detection electrode (recognition element) detects these ions via its receptor sites and a potential difference

based on the difference in ion concentration between the reference and detection electrode is built up. This potential is the quantity that represents the analyte concentration in the place of detection. This was potentiometric transduction. Instead of voltage, in a similar way a current can be measured and these sensors are amperometric. Another option is the measurement using alternating current flowing through the solution and detection of current change. This gives information on the state of the analyte solution and these sensors are in electrochemical impedance category.

- *Optical*: This method uses interaction of photons of light with the recognition element. As the analyte interact with the recognition element (also sensing or active element), the element changes its reaction to the incoming photons and it either changes its reemisive characteristics or refractive index and similar physical properties related to light.

1.1.2 Properties of chemical sensors

Chemical sensing is not a straight-forward task, and practical sensors have multiple limitations. These limitations along with advantages are reflected in the main properties of chemical sensors. These properties are general, so they apply to chemical sensor with any construction. These properties also define the quality of the sensor and viability of use in an environment of choice.

Selectivity: Sensing material is responsible for interaction with gas and providing physical change that can be measured, effectively measuring the gas adsorbed onto the sensing material. Generally however, many kinds of molecules can attach to sensing material. Selecting one concrete molecule is not always possible, but the sensing material's detection range can be reduced by changing its affinity to molecules that attach onto it, and this is done by tuning the energy of the active areas, preventing or allowing chemical interaction of concrete molecules with the active material. One parameter that can be used to tune the energy level of the sensing layer is the temperature. Each gas has some temperature level at which the detection of that gas has best response and this can be used to better detect multiple gases on the same sensing material. Functionalization of the sensing material can improve selectivity too. Some gas molecules almost cannot interact with the base sensing material. By introducing other compounds into it, such as oxides or metal atoms, gases interact with those and the electrochemical effect can be sensed in the sensing material.

Sensitivity: Sensitivity is provided by the sensing material. Sensitivity depends on sensing material's properties over time of interaction with analyte. When chemiresistive sensors are exposed to analyte, sensitivity is defined by the formula $S = (R_0 - R_g)/R_g$, where S is sensitivity, R_0 is the initial resistance of the sensing material and R_g is resistance of the sensing material after gas exposure [7]. It is being discussed, that on materials such as graphene, we can measure gas concentration as little as one molecule.

Stability: Stability of gas sensor names repeatability of sensing capability over period of time. Some sensors degrade over time and have only a finite number of measurement cycles. Stability of these sensors is low. Operating temperature may have impact on sensor's stability.

Response time: Measure of how long exposure the sensing material needs in order to reach 90%+, detection in form of resistance change for example. Short response time means that umpon the exposure to the analyte, sensor quicky adsorbs the gas molecules and its response to gas can be quickly measured.

Recovery time: Time it takes for the sensing layer to get rid of the gas molecules it sensed and recover to 10% of its saturation. Recovery time in some sensors can be as high as 2000s, which means that the measurement cycles can be long. On the other side, there are sensors with 35s down to 11s of recovery time. Recovery time depends on how well the gas molecules can let go of the sensing material. Heavier molecules have problem with desorption, while light molecules such as alcohols let go easily and lead to fast recovery time. Heat can shorten sensor's recovery time.

Operating temperature: Not all sensors can operate in room temperature, although researchers are trying to find a way to accomplish this. In some cases the sensing material is not able to adsorb required gas molecules and the energy of the system must be increased for sensor to work. This is why some sensors operate at about 200°C.

Reliability: This is more of a general property of a chemical sensor. A reliable sensor must be able to repeatedly and consistently report a concentration of gas or a set of gases based on the mathematical function it is tuned to. For example, if a sensor defined to detect NO_2 in air and ten ohms of resistance are to match 10 parts per milion concentration, reliable sensor will adhere to this function for its stated lifespan.

Limit of detection: Smallest concentration of analyte detectable by the sensing material is dependent on the signal-to-noise ratio of the recognition and transducing element. It is measured in parts per milion (PPM) or parts per billion

1.2 Gas sensors

Chemical sensors detect chemical quantities in an environment and this includes detection of ions ions in a liquid, chemical composition of solids, or composition of gas. All these areas of detection are broad and this section focuses on sensing the molecules in a gaseous environment.

1.2.1 Working principle of a gas sensor

Any sensor, not just a gas sensor, is a device that reacts to a change or a state of some physical phenomena in an environment and as a response it produces a signal on its output, that represents the measured quantity. Gas sensors are devices, that transform chemical information, such as concentration or composition of chemicals into a signal useful for analysis [6]. Gas sensor process chain is a simple model that shows how the sensor operates. This chain is composed of several blocks that are visualized in Figure 1.6. In terms of gas sensors, discrete chemical units, such as atoms, molecules, or other more complex chemical structures like dopamine (irrelevant to gas sensors), that are desired to be detected, are called analytes. This chain starts with a receptor and a transducer. Purpose of a receptor is to interact with the analyte and as a result, it changes its physical property that is not directly measurable in this model. It passes the detection information to the transducer, whose task is to respond to the receptor's change and produce an activity that can be directly measured. Since nowadays almost all sensors are connected to some kind of electrical processing circuitry, the transducer reacts to the changes of the receptor, and it responds by changing its electrical properties, such as voltage, or conductance. The rest of the chain is data processing. Different types of gas sensors require different complexity of signal processing, until a measured quantity is produced.

Gas sensors operate on various technologies and principles. There are gas sensors based on polycrystalline semiconductors, which are based on tin or zinc oxide. They require pre-heating and detect gases including NO, NO_2, CO and CO_2 [9]. Gas sensors based on gels can use surface accoustic waves to detect volatile organic compounds (VOCs). These sensors can work on a frequency phase shift that is converted to voltage and to a digital value [10]. Conductive polymer, such as polyaniline (PANI), polypyrrole (PPY), polythiopene (PTH) and poly(3,4-ethylene dioxythiophene) (PEDOT) can be used in gas sensors to detect NH_3, H_2, H_2S, CO_2,

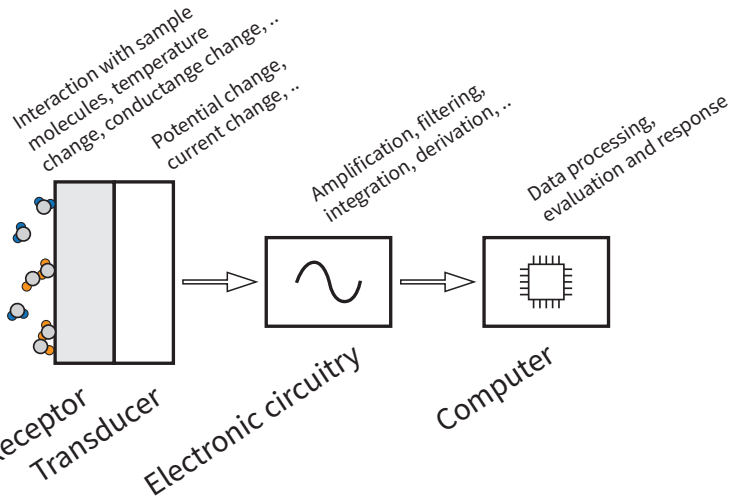

Fig. 1.6: Chemical sensor chain from detection, up to reaction to the measured quantity. [6]

CO, NO_2 and VOCs. Sensing on most polymers happens through gas adsorption onto the polymer and resulting polymer doping through redox reactions [11]. A whole family of gas sensors is built on field-effect transistors. Some of these sensors contain palladium in the gate of the MOS, because it is highly sensitive to hydrogen [12]. MOS gas sensors can be based on silicon, with the operating temperature limit at about 250°C, or on silicon carbide, which pushes this limit to about 800°C [12]. Then there is a family of gas sensors based on 2D materials, which is a primary focus of the thesis.

1.2.2 Methods of gas sensor operation

It has been explained above, that the physical framework allows for many different gas sensors to be created. These gas sensors utilize different methods to sense gases. In this section, several of the most important and used gas sensing mechanism are mentioned. They are based on various recognition type and transduction type combinations that can achieve viable gas sensing.

Chemiresistive Gas Sensors: This category falls into a broader category of electrically-transduced sensing architectures. The basic principle of chemiresistive (chemoresistive) sensors is a resistive or conductive response to the analyte gas. [7][13]. Usually a sensing element (recognition element) is exposed to reducing/oxidizing gases (redox), where the gas atom or molecule adsorbs onto the surface of the sensing element and reducing gas looses an electron and transfers it to the sensing element, while

oxidizing gas withdraws an electron from the sensing layer. Oxidation in this matter is not connected with the word "oxygen". An alternative naming for these gases is electron donating and withdrawing molecules. If the sensing layer (usually also a transducer) is a P-type semiconductor, the electron donating gas (reducing) molecule decreases the conductivity and if it is a P-type semiconductor, the electron increases the conductivity [13]. The sensing element is usually contacted with two electrodes and the resistivity between the electrodes is proportional to the free electrones/holes in the sensing material and this is proportional to the analyte molecules adsorbed on the sensing layer. In case of graphene as a sensing layer, the gases dope the graphene, so gases that donate the electrons are N-doping and withdrawing gases are P-doping. Some electron donating and withdrawing gases are shown here:

Electron-Donating Gases (N-type effect):

- Ammonia (NH_3)
- Hydrogen (H_2)
- Carbon monoxide (CO)
- Methane (CH_4)
- Ethylene (C_2H_4)
- Acetylene (C_2H_2)
- Ethanol vapor (C_2H_6O)

Electron-Withdrawing Gases (P-type effect):

- Oxygen (O_2)
- Nitrogen dioxide (NO_2)
- Chlorine (Cl_2)
- Ozone (O_3)
- Sulfur dioxide (SO_2)
- Hydrogen chloride (HCl)

This adsorption is made possible by Van Der Waal's forces, which is a weak form of molecular interaction. Electrons are exchanged between two atoms. In this case it is an atom of the analyte and an atom of the sensing layer. The electron is transferred to the atom with the higher electron affinity, moving from a valence orbital of one atom to the valence orbital of the other atom.

Catalytic Gas Sensors: These types of sensors are ones of the oldest and are used for detection of combustible gases. The sensor contains recognition element and a transducer. Recognition element is usually a catalytic element coated onto a resistive element, or it can be a catalytic wire directly [14]. This catalyst is heated using a voltage to relatively high temperature (500°C). The combustible gas to be detected,

which would normally burn at an ignition temperature, thanks to the catalyst, the gas can ignite even at lower temperature [15]. It oxidizes on the heated catalyst surface and this chemical process produces heat. The transducer picks up the heat, increases its resistance and this is measured by the connected electronic circuit. Wide range of combustible gases can be measured this way, including:

- Methane (CH_4)
- Ethane (C_2H_6)
- Propane (C_3H_8)
- n-Butane (C_4H_{10})
- n-Heptane (C_7H_{16})
- Methanol (CH_3OH)

Accoustic and Surface Accoustic Wage Gas Sensors: Detection mechanism of these sensors is mechanical, rather than chemical. A receptor film is vibrated by an electrically powered transducer. When analyte binds to the receptor film, its mass and thickness changes. This affects the vibration and wave content such as frequency, amplitude and phase is measured back to figure out the type and concentration of the analyte. This way of analyte detection allows for wireless separation between the sensing layer and the evaluation circuitry [16], which is an unique advantage in the field of gas sensing. For example, the detection system sends a 440MHz excitation wave to the sensing element and the transmitted response is evaluated. Surface accoustic wave sensor is based on the Rayleigh waves. Since the surface waves have the most of their energy localized near the surface of an object, they are easily influenced by the change of the object's surface characteristics [17]. An interdigitated transducer (IDT) receives an electrical signal, converts it into a mechanical wave and then reconverts this wave back to the electrical signal. Two main types of accoustoelectronic sensors are based on a delay line and a resonator. A piezoelectric effect is used in the transducer for both types of sensor. In case of a delay-line sensor, the transducer has an input and output electrode sides spaced by a delay line. An active element such as a thin polymer is placed across the delay line and it absorbs the analyte. Resonator is more difficult to design. It has the interdigitated transducer in the center of the sensor base. Further out from the IDT are reflectors and at the end of the base is an optional absorber. The resonator is coated by a sensing film that absorbs the analyte. Both the resonator and the delay line operate at a usual operating range of 40-600MHz [15]. Gases these sensors can detect include hydrogen and methane [17].

2 Gas sensor measurement

Gas sensors relevant to this thesis operate on a chemiresistive principle. This chapter focuses on practical ways of sensing the target gas and interpreting the received data. Graphene-based gas sensors are studied in this section. Focus is drawn to chemiresistive principle of operation, although some graphene sensors work on optical ways of gas detection [18], change in frequency of the surface accoustic waves [19], Hall resistivity changes [20], Dirac voltage shifts [21] and plasmons detection [22]. All these are sensing parameters that have been tested.

Before the actual graphene chip can be used for the measurement, it must be prepared. Sensors must be sliced from the original wafer and bonded to a contacting array. An example of a prepared sensor sample is shown in Figure 2.1.

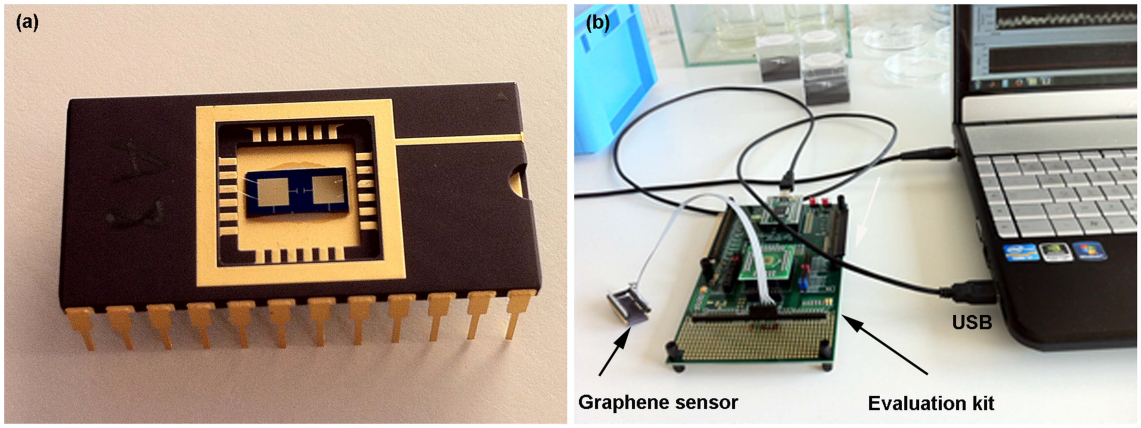

Fig. 2.1: Pictures of a graphene sensors testing apparatus **a)** graphene sensor bonded to a package, **b)** Testing circuitry for the sensor. Image adapted from [23]

One of the most widely used way of measuring a chemiresistive gas sensor, is to acquire a change of conductivity in time, while the sensing material is exposed to the analyte gas. The sensor is usually tested under atmospheric pressure and it is exposed to a mixture of an analyte gas and a carrier gas. If the carrier gas is air, relative humidity is taken into an account. If the carrier gas is not air, it is usually an innert gas, such as argon, helium or nitrogen [23]. An example of a chemiresistive reaction to various gases is shown in Figure 2.2. Sensitivity is denoted in relative conductance or resistance: $\Delta R/R = (R_{carrier} - R_{analyte})/R_{analyte}$ [24].

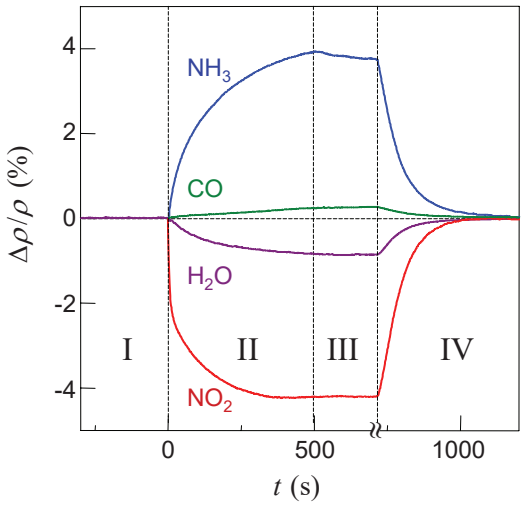

Fig. 2.2: Resistivity of a graphene sensor responding to various analyte gases. In the phase I, the sensor is in an unspecified vacuum. In phase II the sensor is exposed to 5 liters of gas mixture consisting of 1ppm concentration of the analyte gas mixed in helium or nitrogen. Measurement was performed under atmospheric pressure. In phase III the chamber with the sensor was again brough to vacuum. Gas molecules were still adsorbed on the surface. Annealing the sensor under vacuum at 150°C in phase IV was able to bring the sensor to its former undoped state. Figure adapted from [20]

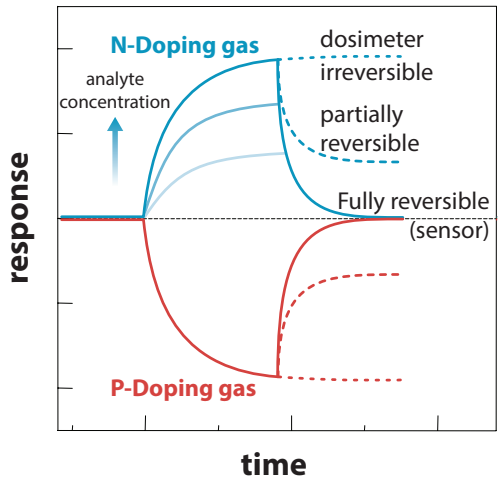

Fig. 2.3: Theoretical response of a chemiresitive gas sensor to an analyte. This figure shows a comparison between electron donating and withdrawing gases, how exposure to various analyte concentrations may look like and how well can a material recover from the analyte. When a material is able to completely recover from the sensing phase, it is suitable for sensing. Figure inspired by [13]

In the same way a transient response (also called a dynamic response) is obtained. A sensor is exposed to levels of an increasing concentration of the analyte gas. The sensor is exposed to a target amount of concentration and the sensor reacts. After a period of time the analyte is removed and sensor is purged. In paper [25], they flush the sensor with argon for 300s and the sensor is exposed to another concentration. Group of R.K. Paul [26] purged their sensors with dry air for 200 minutes. Light can also be used to trigger gas desorption. UV laser with a wavelength of 365nm was able to photodesorb oxygen and ammonia from a pristine graphene surface [27]. The transient response to various gas concentrations shows how well the sensor can recover and how it reacts to an already exposed sensing layer. Figure 2.4 shows this

transient response in time. If some way of sensor cleaning is not used, desorption process can be observed even after 24 hours [28].

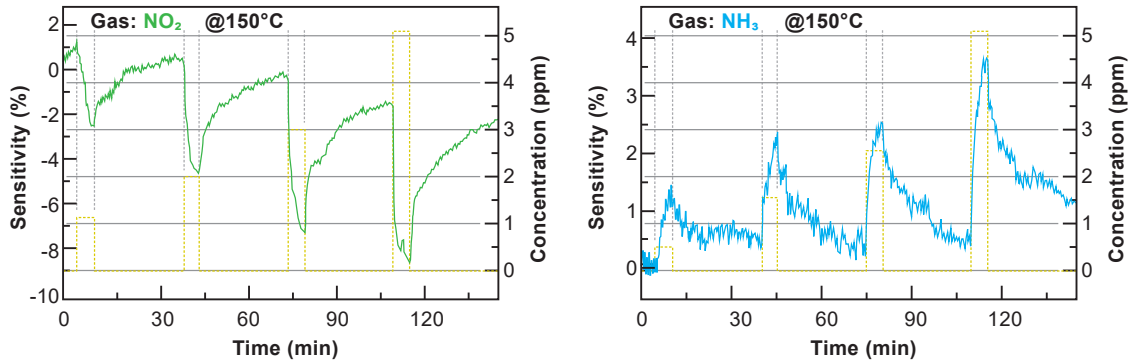

Fig. 2.4: Real-world example of two transient responses of a Graphene/MoS_2 heterostructure sensor to NO_2 and NH_3 gases. Graphs show the ON and OFF phases of the analyte gas exposure and the concentration of the analyte for each exposure. Figure reconstructed from [24]

Instead of the sensitivity difference in percent, a difference in voltage or current can be plotted. Various baselines can be measured and the information obtained should be approached statistically. Response to various gases can be measured too. In an inert atmosphere, different analytes react differently. Reaction with an introduction of humidity may be a viable information too, since it is closer to the out-of-the-lab environment.

After the data from the sensor is acquired, the data can be post processed to increase the accuracy of the detected gas type and concentration. It is known that sensors tend to have long detection and recovery time and this poses problem when the sensor is continuously measuring gas concentration. That is why advanced methods of gas sensor data processing have been developed, such as back propagation neural networks [29].

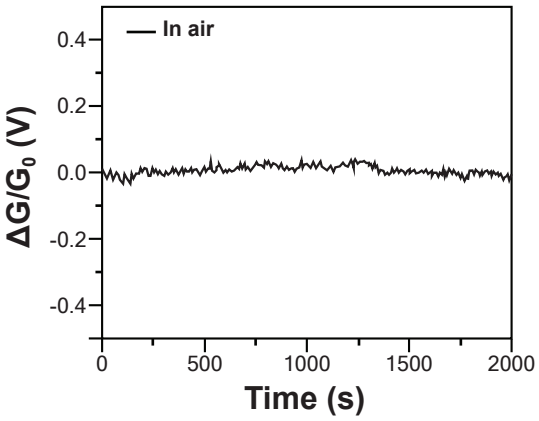

Fig. 2.5: Conductance response of a phosphorene active layer to the air over time. Maximum fluctuation in relative conductance is less than 4%. Figure adapted from [25]

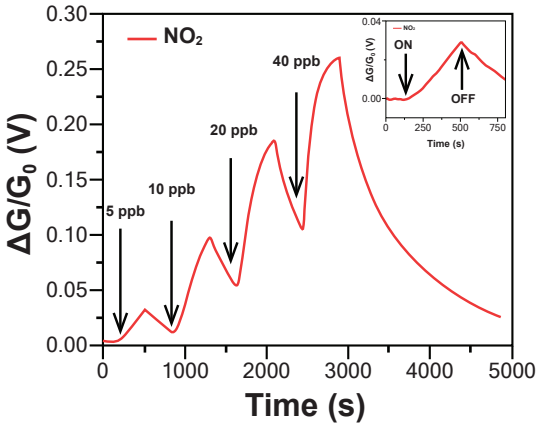

Fig. 2.6: Exposure of a graphene sensor to a varying mixture of NO_2 and argon gas. Inset shows a zoomed window of the 5 ppb area. ON means the NO_2 gas is fed to the sensor and OFF means feeding is switched off. Figure adapted from [25]

2.1 Noise in graphene

There are four main intrinsic sources of noise in graphene:

- Thermal noise (Johnson noise)
- Generation-Recombination noise (G-R noise)
- 1/f noise (Flicker noise)
- Shot noise

During the noise characterization of graphene, contacts to the graphene play an important role, because of the voltage distribution between contacts and the graphene sheet [30]. In the following text these four main sources of noise in graphene are introduced, but they are not presented in a specific relation to graphene, as they happen in all conductive materials in some proportion.

Thermal noise is caused due to random motion change of the free charge carriers (electrons or holes) across the conduction path of a material. This change of motion happens due to scattering of the wave function on the defects in the wave path in the conductor, based on the quantum theory model. In a more classical view, vibrations of the atoms due to temperature, cause the electrons to gain variable amount of kinetic energy and random direction of motion. On the macro scale, this effect statistically manifests as voltage perturbations at the terminals of the conductive path. The spectral density is given by Nyquists formula in Eq. 2.1.

where k_B is Boltzmann's constant ($1.3806504 \cdot 10^{-23}$), T is the temperature of the conductive path and R is the resistance of the conductive path. Thermal noise is present in the material even at no voltage applied across it and because the density is distributed across the whole frequency spectrum evenly, it can be distinguished and isolated from the other sources of noise.

$$S_I(f) = \frac{4k_BT}{R} \tag{2.1}$$

Generation and recombination noise is influenced by local fluctuations of of the steady-state electron and hole densities in the conduction and valence band of the conductive material. This noise can be approached statistically by seeing random transitions of the charge carriers between localized (bounded) states and/or band (extended) states [31]. The spectral density of G-R noise is described by a Lorentzian in Eq. 2.2 [32]. where S_0 is the frequency independent portion of the noise at frequencies below $(2\pi\tau)^{-1}$ and τ is the time constant of a specific trapping state that causes the noise, such as an ionized impurity [32]. In graphnene this electron-hole recombination and generation happens mainly by optical phonon assisted interband transitions [31]. Generation and recombination noise can be seen below 0.1Hz due to the DC current instability [33].

$$S_I(f) = \frac{S_0}{1 + (2\pi f\tau)^2} \tag{2.2}$$

1/f noise is also called flicker noise, or excess noise. It is an important factor for graphene gas sensor measurement, as it limits the sensitivity of sensors [30] [32]. The source of this noise was not fully understood and the state of the art in this field was controversial [32] in 2013, even after many years of research. Its characteristics in graphene and other materials, such as silicon semiconductors is slightly different. It can be formed by various fluctuation processes, such as current fluctuation due to mobility fluctuation and carrier number (carrier density) fluctuation [32]. Mobility fluctuations can arise from electron scattering on various lattice scattering centers, where the scattering center parameters can fluctuate as well. Mobility and carrier number fluctuations can be closely related, since the scattering centers cross sections can fluctuate due to capture or emission of electrons in their vicinity. The 1/f noise in complementary metal-oxide-semiconductors field-effect transistors is described by McWhorter model, which is based on carrier number fluctuation approach. In metals, including graphene, 1/f noise is usually attributed to mobility fluctuations [32]. This noise is present below 100kHz. In graphene, the conduction electrons are exposed to traps (such as charged impurities) in the substrate or the environment, which can result in carrier number fluctuations. Flicker noise in bilayer graphene at $f < 10Hz$ is attributed to "slow" traps, due to contacts and graphene edges

contributions and its behavior is rather $1/f^{2-3}$ than $1/f$ [33]. Grain boundary noise of graphene contributes to 1/f noise [34] too and potentially graphene edges are also contributing to 1/f noise [20]. There are conclusions, that graphene performance can be pushed up to thermal noise limit and that graphene is a low-noise material [35] [36]. It has been found that the bigger the graphene area ($W \times L$), the smaller is the 1/f noise in the system. Since the noise is in direct relation with graphene area, it can be concluded that it is the dominant source of noise and contact do not influence the noise as much as the graphene itself [30]. Single-layer graphene has the most 1/f noise. As the number of graphene layers increases, the noise decreases. This phenomenon is explained by a theory where the band structure in bi-layer or few-layer graphene varies the charge distribution in the graphene planes, which results in screening of the potential fluctuations [32]. This 1/f noise can be used as a sensing parameter to distinguish various adsorbed gases on the graphene sensing layer [21]. The exposure of contacts and graphene to the environment causes contacts resistance increase and charge mobility degradation, which is attributed to increasing of the 1/f noise of the device over time. Since most graphene gas sensors rely on electrical response, their performance is limited by 1/f noise and this noise influence cannot be reduced by extending the measurement time [32]. Reaction process at the sensing material can be so slow, that the 1/f noise of the system may overtake the measurement and it can be compromised. Also, the 1/f noise is the major contributor to the phase noise of the oscillating systems [32]. The 1/f noise of graphene depends on the gate voltage applied to it. With an increasing gate voltage, resistance of the graphene channel decreases and the 1/f noise increases. The 1/f noise in graphene is decreased after low-energy 20KeV electron beam bombardment. By decreasing the mean-free path of the electrons by the lattice change caused by the beam bombardment, the 1/f noise is also reduced [37]. Thus, the noise reduction comes at the expense of mobility degradation. The general spectral density of 1/f noise is shown in Eq. 2.3, where $\gamma \approx 1$ [32]. It decreases with increasing frequency, forming a knee called f_0. At this knee the noise decreased to the point where it equals the thermal noise. This knee can be few Hz up to several kHz wide [32].

$$S(f) \sim 1/f^{\gamma} \tag{2.3}$$

Shot noise is similar to thermal noise. It has a white noise characteristic, which means that its spectral density spans the whole frequency spectrum (the density function does not use frequency in any relation). It is caused by the discrete nature of electric charge and random arrival times of individual carriers crossing a barrier or a junction, such as the one between graphene and its contact interface. Tunneling, quantum interference and scattering on various lattice non-symmetries contribute to shot noise [38]. The spectral density of shot noise is given by Schottky's theorem

in Eq. 2.4, where q is electron charge (1.602176634»10^{19}) and <I> is the average value of an electrical current

$$S_I(f) = 2q < I > \tag{2.4}$$

2.2 Advances in graphene research

As it happens with many other things in physics, graphene was too predicted theoretically at first, in 1947 [39]. Historical progress of graphene research is documented and tracked [40]. It was produced in 2004 by the group of A. Geim and K. Novoselov using famous scotch tape technique. A subsequent paper was published that year [41] and the same two people produced another paper related to graphene in 2007 [42]. Throughout the years graphene has been applied to immunosensors [43], triboelectric nanogenerator in wearable electronics [44], aerogels [45], hexadecaol [46], composites for antibiotics removal [47]. It is being experimentally used as transparent conductive electrode in solar panels [48] or as a part of microwave absorber [49]. An optical modulator has been also build using graphene [50]. This is just a tiny sample from thousands of research papers produced throughout many years. This selection was to depict the scale of possible applications where graphene may be proven, thanks to its properties. This thesis is focused on exploiting noise characteristics of graphene inside of a chemical sensor. To start from the beginning, graphene in its purest form (also called pristine graphene) was used in a chemical sensor and discrete detections of molecules on graphene surface were recorded [20]. Noise parameter has been also studied and proven in characterization of different gasses adsorbing on pristine graphene structure [21]. A review of graphene from 2010 [51] reports (without clear referencing) that the real drawback is a lack of selectivity for pristine graphene sensors, as it responds to different analytes very similarly. This is attributed to the fact that pristine graphene is relatively chemically stable material and it lacks dangling bonds that are good for analyte adsorption [52]. Pristine graphene by itself (omitting graphene edges) has low-energy binding sites and graphene with introduced defects of functionalization has high-energy binding sites [53]. Therefore, as graphene is being used in chemical sensing, various graphene modifications, structural enhancements, doping and topology modifications are experimented with. Graphene nanosheets have been implemented with SnO2 nanofibers that detects acetone and H_2S [54]. Multilayer graphene has been used to detect NO_2 [55]. Graphene/polyaniline (PANI) composite can be used to detect methane [56]. There is a big range of graphene structures used for chemical sensors. Many of them can be found in this review [57].

2.3 Chemical and physical properties of graphene

Interest in graphene and its application into all kinds of fields arises from graphene properties. In this section, well-researched parameters of graphene are listed and some of them are compared to other well-known materials to show how much graphene surpasses other materials. Both physical and chemical properties are listed and these properties are also relevant in setting up the measurement apparatus and in the choice of measurement strategy.
Graphene is one atom thick sheet of carbon atoms organized into a hexagonal array, seen in Figure 2.8. Other literature mentions benzene-ring structure [41] or honeycomb structure [42][58]. Benzene ring with its hydrogen stripped away is like a single graphene cell. The graphene cell is visualized in Figure 2.8.

The unaltered clean carbon sheet is also called pristine graphene [52]. Pristine graphene is made out of carbon to carbon bonds that are 1.420Å apart [59]. Carbon is on sixth place in the periodic table. This means that it has 6 electrons around its nucleus. Two electrons with up and down spin are in $1s$ orbital and they are generally inaccessible to any experiments relevant to his thesis, because they require too much energy to be useful. Other four electrons are in the valence shell and they are all contributing to the structural effects. Two of these four electrons are present in $2s$ orbital with spin up and spin down variant. The last two electrons are in $2p_y$ and $2p_z$ orbital with spin up only. The electrons are visualized in Figure 2.7. This atomic configuration allows for various forms of hybridization, which can create different carbon structures, such as diamond [60] or graphene.

Pristine graphene sheet (layer) can be placed on top of another. These layers are connected together using Van der Waals forces and double-layer or few-layer graphene can be created this way. This compound structure is too called graphene. Stacking many layers of graphene together forms graphite. With 3 and more layers the electronic spectra of graphene become more complicated and thus these structures are taken as a standalone graphene configuration for research[42]. This thesis is however focused on the single-layer graphnene, which is a 2D crystal.

Graphene configuration has three identical sp^2 hybridized orbitals 120°apart and each of these orbitals connects to one of three neighboring atoms in the crystal lattice. These connections share one electron with up spin in one atom and one electron with down spin from the other atom. This way, the carbon bonds have filled shell (orbitals) and thus the valence bond is strong. The structure of these connections is called trigonal planar structure and is made out of σ (sigma) bands. The unaffected p orbital which has one extra electron, can form half-filled pi (π) band, which is available on both surfaces of the graphene sheet [61]. These π bands are in their hybridized configuration referred to as π and $\pi*$ bands [62]. σ electrons

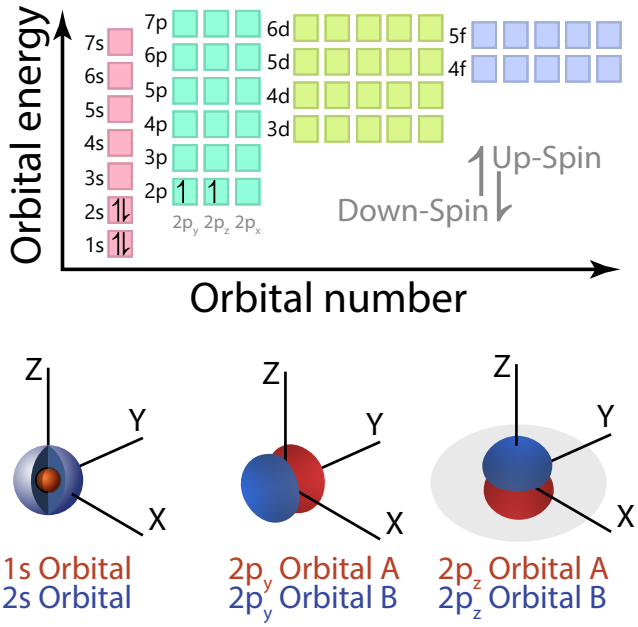

Fig. 2.7: Top of the image represents electron occupation of a carbon atom in SPDF orbitals model. Bottom part of the image visualizes the orbitals. Inspiration was taken from the online PTable project.

form energy bands far away from the Fermi energy [63]. Fermi energy is the highest possible energy that an electron of an atom or a structure can possibly have, while still remaining bound to the atom and not being fee. This is a statistical value and it does not denote physical possible band at that energy.

Graphene crystal structure can be mathematically analyzed to yield some insight into electronic properties of the structure. Tight-binding approximation (also named linear combination of atomic orbitals [65]) was developed for this purpose. This method calculates hopping and overlap integrals (usually nearest-neighbor (nn) and next-nearest-neighbor (nnn) interactions are taken into account) which yield an energy dispersion result. In graphene, 3 of 4 valence electrons are in the sp2 bond, holding the graphene structure together and they are responsible for graphene mechanical properties. The last electron present in the P_z orbital and is a member of π bond with another carbon atom. This bond is made of small orbital overlap and thus it is responsible for electronic properties of graphene [66]. The tight binding method is based on the assumption, that electrons are localized around the atom in their orbital and they do not move freely across the crystal. These electrons can hop between atoms and this phenomenon forms the conductivity of the crystal.

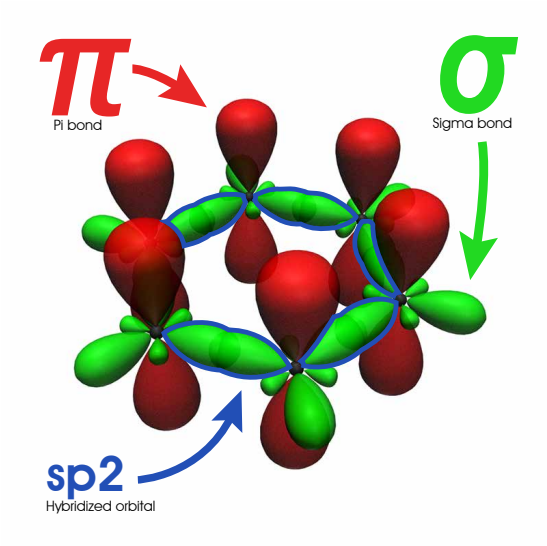

Fig. 2.8: Single graphene cell with its outer orbitals hybridized. This a conceptual visualization and is not a result of simulation. (Inspired from [64])

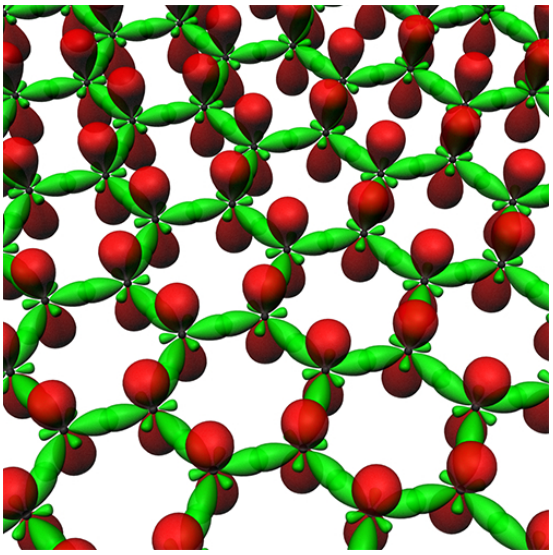

Fig. 2.9: A visualization of symmetric graphene sheet with its orbitals.

The orbital structure of the whole graphene crystal is composed of energy bands, which are made up of the orbitals of individual carbon atoms and if the electron has sufficient energy, it can jump between the orbitals of other atoms within the energy band, or in the conduction band. A conceptual model of this phenomenon is visualized in Fig. 2.10

To calculate a tight-binding approximation, the crystal lattice needs to be described. First, it is necessary to have a physical representation of the graphene lattice. The atoms of the lattice are visualized in Figure 2.11. The lattice is described by two vectors - $\vec{a_1}$ and $\vec{a_2}$. Papers [66][39][61][62][63][67][60] have equivalent vector geometry as in the Figure 2.11, but have different rotation and starting point. The $\vec{a}$ vectors determine the 2D Bravis unit cell in a direct (also real-space) lattice, which tiles an infinite crystal structure. Next, it is necessary to define $\vec{K}$ vectors. $\vec{K_1}$ vector is to be perpendicular to $\vec{a_2}$ and $\vec{K_2}$ is perpendicular to $\vec{a_1}$ in this case. These vectors are defined in reciprocal space and periodicity of this space is defined by a relation to direct space [66]. The $\vec{K}$ vectors are shown in Figure 2.12. The smallest and thus elementary graphene crystal cell that can be physically formed by carbon atoms is the hexagonal cell. K vectors specify the Brillouin zone, which is a primitive lattice cell in the reciprocal space. The results of the tight-binding approximation are available throughout this zone. Lastly, the nearest neighbor vectors must be defined. Graphene atom has 3 nearest neighbors and their vectors are also shown in Figure 2.11.

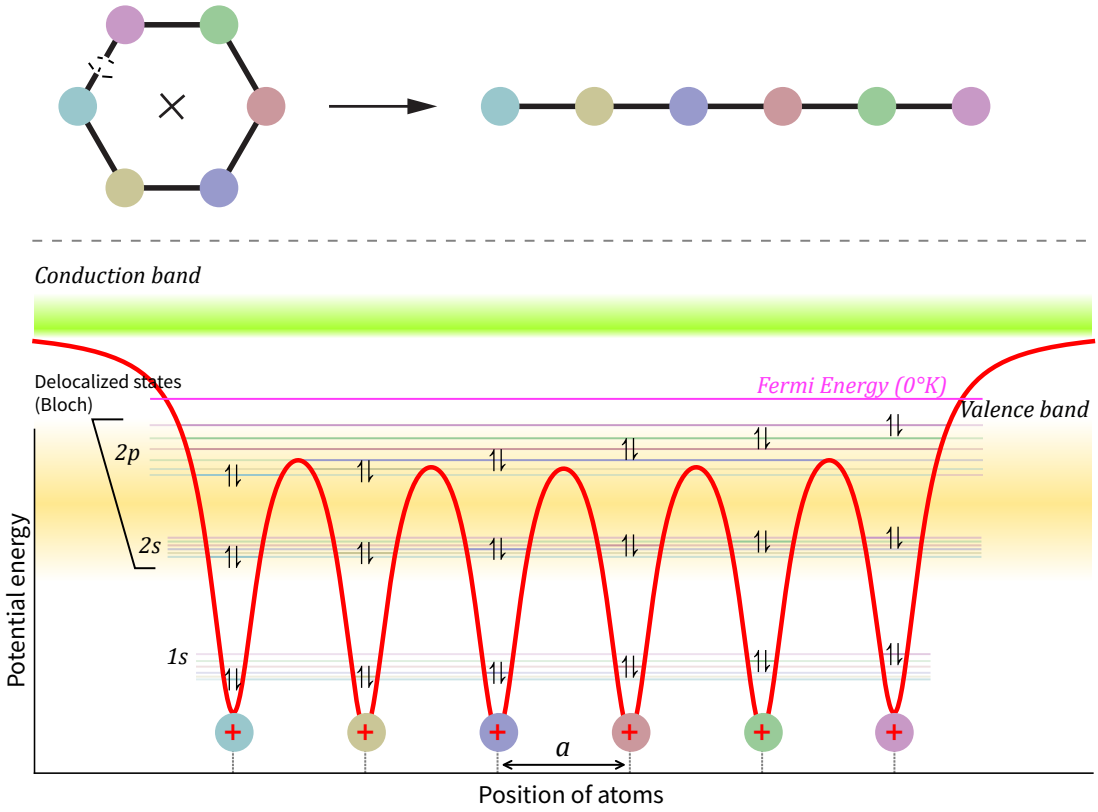

Fig. 2.10: A conceptual view on atomic orbitals and bands in hypothetical line of carbon atoms. Here, the hexagonal structure is broken and the atoms are layed with constant spacing on the line. Each atom has its own orbitals and this is a visualization before their hybridization. The electrons can hop between atoms when they go from an available orbital in one atom to an orbital of another atom. The lines represent orbitals of specific atoms and the arrows represent the electrons with their spins in the orbitals of each carbon atom.

After having all the vectors defined, the tight-binding approximation requires a Hamiltonian for the isolated carbon atoms in graphene [66]. The Hamiltonian is a matrix formed from a wavefunction of the P_z orbital and it is necessary for solving the Shrödinger equation. Bloch's theorem is used while constructing the Hamiltonian. Solution that comes from this method is an electronic energy dispersion, which is included in the electronic band structure of graphene and papers [60] [61] [69] agree on the spatial solution 2.5 with $\gamma = 2.8eV$. The first Brillouin zone's K and K' points there are Dirac points, which are points where the conduction and valence bands of carbon meet (electron and hole energy bands touch each other [68]). The 3D function is a representation of the π and π^* orbital, but this method allows for calculation of other orbitals, such as those in Figure 2.14.

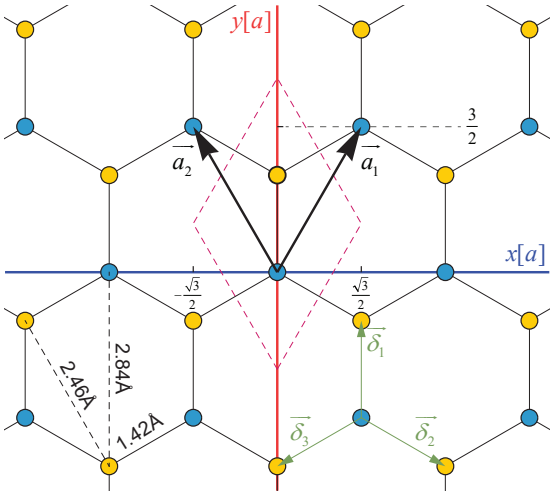

Fig. 2.11: Graphical representation of graphene atomic structure in the physical (also direct) space. The axis is in the unit of atomic distance $a = 1.42$Å. The smallest spatial unit that describes this infinite lattice (Bravis unit cell) is highlighted by purple rhombus. This cell is described by $\vec{a}$ vectors. Nearest neighbors are defined by δ vectors. (Image inspired by [68])

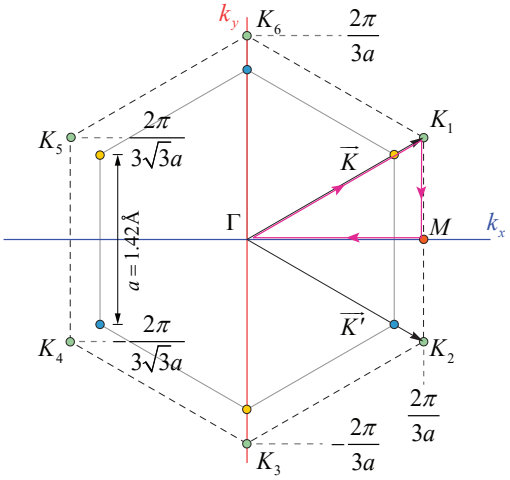

Fig. 2.12: Brillouin zone of the 2D reciprocal lattice. Light-green points are K-points, which are fully defined by two $\vec{K}$ vectors. This reciprocal space is native to momentum space, describing wave vector of particles in a periodic system. This space is indirectly related to the physical lattice space. The Reciprocal lattice vectors $\vec{b}$ are not shown. The violet triangle is an example of traverse for this momentum space, going fro δ through K_1 through M back to δ. This is the X axis for the momentum space diagrams. (Image inspired by [68])

$$E_{\pm}(k_x, k_y) = \pm\gamma\sqrt{3 + f(k_x, k_y)} \tag{2.5}$$

$$f(k_x, k_y) = 2\cos(\sqrt{3}ak_y) + 4\cos\left(\frac{\sqrt{3}}{2}ak_y\right)\cos\left(\frac{3}{2}ak_x\right) \tag{2.6}$$

There is a problem with a disagreement on the band structure among the sources. The Tight Binding Method reports π and π^* crosspoint at -5eV, but The Band Structure of Graphene reports -10eV 2.14. Report [70] shows a symmetrical π and π^* structure peaking at about 8eV. Paper [66] and thesis [71] seems to agree on that. Note [63] and a review [61] disagree on these plots. They show a non-symmetrical graph of dispersion at peaks +t and -2t with $t \approx 3eV$ for [63] and $t = 2.7eV$ for [61] Source [72] reports a non-symmetrical plot with peaks at about -6.5 and 15.5 eV. This is probably due to different choices in modeling.

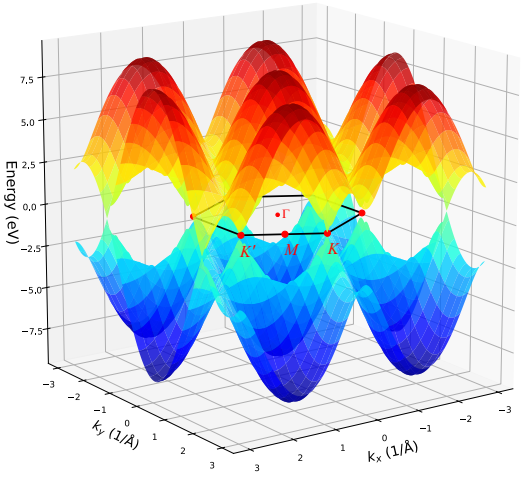

Fig. 2.13: Energy dispersion over the first Brillouin zone of graphene. Red part is the conduction band and blue is the valence band. They are symmetrical. (Image reconstructed from [61])

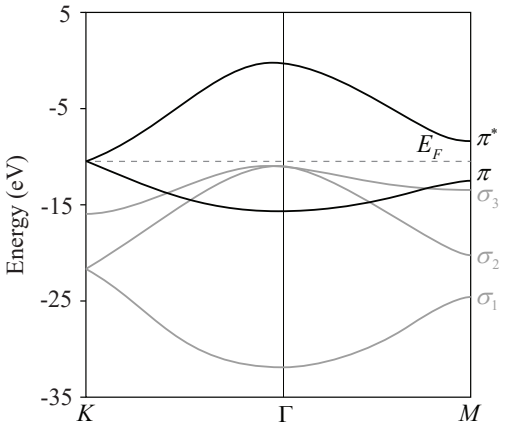

Fig. 2.14: A view of the energy dispersion in a Brillouin zone. Five bonds are computed here. Sigma 1, 2 and 3 bonds are active in the binding of carbon molecules and are not interesting in terms of electronic properties. Interesting is π orbital, which is bonding and π^* which is anti-bonding orbital. (Reconstructed from a youtube video "Lecture 33 The Band Structure of Graphene" uploaded by Pat's Perovskites)

Based on this physical model of graphene and some other calculation, series of assumptions and experiments, a set of physical properties of graphene has been predicted and measured:

Carrier mobility Research team came to a conclusion, that if other sources of scattering are omitted, electron-phonon scattering has such a low effect that a carrier mobility of $200000 \cdot \frac{cm^2}{V \cdot s}$[73] could be observed at room temperature, however typical mobility of graphene on SiO2 ranges from 10000 to 15000 cm^2V^{-1s-1}. Extrinsic disorders that are sources of scattering include charged impurities (such as adsorbed molecules) or microscopic ripples. This quantity defines how fast the charged carriers move through a material when an electric field is applied at the material. At room temperature ($\mu = 300K$), real carrier mobility with value up to $100000 \cdot \frac{cm^2}{V \cdot s}$ can be achieved. The charge mobilitiy due to ambipolar electric field effect can exceed $15000 \cdot \frac{cm^2}{V \cdot s}$ [42]. The mobility depends on the temperature only weakly[42]. High carrier mobility leads to higher conductivity. Concrete geometry and voltage setup for the experiment lead to the values mentioned here is not known.

Ballistic transport A quantity that refers to distance the electron travels without any significant scattering. In graphene, this distance can reach up to $0.3\mu m$ [42], which is about 1050 graphene cells long.

Specific surface area A theoretical value for graphene specific (dependent on mass) surface area is determined to be $1005\frac{m^2}{g}$ [74].

Thermal conductivity Thermal conductivity of graphene is experimentally measured to be $(4.84 \pm 0.44) \cdot 10^3 to (5.30 \pm 0.48) \cdot 10^3 \frac{W}{m \cdot K}$ [75].

Breaking strength Intrinsic strength of graphene is experimentally measured at $42 \pm 4\frac{N}{m}$ [75]. This means that 42 newtons of force are required to break a 1m long sheet of graphene, which is very much, considering its one atom thickness.

Tensile strength The amount of force graphene can sustain before breaking is 130GPa.

Stiffness Young's modulus for graphene is $1.0 \pm 0.1 Tpa$ [75]. This quantity measures how much pressure stress needs to be applied to graphene in order to deform it.

Spring constant Compression and dilatation of graphene is energetically costly. This is because its spring constant is about $57\frac{eV}{}$[61].

Optical transparency Transparency is based on how much can photons with visible energy spectrum interact with the graphene structure. Graphene's transmittance is determined to be 97.7% [62]. Graphene is visible on a substrate (such as SiO2), with visibility being much stronger in reflection, than in transmission [76].

Work function If an electron is able to leave a graphene surface and place itself to the outside environment, it needs at least 4.7eV of energy [24].

Graphene doping

Doping in materials increases or decreases the number of free carriers. For example, in Silicon, phosphorus dopant introduces an electron to the structure's conduction and boron introduces an electron vacancy (hole). Doping of graphene is split into two main categories.

- Electrical doping (Ambipolar electric effect)
  Graphene as a field effect channel can be 'doped' just by introducing an electric field through the sheet (DC gate voltage has to be applied between the graphene layer and the substrate separated by dielectric [68]). This effect is called ambipolar gating. The voltage shifts the Fermi level (chemical potential) above or below the neutrality point (to the upper or lower energy band [68]). Upward shift due to positive external voltage introduces electrons, which become majority carriers and downward shift introduced by negative external voltage introduces holes. This process tunes charge carriers (electron or hole density) along the graphene sheet up to a concentration as high as $10^{13} cm^{-2}$ [42]. The voltage moves Fermi energy away from the Dirac point by 10 to 400mEv [62]. The external voltage influences the conductivity of the graphene linearly [58]. This effect is observable up (but not exclusively) to room temperature. In bilayer graphene with SiO_2 as a dielectric the electric field effect is more pronounced. Electronic band structure can be continously changed by tuning δ E gap from zero to about 0.3eV [42]. Resistivity and conductivity changes on graphene due to this effect can be seen in Figures 2.15 and 2.16 respectively. Methods for doping characterization include photo-emission spectroscopy, angle-resolved photoemission spectroscopy, Raman spectroscopy and transport measurement [77].
- Chemical doping
  Atomic or molecular impurities can be introduced into or onto the graphene structure. Chemical doping can be further categorized into:
  - Surface transfer doping
    An atom or molecule is adsorbed onto the graphene surface by Van-der-Waals forces and an electron is exchanged between the graphene and dopant [77]. It is very often a reversible process. Charge transfer happens between graphene and dopant. The direction of this transfer depends by the relative position of the density of states between the highest and lowest occupied molecular orbital of the dopand and the Fermi level of graphene [77]. If the highest occupied orbital of a dopant is above the Fermi level of graphene, then charge transfers from dopant to graphene and dopant acts as a donor. IF the lowes unoccupied orbital of the dopant is below the Fermi level of graphene, charge transfers from graphene to

the dopant and dopant becomes an acceptor.

- Substitutional doping

  This process replaces the carbon atoms in the graphene crystal lattice by other atoms with different number of valence electrons. The sp2 hybridized bonds would be replaced by a new configuration, based on the type of dopant. Nitrogen or boron are possible dopants.

- Nanoparticles

  Various metals or other substances can coat or be grown on top of graphene. This changes graphnene's topology and breaks graphene's sublattice symmetry [78], which is responsible for the continous energy levels modeled by Dirac cones. This introduces a bandgap for the graphene sheet. This process is also called decoration.

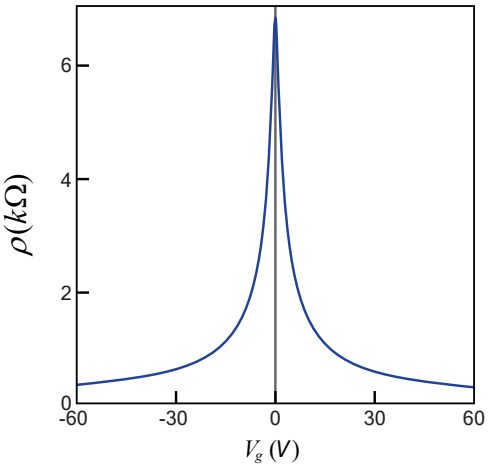

Fig. 2.15: Resitivity of a graphene sheet based on the gate voltage. Experiment was conducted at T=1 Kelvin and at 0 tesla of magnetic field. Adapted from [42].

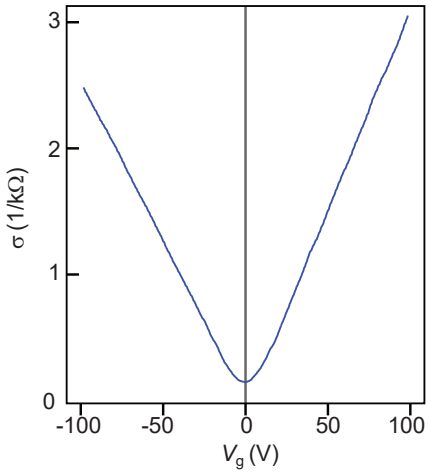

Fig. 2.16: Conductivity of graphene based on the gate voltage. Experiment conducted at T=10 Kelvin and at 0 tesla of magnetic field. Adapted from [58].

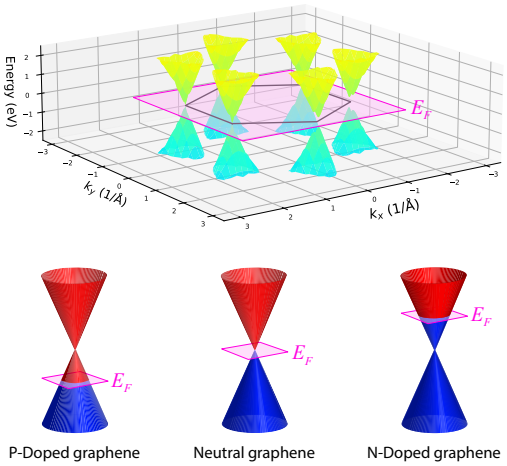

Fig. 2.17: On top is a cutout of the Energy dispersion from Figure 2.13. The cutout shows almost linear characteristics for the conduction and valence band. The bottom part is an approximation of this dispersion by circular cones. These are called Dirac cones and the Fermi energy can be moved up or down with the doping caused by the external electric field.

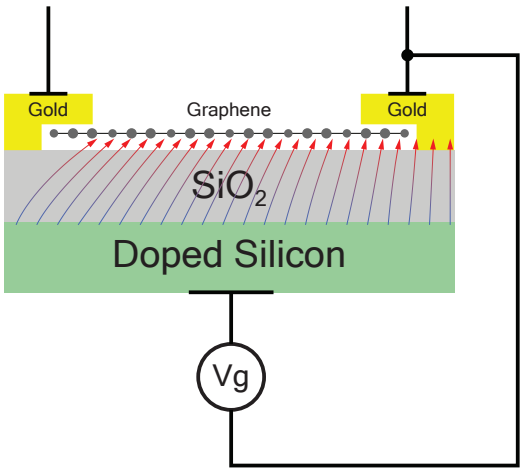

Fig. 2.18: Graphene layer deposited on a silicon wafer with silicon-dioxide as an insulator. The layer of SiO2 is several hundreds of nm thick. An electric field is created between the relatively conductive silicon base and the graphene sheet, interfaced by a golden electrode. This field shifts the Fermi level of graphene and electrons or holes are introduced in the graphene. This is called Ambipolar electric effect.

Dirac fermions in graphene

Due to graphene's highly symmetrical hexagonal lattice, the π orbitals provide continous energy levels between valence and conduction band. This effect can be seen from the energy dispersion modeled over the first graphene Brillouin zone. The Fermi energy of an ideal graphene is at the Dirac energy, which is the energy of a dirac point [62]. Electrons within about 1eV above or below the Dirac energy have a linear dispersion relation. This is why these electrons are better described by Dirac equation for massless fermions, rather than Schrödinger equation, by which the electrons would normally be described. This is because graphene is a zero-gap semiconductor and along the Dirac points in the Brillouin zone, the charge carriers behave as quasiparticles [42]. These quasiparticles introduce properties such as pseudospin and chirality. The quasiparticles in graphene are massless and exhibit little scattering under ambient conditions [42]. They are called massless Dirac fermions (or Dirac electrons) and can be seen as electrons that lost their rest mass, or as neutrinos that acquired an electron charge [42]. These relativistic particles

have effective "velocity of light", which is 299 792 458 m/s [68]. They propagate in waves on the graphene sheet by a potential proportional to the square of the sheet curvature and that increases graphene's resistivity [69].

Conductivity of graphene

In a simplified view, charge excitation has two main sources. Electron hole pairs, which is an incoherent excitation of the Fermi sea and it is governed by Pauli's principle and collective modes, such as plasmons. In usual metals and semiconductors whose lattice has nonrelativistic dispersion, there is a large Fermi surface and energy bands have a parabolic shape. The continuum of intra-band electron-hole excitations can happen down to zero energy. Plasmons also appear as collective charge-density waves and happen outside of the electron-hole continuum [61]. In graphene, where the Fermi energy is at the Dirac point, the Fermi surface shrinks to a point and because of this there are no intra-band excitations. Interband excitations between the Dirac cones can happen. Therefore, neutral graphene has no electron-hole excitations at low energy because they cost energy.[61] When a graphene sheet is exposed to an oscillating electric field between the source and drain electrodes (between the two contact terminals), graphene reacts by frequency dependent conductivity, which concerns linear response theory of graphene. This conductivity has two contributions. Intra-band and inter-band conductivities. Intraband transitions are electrons jumping between the energy levels inside the valence band or conduction band. Inter-band transitions are electron transitions between the valence and conduction band [66]. For the intra-band conductivity, in collisionless approximation (which is dominant at high purity samples), it has the value of imaginary part of the conductivity function and it falls down with growing frequency ($1/\omega$). The inter-band conductivity becomes dominant at high frequencies (infrared, optical) [68]. Its value is from the real part of the conductivity function. The transition point between intra and inter-band happens at frequencies from 10 to 100 THz [68]. According to [60], in a lowly doped graphene, no intraband transitions can take place.

Quasi-classical theory of conductivity and frequency mixing

It is possible to approach conductivity by Quasi-classical theory by modeling the conductivity using Boltzmann kinetic equation. This analysis shows, that at low frequencies the conductivity is imaginary, concerns intra-band contribution (as in classical view) and at high frequencies, quantum inter-band contribution dominates [68]. When the graphene is irradiated (or otherwise affected) by two electric waves with different frequencies and both waves are linearly polarized in the same direction, graphene induces second-order and third-order (produced by low-frequency Drude conductivity) harmonic current. In addition to this, graphene produces fre-

quency mixing effect with complex expression written in [68]. This model is valid for $\hbar\omega \ll |\mu|$, which corresponds to radio, microwave and terahertz range of frequencies [68]. According to quantum theory, where graphene is modeled by a Quantum kinetic equation (including Hamiltonian), the induced currents from two waves are at frequencies $\omega_1, \omega_2, 3\omega_1, 3\omega_2$, $(2\omega_1 \pm \omega_2)$ and $(2\omega_2 \pm \omega_1)$ [68]. These frequency mixing effects are based on non-linear modeling and the non-linear response at lower frequencies is much greater in graphene than in many other non-linear materials [68]. Graphene should also experience frequency multiplication effect. If graphene is exposed to an oscillating electric field, the induced current does not contain only the fundamental driving frequency, but also the odd harmonics (3ω, 5ω, 7ω, ..) The even order harmonics are not to be present because of central crystal symmetry. This should be true for infinite and uniform graphene layer [68].

Influence of wave vectors on graphene conductivity

Conduction in graphene is influenced by its wave vectors. These wave vectors are a result of confining the system by the geometry of the graphene sheet or ribbon. These wave vectors are called transverse modes or sub-bands. Bending introduces flexural modes into the graphene sheet and strain introduces optical and accoustic modes. Sub-bands that cross the Fermi level can carry current. Near the Dirac point, many of these allowed wave vectors end up gapped or pinned in energy, and so their influence on conduction is suppressed. There are three possible sheet configurations. Zig-zag, which is half-metallic, armchair, which is semiconducting [79] and chiral, where it depends on the chirality. The wave vectors determining conductance depend on the length of the ribbon. The transverse channels are dependent on the width and their total contribution to conductance of graphene ribbon scales as a diffusive metal [61]. The shot noise to current dependence of graphene is also that of a diffusive metal. Midgap states which are a result of graphene disorder can enhance conductance emerging from evanescent waves [61] By modifying graphene's geometry, band-gap can be engineered at the Dirac energy and this allows for tuning of graphene's conductance. Modeling of the electromagnetic wave propagation along a graphene nanoribbon can be done for a low-frequency regime where only intraband transitions of the π electrons with unchanged traverse quasi momentum are allowed. The transitions contribute to an axial conductivity along the ribbon and not to the transverse conductivity [67].

Quantum hall effect

Graphene is a material that experiences quantum hall effect. In graphene, this effect can be observed even at room temperature [42]. This effect takes place when a magnetic field goes perpendicular to the current flow. The current drifts sideways based

on the Lorentz force. The ratio between the current flow and the voltage in the drift direction is constant. The general quantized hall resistance is 25812.8 ohms, which is a result of $\frac{h}{2e^2}$. The Hall conductivity ratio in graphene is $\sigma_{xy} = -\left(\frac{2e^2}{h}\right)(2n+1)$ [80], which is the general ratio, with a half-integer shifted sequence of quantized values, reflecting graphene's Dirac-fermion-type dispersion.

Phonons in graphene

Phonons in the graphene sheet can create electon-hole pairs from the Fermi sea. If phonon energy (determined by its frequency) is larger than twice the chemical potential (μ), real electron-hole pairs are created from the filled state of an energy band of a carbon atom. This process "softens" the crystal lattice, which means that the phonon reduces its frequency and the phonons dampen by loosing their energy into the excitation. If the phonon energy (frequency) is smaller than twice the chemical potential (Fermi energy E_F), because electronic states near the Fermi level are already occupied (Pauli principle), electron-hole pairs are not created from the phonon. The phonons thus don't get screened as much and the lattice "hardens". Phonons then have a longer lifetime. Only virtual excitations can be generated here, which leads to polarization [61].

Surface plasmon-polaritons in graphene

When an electron with high velocity enters a material, a portion of its energy can convert to an electromagnetic field coupled with charge density oscillations. It is called a surface plasmon polariton (SPP) and it propagates along the conducting material from which it is excited and a dielectric medium [81]. In graphene, SPP are supported with extremely small mode volumes [82]. These SPP can be used for various light-matter interactions or broadband signal interconnection.

Screening effect in graphene

When an external electric field is applied to graphene, either by introducing a charge on the surface of by applying an external field, electrons from graphene are attracted or repelled the external field, which partially cancels the external field. This response to reduce the external electric field is called screening. Pristine graphene is a semimetal with a vanishing density of states at the Fermi level. Because of this the linear Thomas-Fermi screening length diverges and long-range coulomb interaction is not screened. The electron-electron is also not screened because of zero density of states at the Dirac point [61]. With increased doping the coulomb interaction is screened [61].

Defects in graphene

Due to covalent sigma bonds, it is very hard for external atoms to replace the carbon atoms in the graphene crystal [69]. However, disorders can be present in the graphene:

- Surface ripples (deformation in the direction of a perpendicular axis to the graphene plane)
- Topological defect (similar to grains)
- Structural defects (such as formation of n-tagons)
- Vacancies
- Embedded impurity atoms
- Cracks
- Edges
- Adsorbants (Van-der-Waals-force attached impurity atom or molecule)
- Thermal fluctuations

These disorders create localized charge imbalance that breaks the charge symmetry, increases scattering. Larger defects modify electron trajectories. Local density of states are affected close to the impurities. Point defects, similar to impurities and vacancies can create additional electron energy levels and this can affect conduction of current though the lattice, if the number of point defects is significant. Local charge density decays by $1/r^3$ and local electronic density decays monotonically by $1/r^2$ at large distances [61]. Some disorders change the angles between p_z orbitals and this changes the hopping energies between different sites. This leads to the need to remodel the Hamiltonian for the graphene configuration [61]. Such a change can happen when the graphene sheet is bent. Breaking the perfect electron-hole symmetry around the Dirac points may lead to localized self-doping [61]. Self-doping breaks graphene sheet charge neutrality also because of the zigzag edges of the graphene sheet. Energy bands are slightly shifted in these areas. If the Fermi level stayed at the original Dirac point energy, those bands would end up filled, which brings additional charge in and this breaks graphene sheet neutrality. Graphene sheet restores the charge neutrality across itself by globally shifting the Fermi level from the Dirac point. This virtually unfills some bands near the Dirac point and balances out the electrons near the edge of the graphene [61]. At the neutrality point, graphene remains metallic [42]. Standard area of the graphene unit cells can be disturbed by dilatation or contraction of the sheet. This disturbance changes local density of electrons, which changes local chemical potential around the disturbed graphene cells. Magnetic impurity (introduced by deposition or doping) changes Kondo resonance betweeen the magnetic impurities and the graphene's electrons. Adsorbing alcali metal atoms changes chemical potential of the graphene and adsorbing transition elements can lead to strong hybridization, which changes electronic propery

of graphene [61]. Doping the lattice with d-electron and f-electron atoms changes electron-electron interactions [61]. Ultra thin materials tend to be thermodynamically unstable and stabilization for example by a matching substrate lattice may be necessary. Decoupling, bending and stretching modes can stabilize these thin films as well [72]. When graphene is suspended on a microfabricated metallic scaffold, it has localized π electrons throughout the sheet. This leads to an assymetric distribution of carbon-carbon bond lengths and this forces the graphene to minimize the energy by rippling up to 1nm in height and during this process graphene becomes non-polar. These ripples in the suspended graphene are dynamic and are denser near the graphene edges [72]. Ripples and wrinkles of graphene are thus a common source of disorder. Some of these defects are totally unwanted for gas sensing applications and some (such dopants) are deliberately introduced to functionalize graphene surface and adjust its adsorption properties for gas sensing applications.

2.4 2D materials for chemical sensing

Extraordinary properties of graphene lead to the research of other 2D materials that might be usable for gas sensing. These chemical sensors may detect gas molecules, but solid particulate detection and even detection of bacteria or other biomolecular systems are in this category. More over, these sensors may have their transduction based in optics, electrochemistry, temperature or gravimetrics [13]. Chemical sensors based on 2D materials are primarily chemiresistive, which are in the category of electrically-transduced sensors. Other way of electrical transduction is piezoresistive [83]. This thesis is focused on electrical transduction method and gas sensing usecases. Sensing of the gas molecules can be usually done via adsorption, which is further categorized into chemisorption and physisorption. Chemisorption occurs when an analyte binds to the sensing surface and forms a chemical bond. Physisorption occurs when the analyte binds to the sensing material by Van-der-Waal's force or dipole interaction [7]. Chemisorption is a slower process than physisorption and it often requires more energy. According to first-principles density-functional theory, gases that experience chemisorption to graphene are CO, CO_2, O_2, H_2, and NH_3. Physisorption experience N_2, H_2O and H_2S [84]. This sensing process can be a funcion of conductivity, work function or electrical permitivity and can be transduced as a change in capacitance, resistance or inductance [13]. Magnitude, frequency and phase of the measured quantity can provide the insight into the sensing event. Materials that have been discovered and are relevant to chemical sensing include graphene, phosphorene (Figure 2.19), hexagonal boron nitride (h-BN), transition metal dichalcogenides (TMDs), layered metal oxides (MoO_3, SnO_2), 2D metal-organic frameworks and covalent organic frameworks. These materials

are used for an active (sensing) layer for an analyte and they are interfaced with electrodes that can be under the sensing material [85][86][85][23] or over the sensing material [87][88].

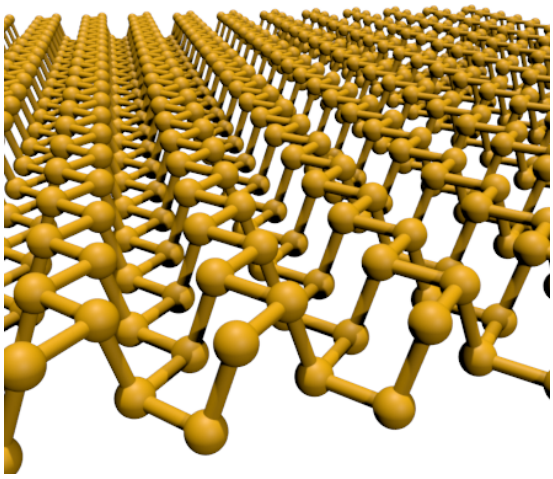

Fig. 2.19: 2D material - Phosphorene.

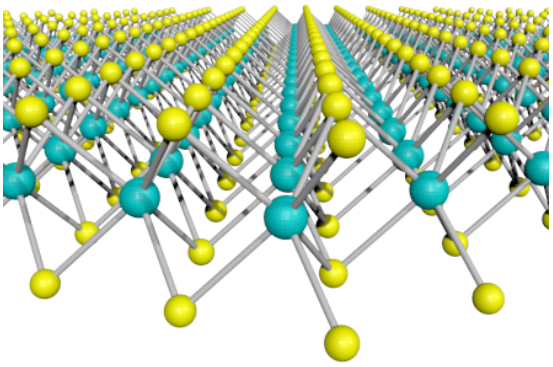

Fig. 2.20: 2D material - Molybdenum disulfide. The turquoise colored atom is molybdenum and yellow is sulphur.

2.4.1 General advantages of the 2D materials

The most common advantage for 2D materials in comparison to others is their large surface-to-volume ratio, which provides direct interaction with all or most of the atoms of the sensing material with the analyte. This infers, that the sensing material could detect most of the interactions of the sensor with the gas, which increases sensitivity. Another advantage is the ease of surface functionalization. The goal of electrically transducing sensing element is to easily receive the analyte of choice in a way that would change its electrical conductivity in most cases. The analyte must be able to easily bind with the sensing 2D element and for that, the sensing element must have binding sites available. Many 3D materials by themselves have binding sites for the analyte. Binding sites on graphene are visualized in Figure 2.21 It can be seen that the edges have electrostatic field around them and this field creates sites that the analyte can bind to. The surface of the graphene however, is not that reactive [89]. The binding sites depend on the hybridized nature of the atomic orbitals around the sheet. For example, graphene has π orbitals available per each carbon atom. Each phosphor atom of phosphorene can potentially function as an active site [13]. In cases where the surface itself does not provide an electrostatic configuration for binding the analyte, since the electrostatic configuration of the sensing layer depends on the orbital configuration of the atoms the sensing layer is made of,

there are ways to modify the atomic structure of the sensing material to allow for new binding sites. Graphene can be easily functionalized. Functionalization can be performed by introducing various defects in the lattice of the 2D material. Vacancy defects break the symmetry and atoms around the defect rehybridize. The new hybridization configuration may allow for better analyte binding. Surface oxidization introduces many new binding sites [90]. Process called decoration which introduces mainly metal particles onto the surface of 2D materials provides active binding sites. Performance of the sensing layer is mainly dictated by its band gap [13] between the valence and conduction band. Presence of a band gap decreases the initial conductance of the sensing element and improves the signal-to-noise ratio. This bandgap can be tuned using functionalization [79] and in graphene a bandgap is introduced by breaking its crystal symmetry. Many of the 2D materials have thickness-dependent bandgap. This is why the semiconducting tendency and a band gap that can be modulated are advantages of specifically 2D materials.

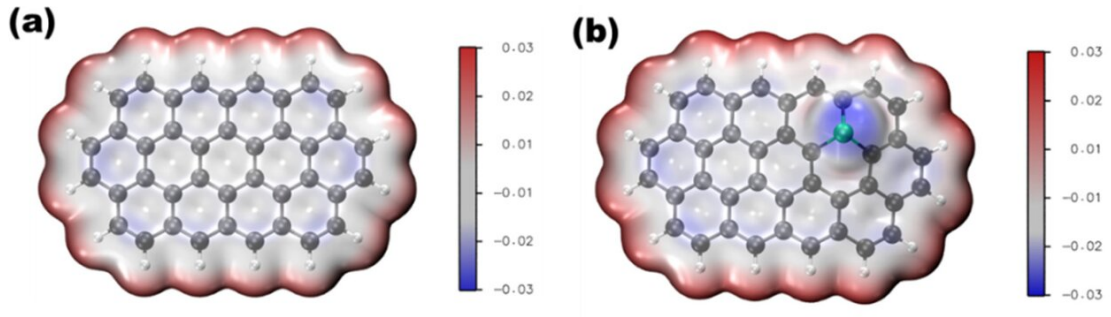

Fig. 2.21: (A) Electrostatic potential around pristine graphene terminated with unknown molecule. (B) Electrostatic potential of a pristine graphene with one phosphorus dopant. Negative electrostatic field creates a binding site for various analytes, primarily with molecule with positive electrostatic field. Figure adapted from [91]

Contacting the active layer

Generally, a sensing material of an electrically transducing sensor is not directly integrated into the evaluating circuitry and is rather provided as a standalone block. Usually, the sensing layer is interfaced via electrodes, which are in most cases from a different material, like gold or platinum. Flexible sensors (not necessarily based on 2D sensing material), can have other electrodes, such as silver pads with reduced graphene-oxide [92]. The problem when interfacing two different materials is the broken crystal symmetry at the interface. Namely, each metal has its work function, which denotes a minimum energy required to remove an electron from the surface of the metal to a point in vacuum just outside the metal. When two materials with different work function are connected together, the electrons tend to flow from

the metal with lower work function to the one with higher work function. This creates a voltage at the metal junction. When a metal and a semiconductor are in contact, their difference in work function creates a barrier, which lowers the transport of charge carriers between the materials, because not all of the carriers have enough energy to jump up the barrier when going in the direction of the barrier [13]. Semiconductor side of the junction can be doped by impurity dopants or by an electric field perpendicular to the graphene sheet [93]. This doping modulates the Schottky barrier [13]. A bias voltage applied to the can bend the barrier lower from the semiconductor side, but the barrier from the metal side does not change and this forms the Schottky barrier, which conducts the charges for one bias polarity, but not the other [13]. Even analyte adsorption can modify the Fermi level of the semiconductor and alter the work function, which leads to the modulation of the barrier height. Electron donor and acceptor modulates the barrier in the opposite direction [13]. This effect is mainly present in semiconductors such as $MosS_2$ and the a sensor can be built on this principle and it is called a junction-controlled device [13]. Electrode and sensing material interface's primary function can be a simple ohmic contact. This junction has a negligible modulation of the Schottky barrier and the effect on the conductance is neglected. When graphene is used as a sensing layer, its interfacing type is ohmic contact. When graphene is transferred onto pre-patterned electrodes, the Cu electrodes contact resistance can have a range 1.25 $\pm$ 1.54 KΩ. Resistance of Au electrodes can have resistance of 30 $\pm$ 10 Ω [94]. The electrodes have significant resistance in the spectral domain and are a contributing factor to flicker noise [95]. For graphene, the electrodes themselves, according to density functional theory act as a dopant. The metal electrodes that weakly bond onto the graphene, like gold, copper, platinum or aluminum can raise the Fermi level of graphene by up to 0.5 eV and they preserve the graphene band structure [96]. High-work function metals relative to the work function of graphene (~4.5 eV) [96] like silver or titanium pull electrons from graphene, thereby P-doping it and low-work function metals like silver and titanium push electrons into graphene, thereby N-doping it [94].

2.4.2 Phosphorene (black phosphorus)

Black phosphorus is made up of P_4 atoms that forms sp^3 bonds with bond angles 96.34°and 103.09°[97]. This material is similar to graphene, because from a top view, the atoms are arranged in a hexagonal lattice. It is produced by mechanical or liquid exfoliation under high pressure. Phosphorene is the most stable allotrope of phosphorus [97]. Monolayer of phosphorene exhibits a direct band gap of up to ~2.0 eV. The bandgap of phosphorene depends on the thickness of the stack where

phosporene layers are placed on top of another. By stacking the sheets of phosphorene on top of one another, direct bandgap can be modulated from 1.51 eV to 0.59 eV [13]. The thicker the stack, the more redshifted the trasmitted light is. Carrier mobility inside phosphorene increases smoothly with an increasing number of layers up to a thickness of 10nm, exceeding $1000 cm^2 V^{-1s-1}$ [97], which is comparable to graphene. Phosphorene works as a sensing layer because gas molecules get physisorbed on the surface using van-der-Waals forces, which changes phosphorene electronic properties [35]. Because phosphorene has a puckered surface, many adsorption sites are available on its surface. An NO_2 sensor based on few-layer phosphorene FET was created with surprisingly high sensitivity (Figure 2.22). This sensitivity was attributed to the fact that phosphorene's out-of-plane conductance is lower than the in-plane conductance. Also, high adsorption energies of NO_2 to phosphorene may increse sensor's sensitivity [25]. A nanoribbon of phosphorene can be functionalized by the following groups: H, F, Cl, OH, O, S and Se [13]. Biggest challenge of practical phosphorene application is its tendency to form phosphoric acid spieces in the presence of moisture. To overcome this issue, the phosphorene surface must be coated or decorated to prevent chemical degradation in ambient conditions [13].

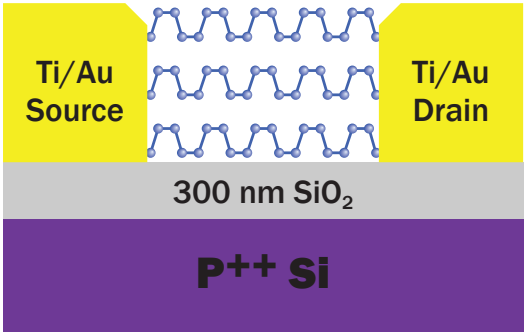

Fig. 2.22: Conceptual material composition of a phosphorene sensor. This is a field effect device with heavily doped silicon as a gate. Phosphorene layers are stacked on top of another and are interfaced with an electrode. Figure adapted from [25]

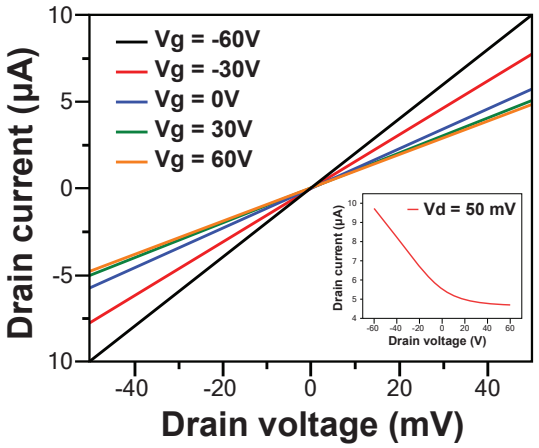

Fig. 2.23: Relationship between a drain current and voltage at various gate voltages. Linear relationship means the electrodes are of an ohmic contact type. Inset figure shows a change of drain current constant drain voltage and changing gate voltage. Figure adapted from [25]

2.4.3 Transition Metal Dichalcogenides

This is a whole family of 3D materials. TMDCs are composed of a hexavalent transition metal ion and a divalent chalcogen (Sulfur, Selenium, Tellurium). Commonly researched materials that fit into this category are HfS_2 (insulator), MoS_2, WS_2, ReS_2, $ReSe_2$ (semiconductors), WTe_2, $TiSe_2$, $PtSe_2$ (semimetals), NbS_2, TaS_2. The most popular of them is MoS_2, visualized in Figure 2.20. They can be synthesized both by mechanical or liquid-phase exfoliation, which is a top-down approach, or by chemical vapor deposition (CVD), a bottom-up method. Exfoliation provides higher purity samples than CVD [98]. This family of materials is a competitor to graphene because materials in TMDC category has intrinsic direct bandgap. Monolayer of MoS_2 is a direct bandgap semiconductor [98], however it has much lower charge carrier mobility compared to graphene. Intrinsic structural defects may be the cause, because electron hopping happens in defect-induced localized states [98]. Sulfur vacancies in MoS_2 introduce localiyed donor states inside the bandgap. Nearest-neighbor electron hopping happens utilizing these donor states, especially at high temperatures. In pristine MoS_2, the electron density is periodic in space and transport is band-like [99], but in defective MoS_2 the electrons are localized near the defects and the transport happens through hopping [99]. Figure 2.25 visualizes this effect.

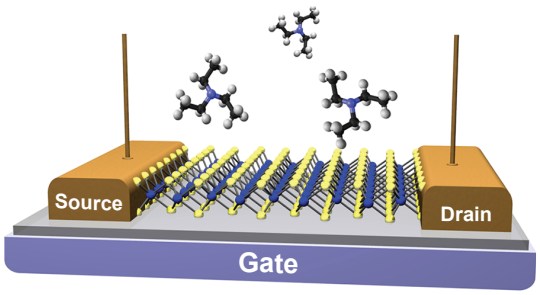

Fig. 2.24: A conceptual view of a single-layer MoS_2 sensor. Figure adapted from [98]

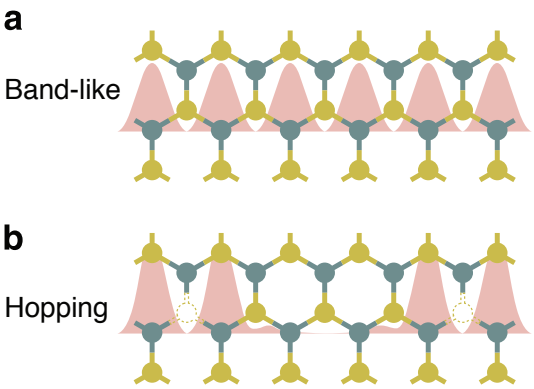

Fig. 2.25: Visualized electron transport in perfect **a** and defective **b** MoS_2 lattice. Figure adapted from [99]

As a sensing layer for gas detection, TMDCs can exploit Schottky barrier modulation effect, for example by adsorption of NO_2 and HN_3 gases to the active layer, that is interfaced with Ti/Au electrodes. NO_2 increases the barrier and thus the contact resistance and NH_3 decreases it. Schottky barrier modulation can be used to

increase sensor sensitivity to compatible analytes [35]. Gas sensors with structures from TMDC category have been experimentally made to sense NO_2, NH_3, H_2O, TEA, Acetone, Toluene, CH4 and some others. Response time tends to be about 30s, but recovery time of some sensors is of more than 10 minutes [35]. Single-layer MoS_2 behaves differently than multilayer stack. In an experiment, single layer showed a fast but unstable response and multilayer (2-4 layers of) nanosheets showed much better performance [100]. MoS_2 sheets can be also aligned vertically between the electrodes to increase an exposure of the environment to the edges of the sensing layer, which is more reactive than the flat periodic surface. When the whole surface is composed of the edges of the vertically stacked sheets, with a 15nm width the response can be 5 times greater than that of a 1nm thick film for NO_2 detection. The NO_2 molecules have a high adsorption energy and this sensor has still long recovery time when N_2 purging [101]. The surface of dichalcogenides can also be functionalized with compatible elements including Ag, Pd, Pt, Sc, Y and Au [35] , which dopes the sensing layer, modifies the response of the active layer and thus favors adsorption to some analytes.

2.4.4 Graphene 2D materials for gas sensing

Electrochemical sensors based on graphene have been investigated probably the most so far, because they provide direct electrical response to the sensing events and they have low resistivity and electrical noise [13]. Ambipolar character of graphene is viable for sensing both electron withdrawing and donating groups of analytes. Zero rest mass (Dirac fermions) property of graphene may also be useful in gas sensing [90]. Electrical noise of graphene can be pushed to the thermal noise limit and thanks to this, the limit of gas detection can be very low [35]. Because of the metallic conductivity of graphene, it has low Johnson noise (noise due to thermal agitation of charge carriers [102]) and it exhibits low levels of 1/f noise due to its high crystallinity [13]. Graphene is a very versatile framework for gas sensing. It can be contacted by vertical carbon nanotubes [103], can be used as electrodes for other sensor architectures [24], it can be doped by nitrogen (n-doping, shifting fermi energy upwards, adding electrons) or boron (p-doping, shifting fermi energy downwards, adding holes), it can be covalently bonded by aryl groups, alkyl chains, organic azides, various aromatic molecules via $\pi - \pi$ stacking, it can be decorated by metal atoms (Au, Ag, Pt, Pd, Rh), graphene oxides can be attached to graphene (SnO_2, Mn_3O_4, Co_3O_4, TiO_2, ZnO_2, ..), quantum dots can be attached to it (CdSe, CdTe, PbS, ..), functional polymers and DNA, proteins, enzymes, peptides and so on can be be wrapped around or adsorbed to graphene [104]. Here, the three main derivatives of graphene for gas sensing are introduced:

Pristine graphene

This is the most elementary and clean form of graphene. It is a hexagonal pure-carbon structure without any defects. Pristine graphene can be produced by solution-phase exfoliation from graphite, chemical vapor deposition, organic synthesis-based methods, epitaxial growth and by micromechanical cleaving (famous Scotch tape method), which produces highest-quality graphene [13]. Pristine graphene experiences zero band-gap at its Dirac points [42]. The conductance in undoped pristine graphene is expected to be at the minimum [36]. Its surface is chemically stable [105] (or inert [23]) and its sensitivity to many gases is lower than the sensitivity of a functionalized graphene. Chemical reactivity is higher at the graphene edges than on the surface [104][89]. Investigated gas molecules (CO, NO, NO_2, NH_3) adsorption on pristinge graphene show low adsorption energies and little charge transfer [106]. SO_2 and H_2S adsorb weakly on pristine graphene surface as well [13]. This may be concluded as unmodified graphene being a non-ideal material for gas sensing [106] or as graphene being easily recoverable by easy analyte desorption [36] and with rapid response [13]. Pristine graphene can detect even one molecule [20], but only under specific conditions. Measurements using Hall effect can provide the strongest response to a change in carrier charge carrier density near the dirac point [36]. Pristine graphene should be able to detect an analyte at concentration as low as 158 parts-per-quadrillion (ppq) [107]. Due to low adsorption energy of a particular molecule onto graphene, such as H_2, the detection remains challenging even at high analyte concentration. Pristine graphene tends to have a resistance of about $3k\Omega/\square$ and thermal annealing can shift the Dirac point down to 54V and heavily p-dope the graphene, which greatly degrades graphene mobility [23]. Pristine graphene may produce a signal reversing effect during gas measurement. Epitaxially grown graphene was n-doped by the SiC substrate. At low NO_2 concentrations the graphene conductance decreased after gas adsorption. At high NO_2 concentrations however, the graphene conductance increased. Authors attribute this effect to dynamic N-P type shift of the material during sensing NO_2 [108].

Graphene oxide

The main modification a surface of graphene can have is its oxidation. When pristine graphene is exposed to a strong oxidizing agent (highly acidic environment [13]), an oxide layer is formed on top. This produces graphene oxide, which is a graphene sheet with many oxygen-containig functional groups [13]. These groups are for example epoxide, carboxyl, hydroxyl, carbonyl,.. groups and they are mostly present on edges and basal planes of an oxydized graphene [109]. Usually, graphene oxide is a product of graphene synthesis, rather than modification of a pristine graphene.

Hummer's method is used to make graphite-oxide. When graphite is oxidized and put into water, graphene oxide layers exfoliate into the water because of negatively charged oxygen that are on the basal plane and edges. Graphene oxide is studied in the field of gas sensing because of its ease of functionalization, especially by positively charged molecules [35]. This material is however an insulator (or less-conductive than pristine graphene [35], or it shows high resistivity [110]), because graphene oxide is bound with the original sp^3 C-C bonds too many times. To increase the conductivity of graphene, some oxygen is stripped away from graphene surface through a reduction process. The ratio of carbon to oxygen molecules on the surface of the sheet can range from 1.98:1 to 2.5:1 with sources [111] and [112] respectively. Graphene oxide is made also to break the zero band-gap property of the pristine graphene, which tends to have a negative effect on gas sensing applications [110].

Reduced graphene oxide

It is difficult to fabricate gas sensors based on pristine graphene with high sensitivity. There are even some research inconsistencies on the making and properties of pristine graphene sensors, which lead to research of another framework for gas sensing - reduced graphene oxide [113]. Graphene oxide (GO) can be reduced by various reduction methods [109] including an exposure of graphene oxide to hydrazine vapors, or to hydrogen plasma [105]. Sluggish and irreversible recovery in sensors based on reduced graphene oxide are a problem because polycrystalline and cracked structure of rGO reduces graphene conductivity [114]. Some graphene oxide (multilayer) flakes can have a resistance on the order of $10^9\Omega/\square$ and can be reduced by thermal annealing (further reduction) to an order of $40k\Omega/\square$. Thin films made of solvent exfoliated graphene have resistance of about $6k\Omega/\square$ and can be reduced by chemical doping to $50\Omega/\square$ [105]. Reduction of graphene oxide affects both the sensitivity and the level of 1/f noise. The more the layer is reduced, the lower the 1/f noise [28]. Oxygen functional groups act as high-energy binding sites and the reduced pristine portions of graphene surface allows for low-energy binding sites. Fast gas response is when the analyte uses low-energy site and slow response is when the analyte uses high-energy site [90]. Reduced graphene oxide can be used as a base platform for many sensor varieties. It can be decorated with polymers, metal particles, or other structures, as it graphene oxide and pristine graphene counterparts. The advantage of rGO is that it can be functionalized with relative ease [36]. PPy, PANI and PPD are popular polymers used with rGO and they have been used to detect mainly NH_3 and NO_2 [90] Proportion between carbon and oxygen can vary from 3:1 to 10:1 [28] based on the exposure time to a reducing agent.

3 Sensor characterization

Goals of this thesis include:

- Describe the mechanism of sensoring
- Study mechanism of operation of graphene-based sensors
- Measure their electrical characteristics
- Study changes in resistance of the sensing layer in the presence of various liquids and gases
- Study noise signals during the presence of various liquids and gases
- Analyze effects of sensor geometry and propose possible optimization
- Propose definitions of conditions for sensor reliability testing

Goal 1 is covered in chapter "State of The Art", Physical background of point 2 is covered in section "Advances in graphene research" and theory is covered in chapter "Gas sensor measurement". This theory is composed from multiple research papers, reviews and online published articles. It is written to span the field of gas sensing well, including new technologies, methods of sensing and findings. To fulfill points 3 through 7, it is necessary to study the graphene reaction to various chemical environments. Sample array of graphene sensors has been obtained from Graphenea company.

3.1 Visual analysis

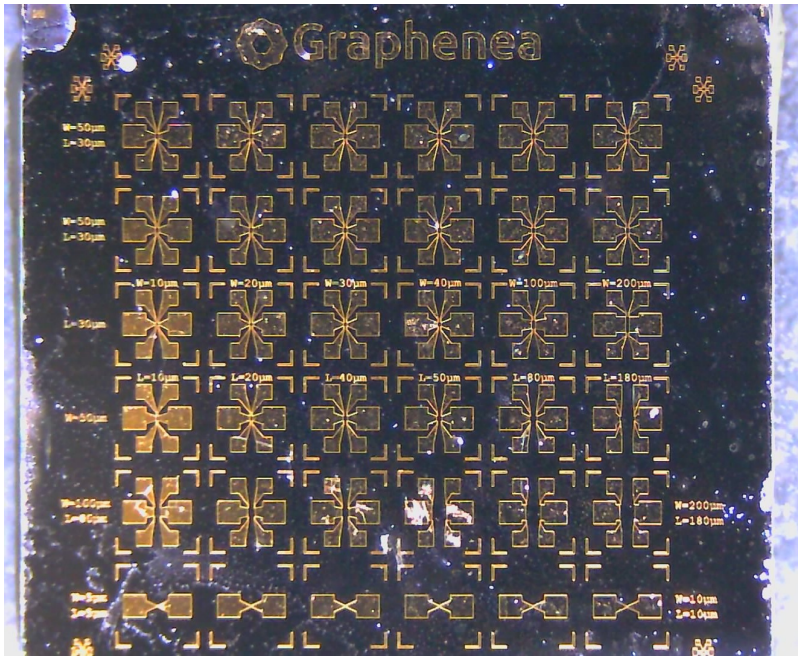

Fig. 3.1: A photo of the graphene sensor array used for experiments in this thesis.

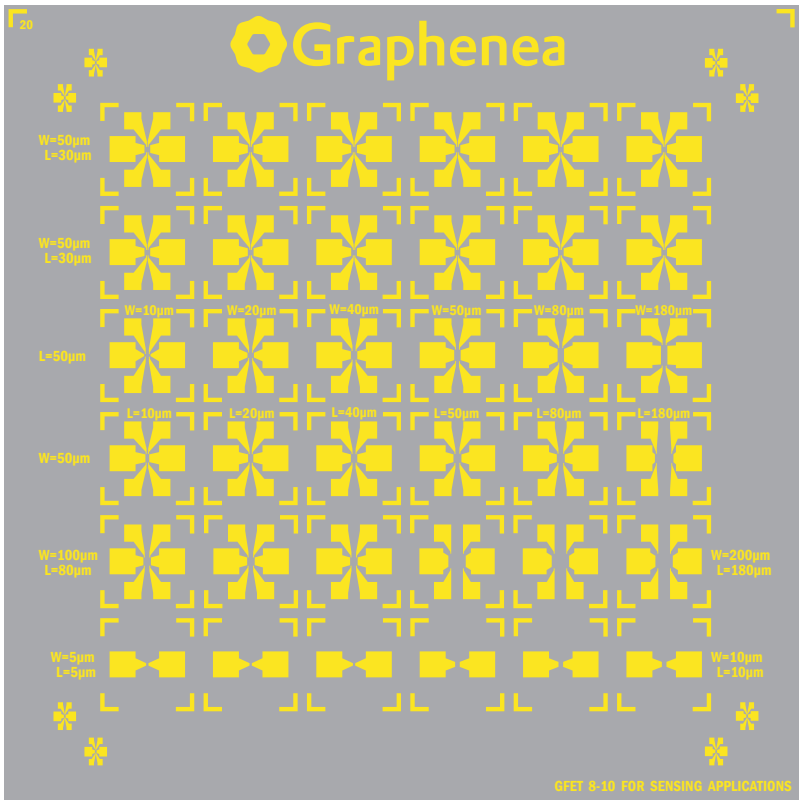

Fig. 3.2: Recreated vector form of the sensor array. Yellow color is gold and gray is a silicon oxide.

The die is pictured in Figure 3.1 and its vector reconstruction is in Figure 3.2. It appears, that the die was first sliced with a saw to about 2/3 of the depth and then it was broken off.

Many of these sensors are contacted using Hall-Bar geometry. Use of this geometry allows for contact resistance elimination. Constant current is injected on two terminals and voltage is sensed on the other two. Carrier density can also be detected using this geometry. Options for measurement on these samples are shown in Figure 3.5. The bottom surface is heavily doped silicon which acts as a gate for the graphene sheets, effectively creating a field-effect transistor structure. The gate is visualized in green color in Figure 3.3. This gate can be used for electrical graphene doping (shifting the Fermi level of graphene away from the neutrality point). This effect directly affects graphene conductance.

Graphenea datasheet for our graphene samples shows the following parameters expected:

- Field-Effect mobility: >1000cm^2/V·s
- Residual charge carrier density: <2 x 10^{12} cm^{-2}
- Dirac point: 10-40V
- Yield: >75%

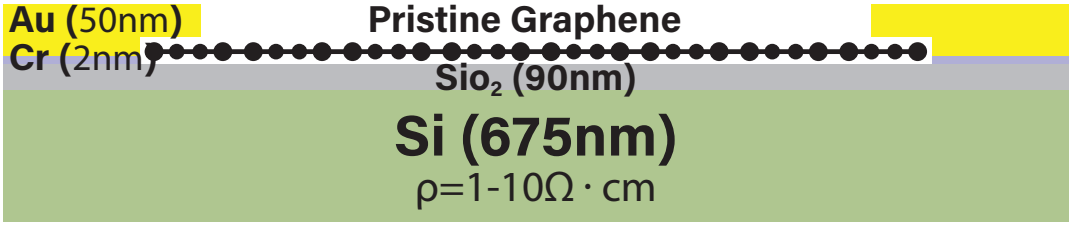

Fig. 3.3: Thickness of various layers in the tested Graphenea samples.

- Maximum Gate-Source voltage: 50V
- Maximum operating temperature: 150°C
- Maximum Drain-Source current density: 10^7 A/cm^2

Manufacturer recommends not to sonicate the chip and not to expose graphene surface to strongly oxidizing agents. Graphene was grown on a base lattice using chemical vapor deposition and was transferred using a ploymer. Graphene has been patterned using photolitography. A layer of chromium and gold is deposited onto the silicon oxide and graphene to make contacts.

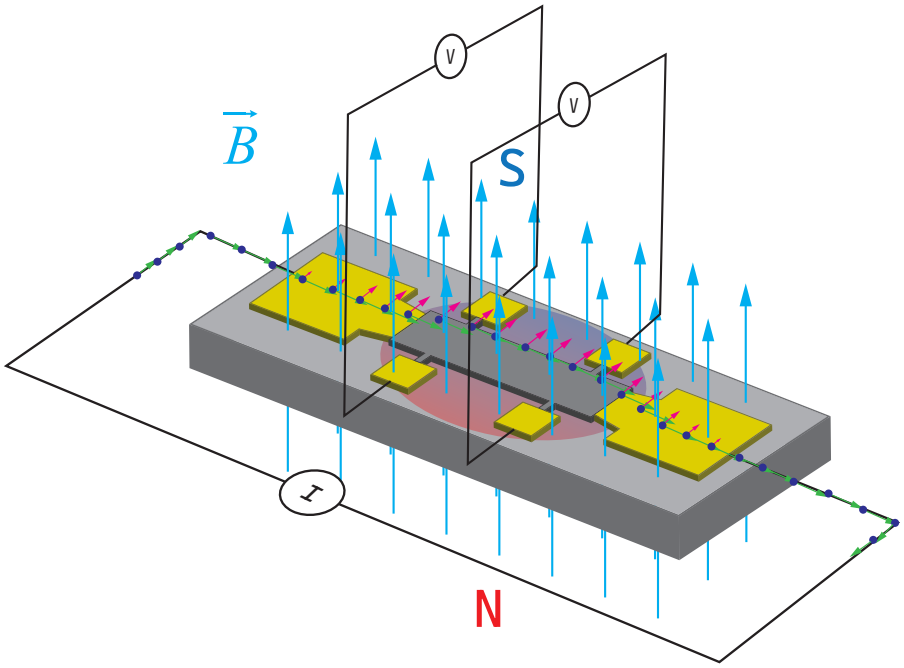

Fig. 3.4: Working principle of the hall-bar sensor. Due to the Lorentz force, the electrons as charged particles are pushed to one side of the geometry, based on the orientation of the external field. This electron concentration difference can be measured as voltage.

3.2 Gas sensing using sample sensors

Graphene sensors obtained operate on a chemiresistive principle in current domain and on a voltage-change principle in the spectral domain. This means, that as gas adsorbs on the surface, the cause and effect can be traced from the adsorption of the molecule onto the surface, to the change of conductance between the points of measurement. If many gas molecules adsorb onto the graphene surface, if graphene is measured under right conditions, cause of the adsorption process is possible to be traced to the voltage changing at various frequencies, which may also be traced from the spectral measurement down to the gas that was adsorbed. The whole art of designing a proper gas sensor is to understand the physical model as much as possible and from this understanding one should be able to design such a sensor, which minimizes the influence of unwanted effects onto the measured quantity and maximizes the desired effect. The measured quantities in this case are the two mentioned - change of conductance and change of voltage in the spectral domain. The fact is, that from the current understanding of physical model of reality, focused on graphene sensors, there are many causes and effects that affect these measured quantities. Great care has been put into finding as many effects as possible and these effects are shown in Figure 3.6.

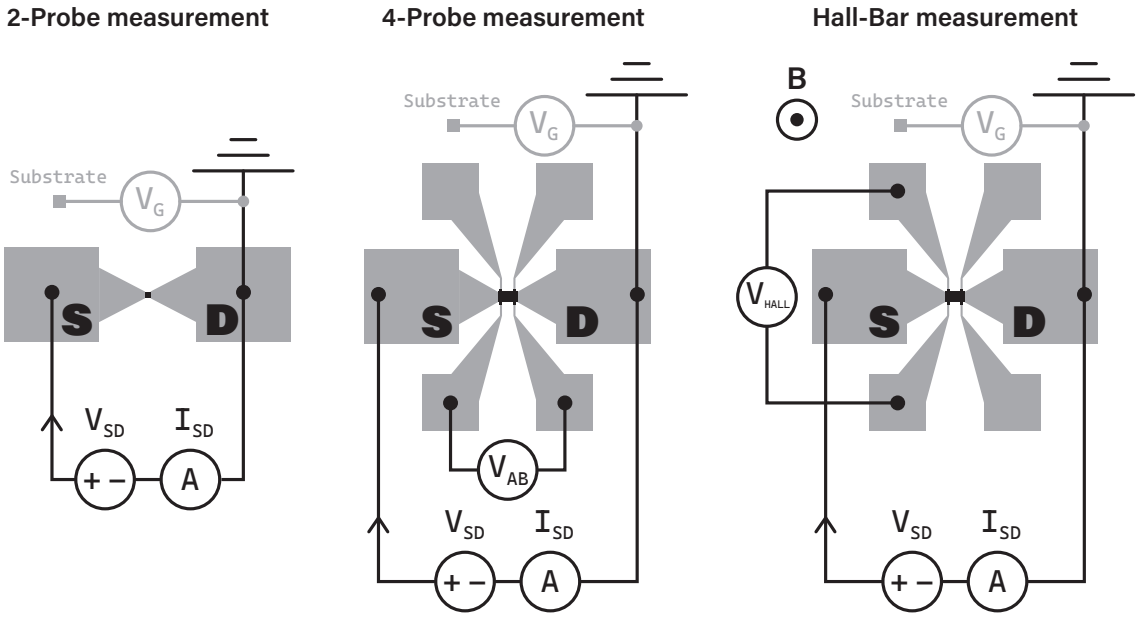

Fig. 3.5: Samples used in this thesis can be measured using various methods. Gate connection is optional and it will influence the measurement.

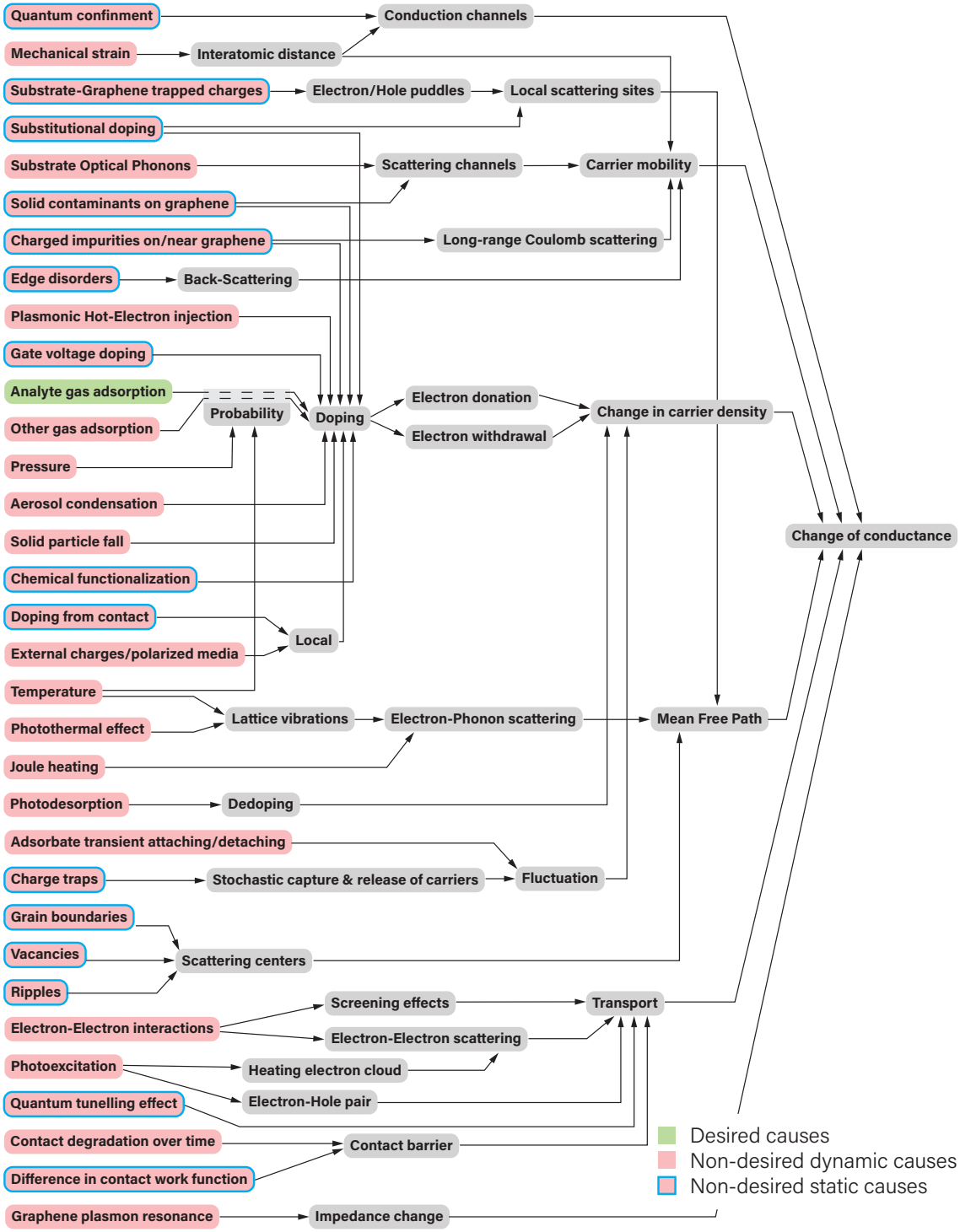

Fig. 3.6: Based on our current understanding of physics and the ability to model real world, this is an exhaustive, but not complete and not fully correct list of physical phenomena that influences the desired measured quantity. All other causes must be minimized, or at least understood, to be isolated. Fortunately, some of these undesired causes have a very small influence to the measured quantity. Causes with a blue border have fixed type of effect on the measured quantity and causes without a border change based on some other input to the system.

Ideal measurement setup

To properly address this complex system, a proper testing apparatus must be created in order to isolate the undesired effects and quantities and focus on the research of the desired ones. Here, a rather ideal testing apparatus is proposed to use the full potential of the graphene samples. The apparatus is visualized in Figure 3.7 and it should be able to allow the detection of single molecules on the graphene surface.

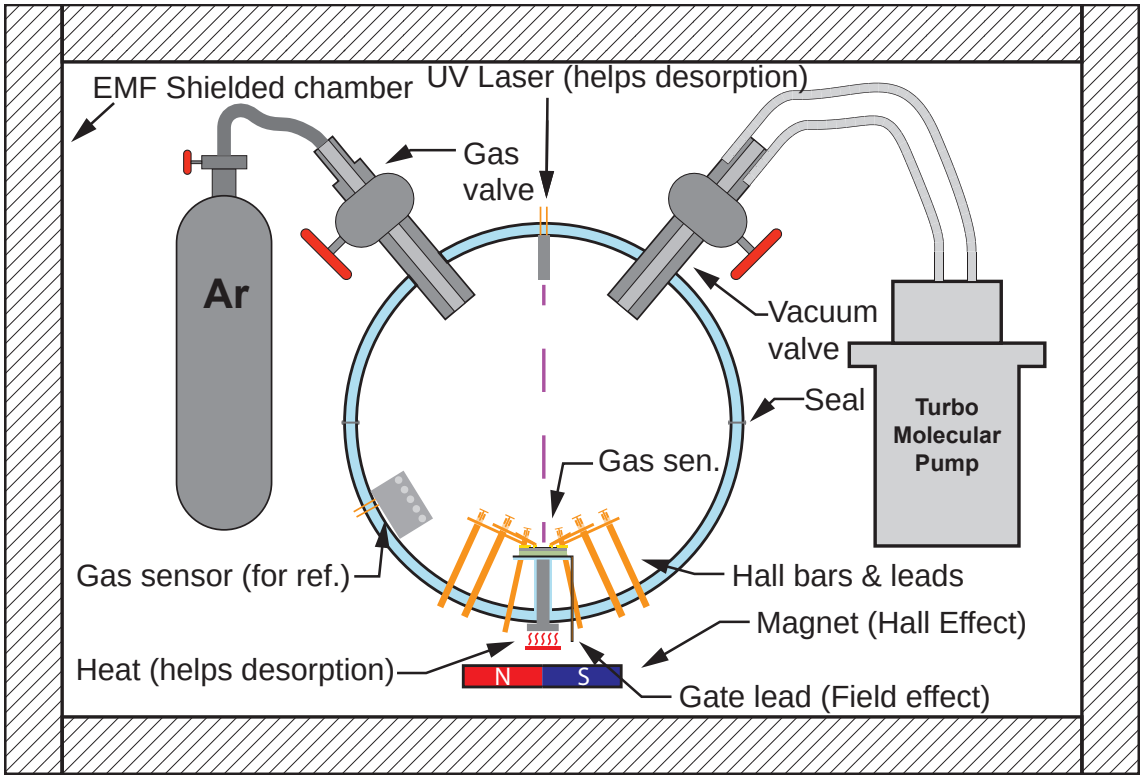

Fig. 3.7: This apparatus would provide good ability to test various graphene sensors. It supports portability, injection of various gases, vacuum, laser-aided desorption, 2, 4 or 6-probes measurement, hall effect and other advantages.

Actual setup

The proposed theoretical setup, although realizable, was not created for time and financial reasons. Instead, a more simple configuration was designed for the sensor testing, consisting of:

- *Witec Alpha 300R*: For raman surface characterization. It is useful to see if the graphene is intact or damaged and it provides an insight into the atomic composition of the surface. It is a non-destructive method of measurement.
- *TESCAN LYRA3 FIB-SEM*: Scanning electron microscope to see the microstructure of the sensor surface and to see possible defects on the sample.
- *Signal Recovery model 5184*: A 1000x gain (60dB) 0.5Hz to 1MHz ultra-low noise preamplifier used to amplify the noise from the sensor.

- *PA15 preamplifier*: $<2/nV/\sqrt{Hz}$ preamplifier, 3Hz to 1MHz with 100x gain (40dB) to amplify the noise from the sensor.
- *Agilent 35670A*: Dynamic signal analyzer is used to detect and measure the noise in spectral domain
- *Ramsey STE3300*: A microwave shielded chamber with $\geq$ 100db shielding from 20MHz to 1GHz waves and with decreasing shielding as the frequency goes up. This chamber encoses the tested samples for isolation of external radiation that would influence the measurement.
- *Agilent U1252A*: Handheld voltampermeter for quick measurement of batteries and resistors used in the measurements.

These instruments allow for an acceptable scientific measurement of volt-ampere characteristics and noise spectrum. The equipment shown above was combined in several ways to make testing rigs for various measurements. They are all mentioned below the sample preparation section.

3.3 Sample preparation and checking

Arguably the most important step in measurement is proper sample preparation, because when the samples are damaged during this step, all the measurements are spoiled. Also, it is good to know good practice of samples preparation, before starting to work on the sensors obtained, as experimentation decreases the yield and these sensors are not cheap. This is why this section provides documented procedures and discussion of sample preparation. As mentioned beforehand, Graphenea sensor array was obtained. These sensors have small contact pads that are suitable for direct micrometer probe connection, but for practical reasons of further measurements, it is desired when the volume of the whole sensor with its electrical leads is less than $1dm^3$. For this purpose, the sensors were cut. The machine used for cutting was *Laser dicer Oxford Lasers A-Series*. Because laser cutting creates a lot of tiny shards-like partices, the sensor array is coated with a protective polymer. Then the machine can start cutting. This machine was able to cut the section of these sensors, but from the subsequent electron microscopy it was concluded that the heat produced from the slicing process damaged the polymer and thus the sensor. This process in not desirable, however it proved that the sensing surface was still operational. Figures 3.8a and 3.8b show the sensor after laser dicing.

It is very possibly the protective polymer that got burnt on the sides of the sensor. This polymer also cracked at various places on the surface, as seen in Figure 3.8b. At the time of scanning using the microscope, the polymer was not removed and to penetrate the top polymer layer, voltage of the electron beam had to be risen to 20kV. Figure 3.9 shows the sensor under an optical microscope. The glossy

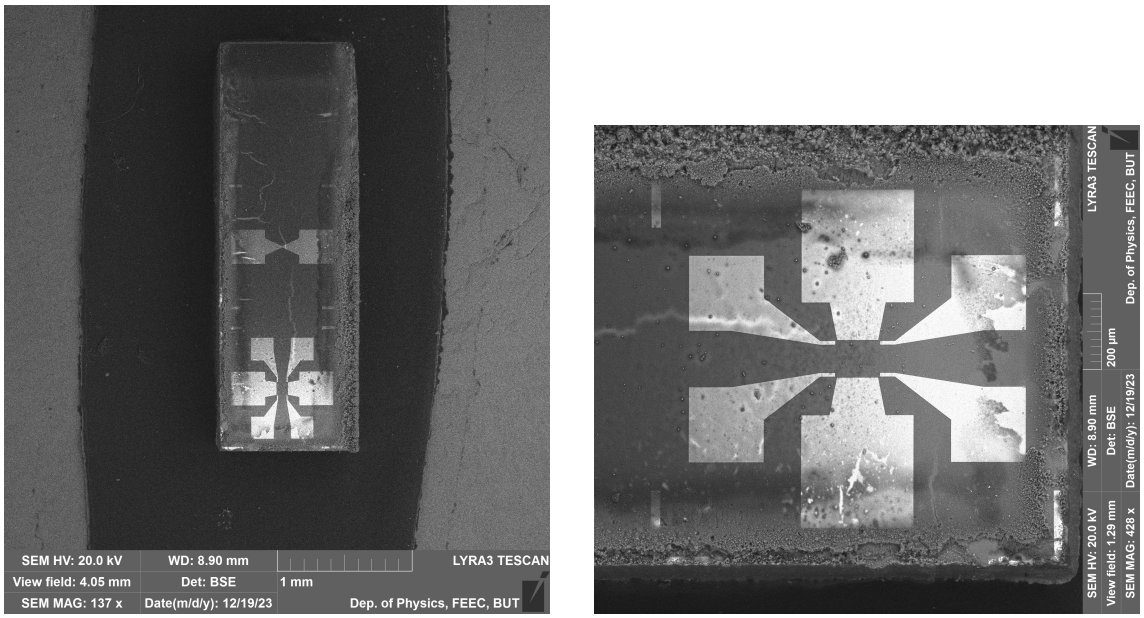

(a) Top view under SEM

(b) Pattern of the more complex sensor

Fig. 3.8: Both sensors under an electron microscope. The surface is not so visible because there are burn marks and contamination.

polymer is visible on the whole surface. This polymer was exposed to sonication process at the temperature of 60°C under acetone and isopropylalcohol. It couldn't be cleaned using these chemicals. A physical method of cleaning was therefore tested. The sample was submerged into an ethanol solution and it was scratched by an iron tool. This very effectively released all the coating under a weak pushing force. Flakes of polymer were then removed by flushing them with ethanol and this process left a nice surface. The graphene area was avoided to prevent damage. Wood is a better alternative to iron and it removed the sediment only by directly pushing into it. This method is more gentle to the golden layer. Cleaned sensor is photographed in Figure 3.10. It was later discovered that this process may still have destroyed the graphene layer, as this particular sensor after bonding was showing open circuit. Analysis of this coating is still a task, as well as its proper dissolving to achieve a clean surface without affecting the graphene portion. This problem is not addressed in this thesis anymore.

Several sensors were diced in this way and for their proper handling, a custom PCB design was made. This PCB was designed to contain minimal amount of small surface-area inter-metallic connections. The PCB making process is shown in Figure 3.11. The sensor was then glued by a metallic paste, which hardens at 110°C. Sensor was then bonded by *HB16 - Semi automatic wire bonder*. Recipe: Bond1 - US 340, Time 230ms, Force 350mN; Bond2 - US 440, Time 320ms, Force 430mN. Bond 1 is

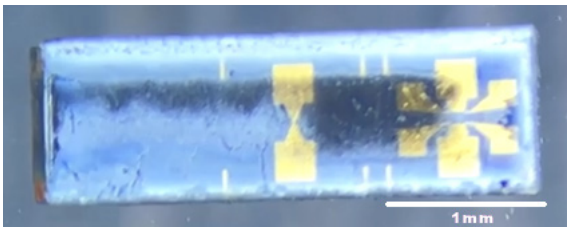

Fig. 3.9: Two distinct graphene sensors with a layer of contamination.

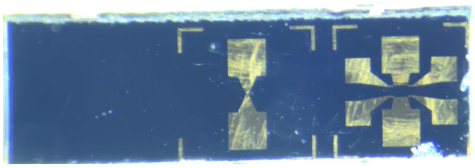

Fig. 3.10: Sensors with removed contamination.

on the chip pad and bond 2 is on the PCB. The bonded sensor is shown in Figure 3.12 and the finished sensor ready for measurement is in Figure 3.13. This sensor PCB allows for easy probe connection and disconnection using U.FL connectors.

Fig. 3.11: Process of creating a custom PCB for sensor handling. First a photosensitive layer was laminated onto a one-layer PCB. An image of the design was exposed and developed.

This way a sensor was prepared and as it has been noted before, this sensor piece got damaged. There were several other sensors prepared by a less sophisticated method. Pieces diced by the laser were glued onto a ceramic silver-plated base and they were bonded by a silver wire (Fig. 3.14 a, b). The whole graphene sensor array was glued onto the PCB and was bonded to the available contacts (Fig. 3.14 c). Information about these sensors are shown in Table 3.1. Both the sensor array and

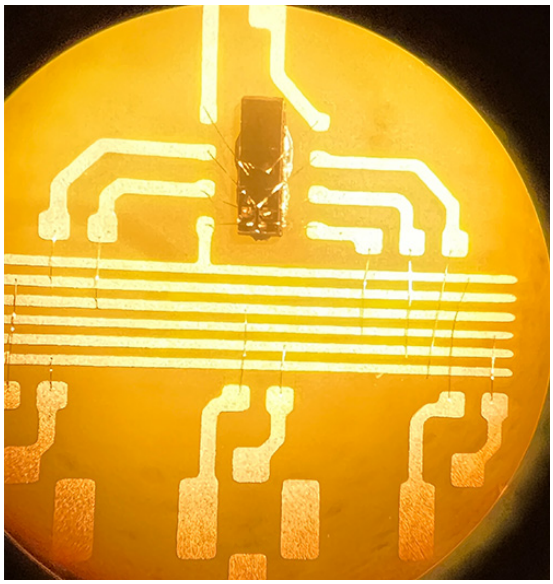

Fig. 3.12: Bonded sensor

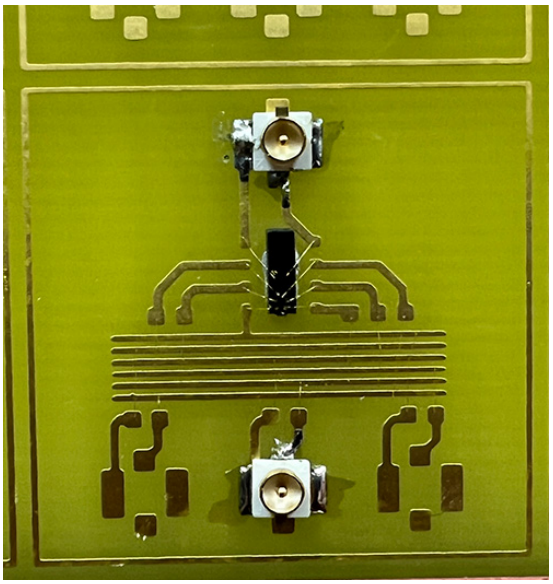

Fig. 3.13: Sensor ready for measurement

the diced pieces were operational and the test results on these pieces are provided below in the experimental section.

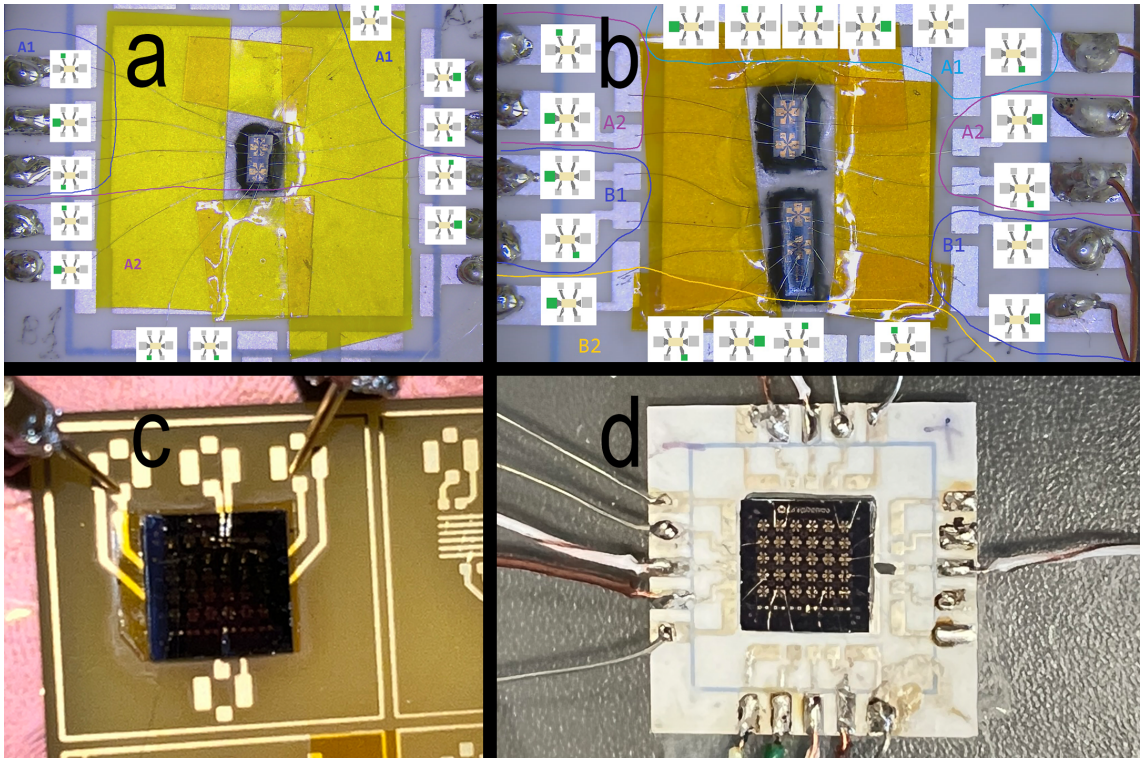

Fig. 3.14: All the sensors used in testing. Top sensor in a) is S5, bottom is S6. Sensors in image b) are listed from top to bottom as S1, S2, S3, S4. Sensor in c) is VID and the sensor in d) is HR.

Sen. num. in thesis	Internal naming	Has polymer	Graphene W	Graphene L
S1	#1A1	YES	50	40
S2	#1A2	YES	40	50
S3	#1B1	YES	50	30
S4	#1B2	YES	50	30
S5	#2A1	YES	50	80
S6	#2A2	YES	100	30
S7	VID	NO	50	30
S8	HR	NO	50	30

Table 3.1: Information about sensors used in testing. First column indicates the naming used in this thesis in the experimental section. Internal naming is listed for the author's reference.

3.4 Experimental section

In this section, all the procedures, experiments performed and conclusions are listed. Various sensors were used in these tests and several parameters were analyzed. This is why each measurement kind is placed in its own section. All the measurements were performed at room temperature, shaded or no light, relative humidity of about 67%, 0T of magnetic field and under no gate voltage.

3.4.1 Raman spectroscopy

To see the quality of the graphene samples, several samples were analyzed under Raman scattering. Raman spectroscope fires a laser at every point of a 2D plane and a CCD sensor captures the scattered light. This scattered light is shifted from the original wavelength. A sample in Figure 3.13 was tested for graphene defects under raman spectroscopy and the results are shown in Figures 3.15 and 3.16.

Peaks for carbon were found at delta 1593 and 2681.93.
Peaks for silicon were found at 526.0 and 974.7.

Conclusion
From the measured data it can be concluded that graphene layer is heavily damaged and this sensor is not suitable for measurements. It has been discarded and the other measurements are done with the other sensors.

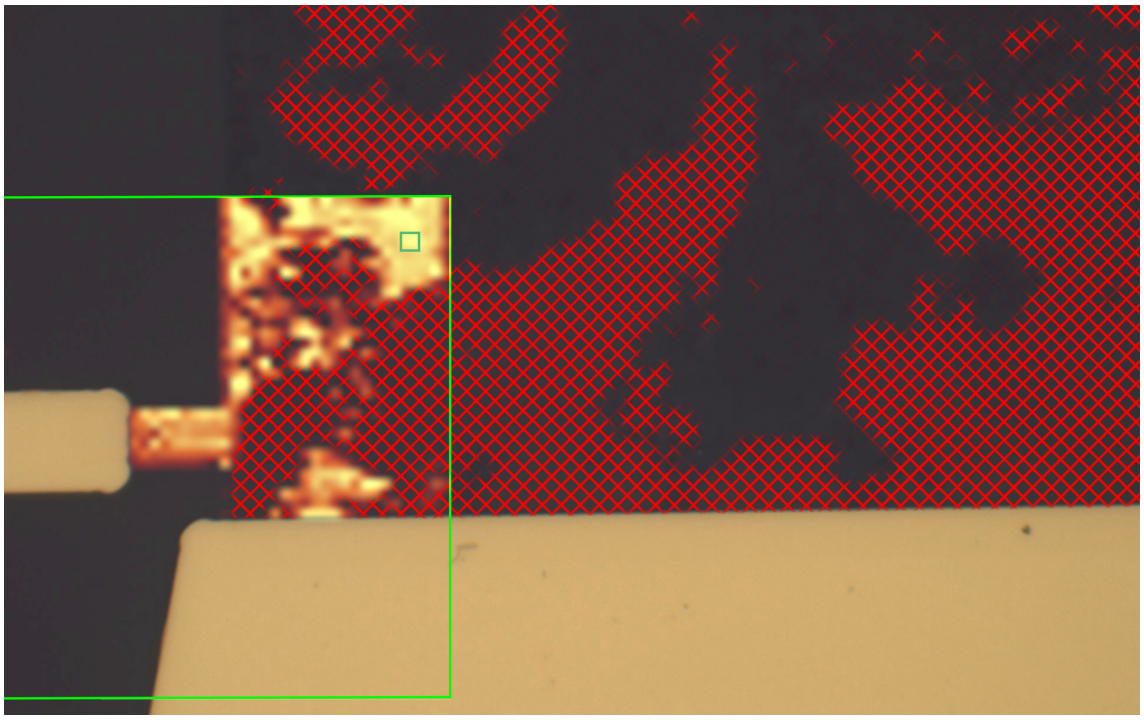

Fig. 3.15: A composite image made up of imaged piece with isolated color change due to grapene being somewhat opaque. A green square shows a result of a spectral filter applied to the carbon band. The inner green square shows which point was chosen to display the measured spectrum. Red mesh shows where the graphene should be, but it is missing.

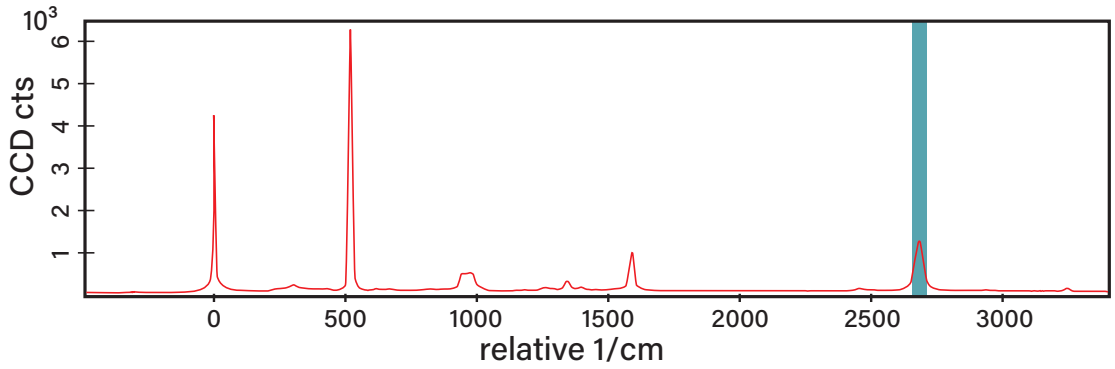

Fig. 3.16: A refracted spectrum of one point in the 2D data capture. Small green square in Figure 3.15 shows the selected point. Blue strip is a spectral band filter applied to the data sample. It colors the 2D image based on the intensity of the wavelength passed by the filter. Current filter is at 2681.93, with the width of 50 units.

3.4.2 VA Characteristics and resistance measurement

Goal of this measurement is to know the resistance of the sensors with a polymer, exposed to the air for a long period of time (> 1 week) and to see the influence of the graphene width and height on the sensor resistance.

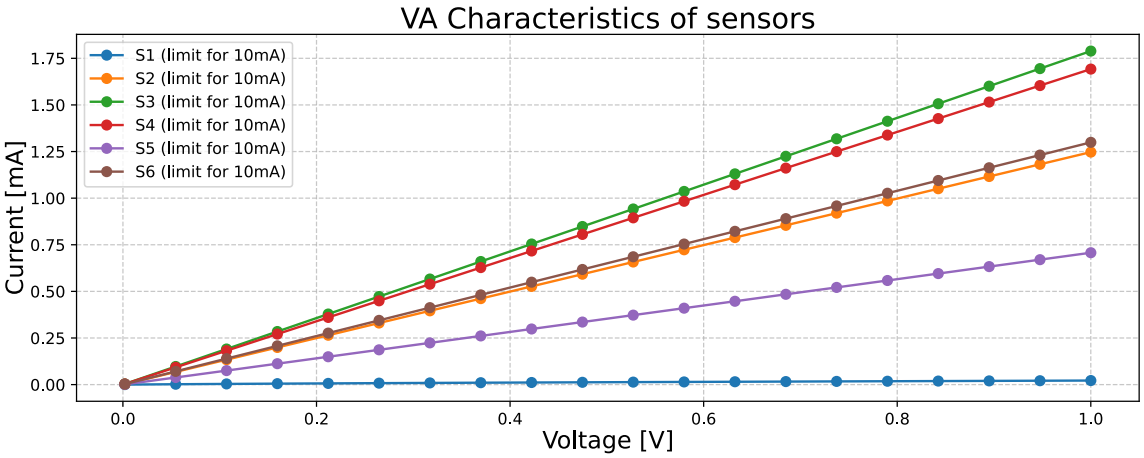

Fig. 3.17: Volt-Ampere characteristics of the sensors with polymer coating. The current limits was not triggered for any of the sensors.

In theory, if the graphene channel has its constant resistance per $\square$, the resistance of the channel with varying width and height should be computable by the formula 3.1, where R_s is the resistance per $\square$.

$$R = R_s \cdot \left(\frac{L}{W}\right) \tag{3.1}$$

Sen. num. in thesis	Resistance (Ω)	(R_s $\Omega/\square$)
S1	48074.15	60092.69
S2	802.03	641.62
S3	558.91	931.52
S4	590.86	984.77
S5	1413.08	883.18
S6	769.86	769.86

Table 3.2: Resistance of the sensors coated with a polymer. R_s should ideally be constant.

Conclusion

In theory the R_s values in table 3.2 should be constant. The resistances of these sensors are widely different. This can be caused by damage to the conductive channel in case of S1 and the variation in the other sensors may be caused by the polymer interacting with graphene layer, or by adsorbants on the surface from possible previous exposures.

3.4.3 VA Characteristics under light and gases

Resistance of the samples may change on certain external influences, such as light or gas. This experiment was performed to see if a change in gas exposure or light changed the resistance at various voltages. VID sensor was measured under a shade from the ambient light, subsequently an iphone 13 pro max torch at full brightness was shined 12cm away from the sensor. Then, concentrated acetone-air vapor was slowly blown onto the sensor. Then, air was blown onto the sensor, until the sensor settled to about 975Ω. Then a concentrated ethanol-air vapor was blown onto the sensor. Results of the VA characteristics are shown in Figure 3.18.

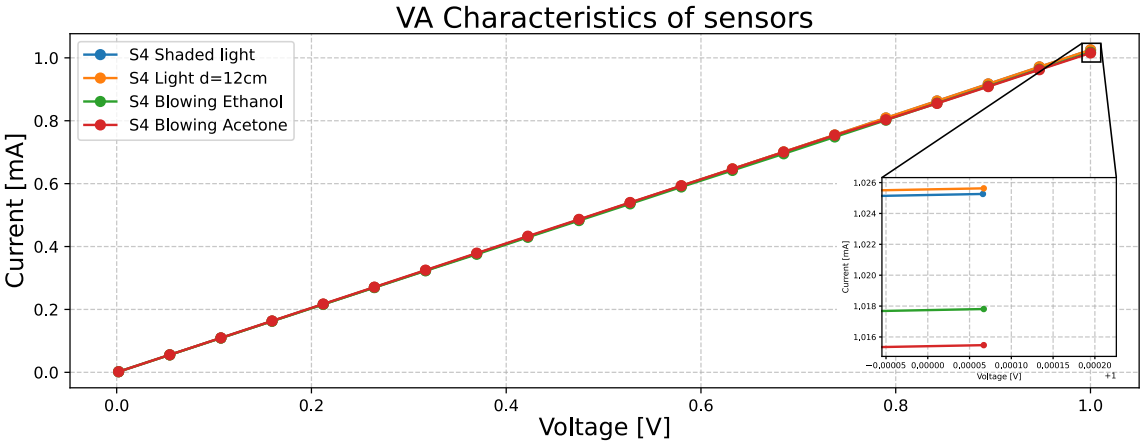

Fig. 3.18: Volt-Ampere characteristics of one sensor under various environmental conditions.

Sensor	Condition	Resistance (Ohms)
VID	Shaded light	975.47
VID	Light d=12cm	975.03
VID	Blowing Ethanol	984.09
VID	Blowing Acetone	984.95

Table 3.3: Resistance values for VID sensor under different external conditions.

Conclusion

Table 3.3 shows the highest resistance of all without a light. This is a proper value for the sensor. Excitation of the sensor by light decreased the resistance very slightly. This decrease should be larger and the reason for the small decrease is unknown. Ethanol and acetone increase the resistance of the sensor, which is theoretically correct, as ethanol and acetone may have P-doping effect on graphene surface, which may be N-doped by external sources, effectively decreasing the free-carrier concentration.

3.4.4 Swept sine measurements

Devices may respond to time-varying phenomena. Graphene sensors may respond to oscillating voltages in the range from 1Hz to 50kHz. Agilent 35670A was used to produce the sine-waves at a defined amplitude and it also detected the response. Phase and amplitude of the returned wave can be measured. In this case, phase shift was not investigated, only the amplitude of the sensor's response. Experimental setup is shown in Figure 3.20. Analyzer was configured to an up sweep direction, 100 frequency increment, 200 PNT/SWP units of resolution, linear spacing, auto sweep mode and 0.5s of integration time (0.5s used when mentioned). VID sensor was used in this measurement.

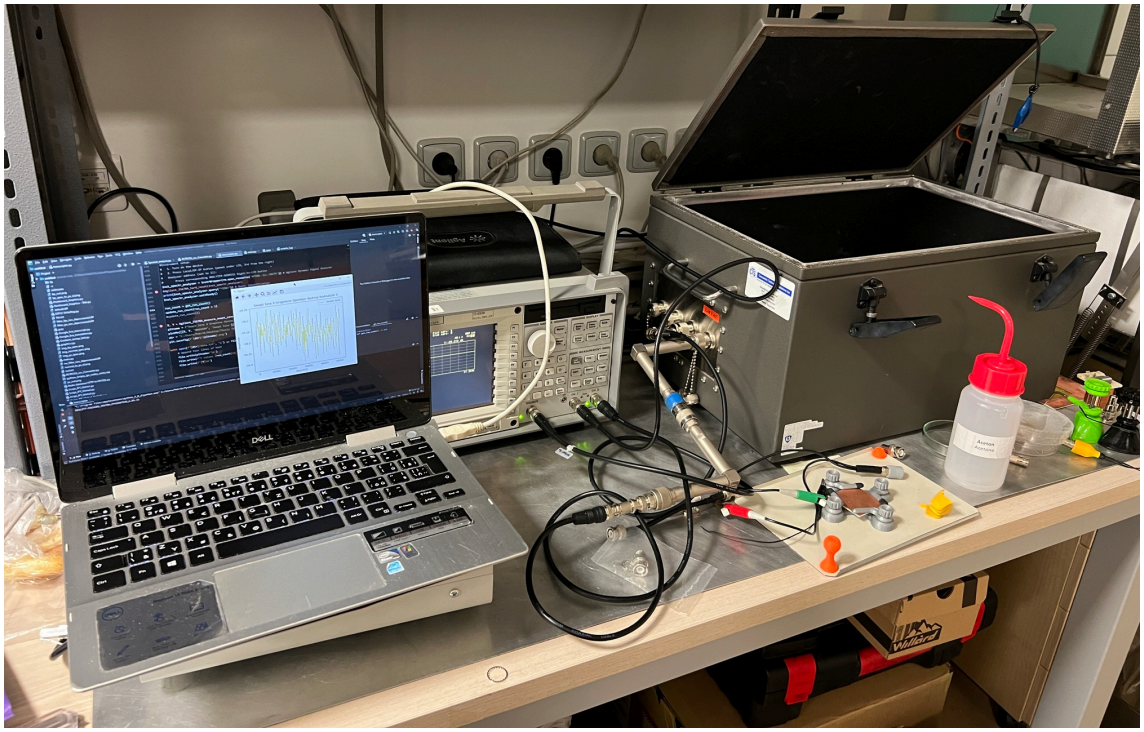

Fig. 3.19: Measurement setup with a computer on the left controlling the analyzer.

Influence of the following variables was tested using swept sine:

- Opened or closed shielding chamber
- Reaction of the sensor to acetone and isopropylalcohol (IPA)
- Various sine amplitudes (voltages)

The measurements without an integration time were performed 10 times. Their character is shown in Figures 3.21 and 3.22. Picture of the experimental setup is shown in Figure 3.19.

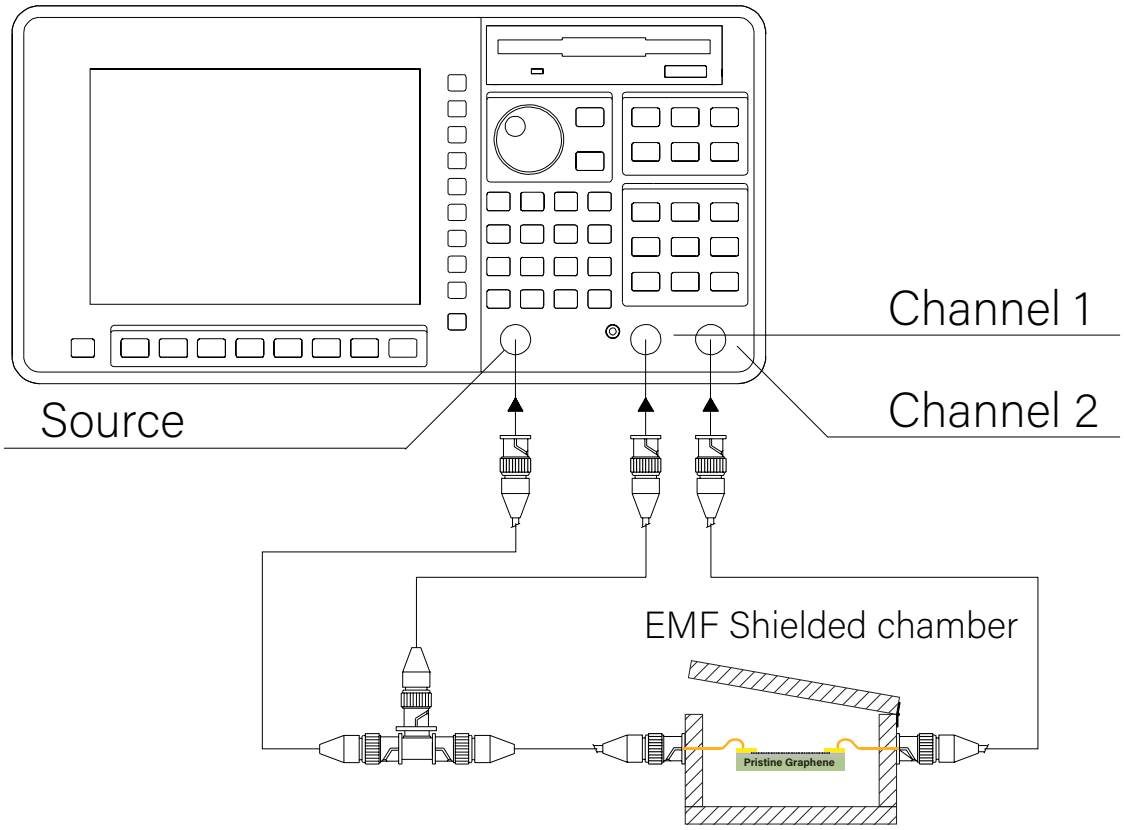

Fig. 3.20: Dynamic signal analyzer's output is connected through the shielded chamber interface directly to one side of the sensor. The other side of the sensor is connected to the channel 2. Source outputs the sine wave and channel 2 reads the measurement. The chamber can be opened or closed.

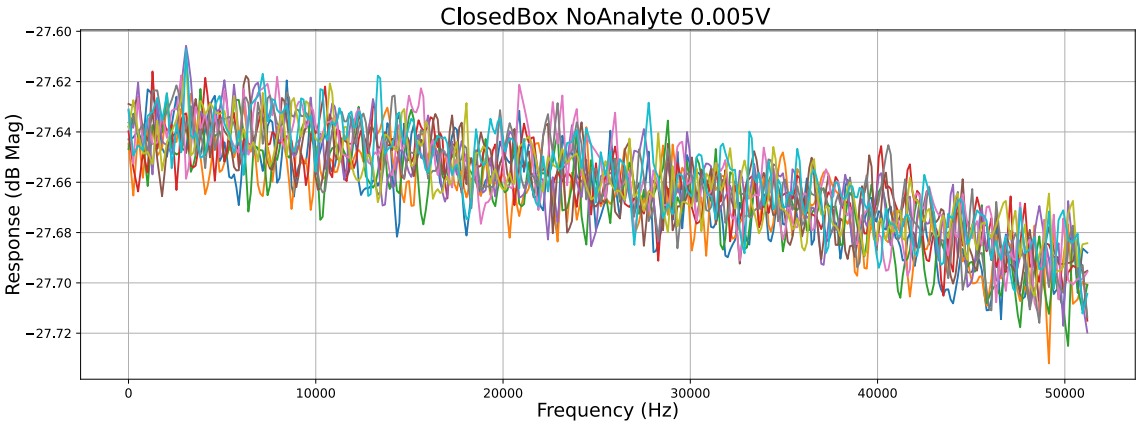

Fig. 3.21: 10 individual measurements of a sensor inside a closed shielded chamber (box), in air (no analyte), with 0.005V peak to peak. Each line represents a distinct measurement.

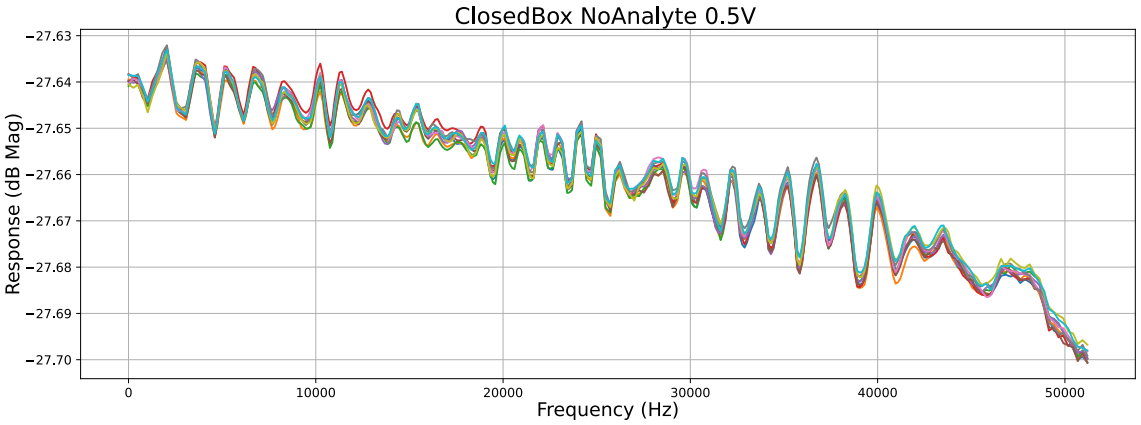

Fig. 3.22: 10 individual measurements of a sensor inside a closed shielded chamber (box), in air (no analyte), with 0.5V peak to peak. Each line represents a distinct measurement.

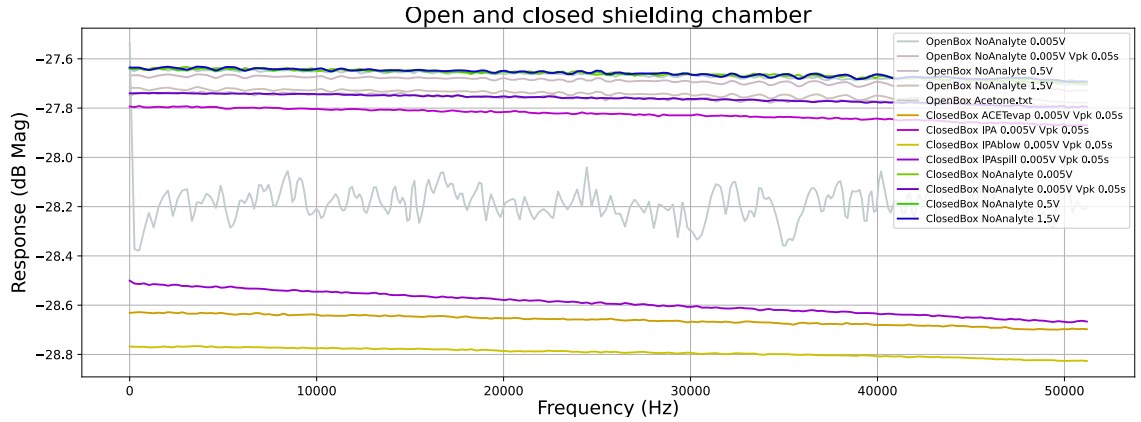

Fig. 3.23: Averaged values of all swept sine measurements. Saturated are measurements performed in a closed chamber.

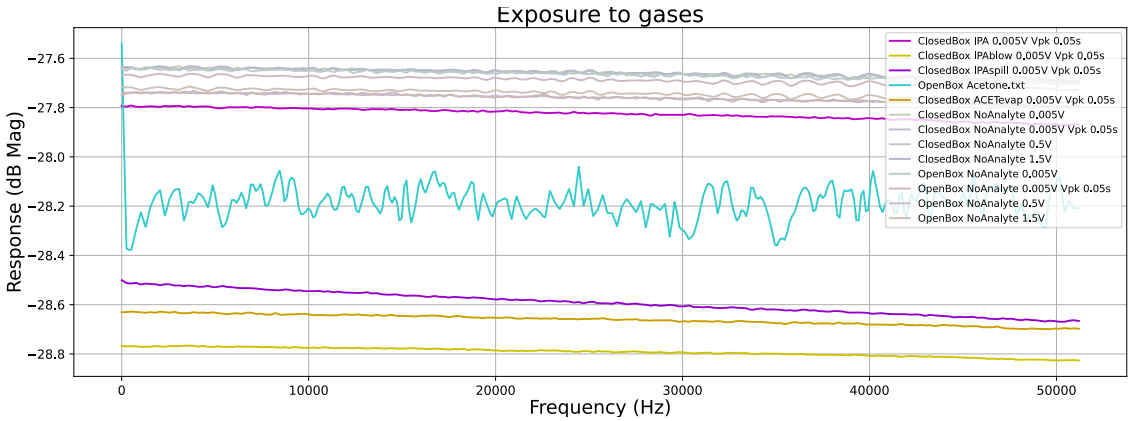

Fig. 3.24: Averaged values of all swept sine measurements. Saturated are measurements of an isopropylalcohol (IPA) evaporation, IPA blow, IPA spill, acetone blow and acetone evaporation. Evaporation was done by placing a dish with the evaporating liquid. Liquid was evaporating 5 minutes before the measurement started. Acetone measurement is very noisy, as only one measurement was performed, without averaging. It still shows a useful mean value. Blow was achieved by placing a nozzle with concentrated vapor about 4 cm above the sensor, weakly blowing on the sensor. Spill was achieved by placing a tiny droplet of liquid onto the sensor.

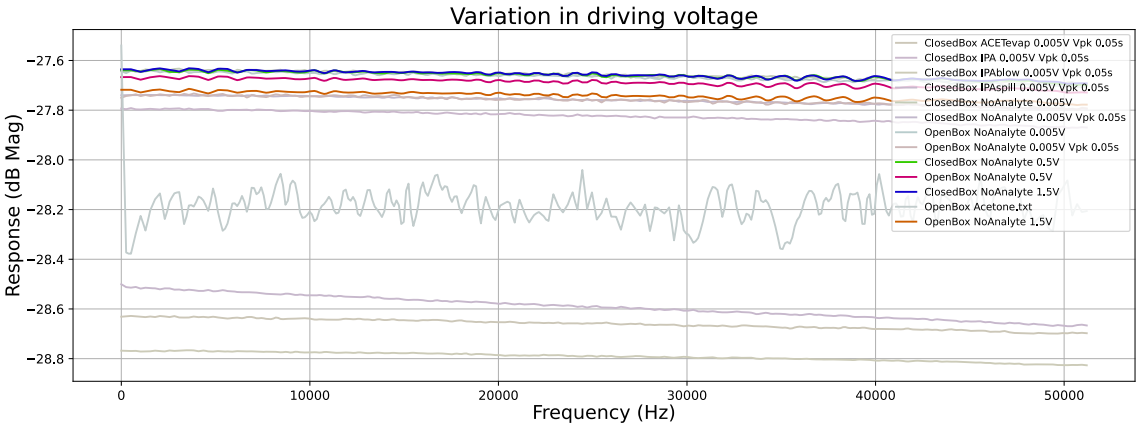

Fig. 3.25: Averaged values of all swept sine measurements. Saturated are measurements with driving voltage above 0.005V.

Conclusion

Each of the influencing variables on the swept sine measurement are concluded here. In Figure 3.23 a difference between measurements performed under opened and closed. As the no-analyte measurement of both opened and closed box are located at the top portion of the graph, openness of the chamber has negligible impact on the measurement. This is expected, as the driving quantities used here are orders of magnitude higher, than the EMF radiation. Figure 3.24 shows swept sine under various gases. Blow of the isopropylalcohol on the sensor increased its resistance the most. Evaporation of acetone inside the chamber also significantly increased the resistance from the baseline value. Little weaker effect on resistance had a droplet of isopropylalcohol on the sensor. Acetone blow did not increase the resistance as much as its evaporation inside chamber. This is unexpected and it may be as a result of N-P type inversion, or this measurement is not trustworthy and should be repeated. IPA evaporation had the weakest effects on the resistance. All of the gas interactions with the sensor decreased the resistance. Lastly, Figure 3.25 shows a difference between very small driving voltage and significantly higher driving voltage. Interestingly, repeating oscillation-like patterns are visible on the frequency response. The resistance levels (based on attenuation response) are relatively well kept, no matter the driving voltage. Although the oscillating character in frequency response is more pronounced at higher driving voltages. These oscillations are not as pronounced when the resistance increases due to gas adsorption on the sensor. Based on the dB magnitude scale, the highest placed measurements are at about -27.65 dB. If the input impedance of the instrument is 50Ω, this level corresponds to a resistance of 1.156kΩ. The start of the IPA blow signal would correspond to 1.321kΩ, which are realistic values. Also, the resistance increase proportional to gas exposure, although not in scale, but in direction, agrees with the DC analysis. The equation 3.2 is used to convert the gain values to resistance, where G is the input gain.

$$R = -\left(2^{1-\frac{G}{20}}\right)\left(5^{2-\frac{G}{20}}\right)\left(10^{\frac{G}{20}}-1\right) \tag{3.2}$$

3.4.5 Dynamic changes of graphene resistance to IPA, heat and breath

Chemiresistive samples obtained to be studied can react to various external quantities. Time variance of these quantities is studied in this experiment. VID sensor was placed into an ambient environment. A measurement of resistance was taken every 250ms. The whole measurement can be seen in Figure 3.26. During this measurement, the sensor was exposed to a blowing IPA gas, shown in Figure 3.27. Isopropylalcohol was contained in a flexible plastic bottle. This bottle was squeezed to release the evaporating IPA mixed with air. As a reference, empty bottle squeezed and the air inside was blown onto the sensor, which resulted in a very minimal effect on the measurement. For the period of the air blowing, an increased noise was seen in the measurement. Thermal effects were also studied during the meaurement process. Figure 3.28 shows the response of graphene to a changing temperature. Heat was delivered by a resistive wire brought to a distance of 6mm over the graphene surface. This wire was heated to about 260°C. Lastly, by accident, a sharp temporary decrease of resistance was detected in the measurement. Consequently, breath exposure was tested on the graphene sensor. Every time the sensor was exposed to human breath, sensor responed in the same way. Zoomed-in portion of the measurement is shown in Figure 3.29. Breathing was performed by mouth and by nose. The depth of the response peaks correspond to the pressure and time of the gas exhaled. Exhalation was performed at a distance of 10cm directly above the sensor.

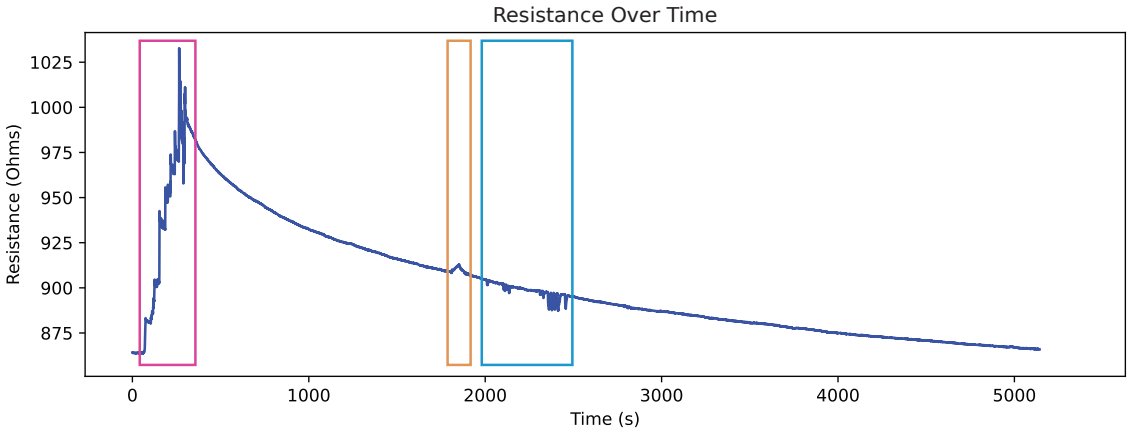

Fig. 3.26: Resistance measurement over a course of 1h25m. Three experiments were performed during this measurement time. Each experiment is isolated by a window that is enlarged in the other figures. Pink window contains IPA blow experiment, orange window shows a response to an increase of temperature and blue section shows a response of the sensor to a human breath.

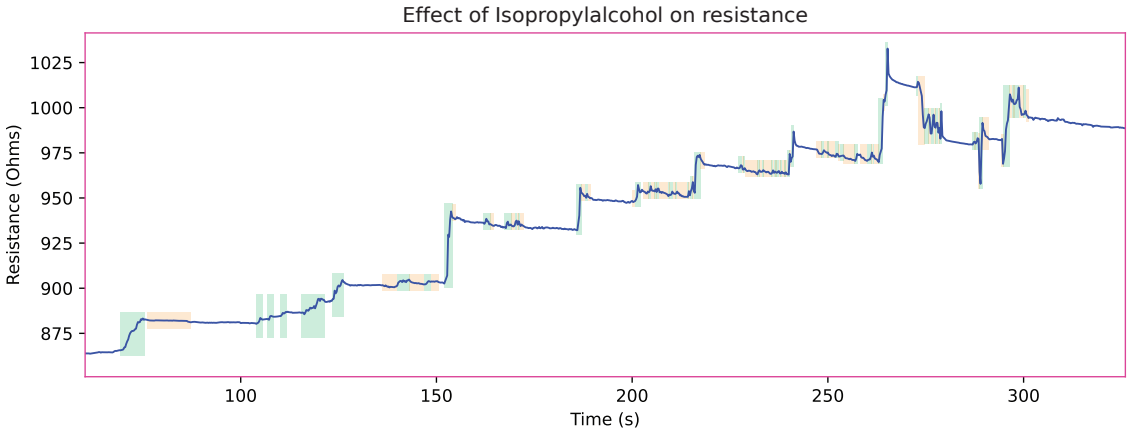

Fig. 3.27: A zoomed-in pink section of the Figure 3.26. All the rectangles show the time when the IPA was blown onto the sensor from a plastic bottle terminated with a nozzle. Green rectangles show the effect of increasing resistance from the blowing gas and orange rectangles show decreasing resistance effect on the same gas source.

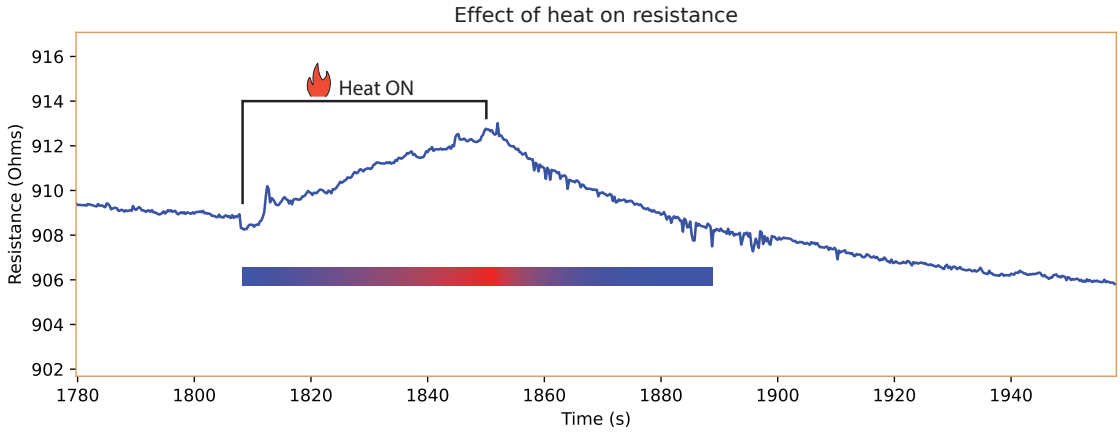

Fig. 3.28: A zoomed-in orange section of the Figure 3.26. As heat was turned on, resistance was gradually increasing. When the heating element was turned off, resistance decreased back down. A temperature gradient is shown under the curve for a representative purpose.

Conclusion

All of the studied quantities have prominent effect on the resistance of graphene. From the reaction of graphene to isopropylalcohol, an increasing resistance agrees with the swept-sine and DC measurements addressed in this thesis. Increasing resistance trend due to an IPA exposure can be explained by molecules adsorbing onto the graphene surface. It might be possible, that with the higher concentrations, condensation of IPA can take place on the graphene surface. Graphene may be n-doped from the environment causes and IPA adsorption provides charge transfer and

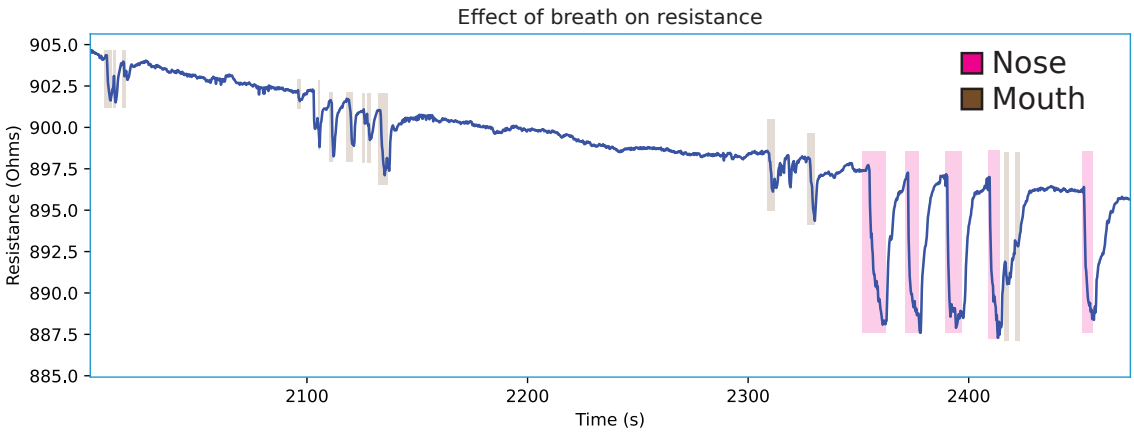

Fig. 3.29: A zoomed-in blue section of the Figure 3.26. Two sources of human breath - mouth and nose were tested. All rectangles show time portions where gas was blown onto the sensor.

dipole interactions effects, effectively p-doping the graphene and thus decreasing its resistance. It seems like the sensor, even after several exposures, did not reach the saturation point. However, after the resistance passed 970Ω, peaks started to drop off faster than under this resistance. Additionally, when the bottle was pressed and IPA-air mixture was released onto the sensor, accelerated decreasing of resistance was recorded, even though resistance increase always majorly dominated. Decreasing effects on resistance from the same gas source may be because of higher air-to-IPA content in the bottle after a suction phase, as well as potential drying effect on the sensor surface, before the adsorption process kicked in. These preliminary studies show the need for a better testing apparatus and more gases to be investigated, as the measurements show promising response ability of the sensor to various useful gases. Temperature investigation showed rather expected behavior. During the heat input, resistance increased linearly, most possibly due to the heat distribution throughout the sample. After the heat source was turned off, resistance decreased exponentially, due to the decreasing difference of the sample temperature and the ambient temperature. Interestingly, little effects of desorption were seen from the heat input. Resistance decrease continued to the original exponential trend caused most possibly by the analyte desorption. Human breath had drastic and fast influence on the graphene surface. Detection of the substances present in human exhaled gas as well as recovery happened practically in real-time, contrary to IPA recovery, which was measured throughout all the experiments. Each recovery from the exhaled gas reached the desorption trendline from the IPA exposure. Even greater response was measured during exhalation from nose. Generally, nitrogen concentration (∼)74-78% is the same between ambient the ambient air and the exhaled gas.

Concentration of oxygen in exhaled gas is about 21% lower than the environment. CO_2 concentration in exhaled gas is more than 1000x more than in the environment. This decrement of resistance is therefore attributed to CO_2. Trace amounts of biological material can also be a causing factor for this effect. It is also possible that the rate of gas exhalation was higher in this experiment that that of mouth, as gas flow was not controlled, nor measured. From the view of Density Functional Theory, CO_2 has a higher adsorption energy that H_2O, but lower than IPA. It also acts as an electron donor (n-dopes the graphene), while H_2O and IPA act as electron acceptors (p-dope the graphene), which in an n-doped graphene would decrease the resistance. Later experiments with water vapor showed that this sensor slightly increased the resistance when exposed to H_2O.

3.4.6 Response of graphene to gas in the spectral domain

Spectral signal domain of the graphene sensor may be a useful source of information where various phenomena can be identified. Therefore a test setup has been created to see the difference between acetone and isopropylalcohol reactions on the graphene sample. It consists of the graphene sensor connected to a battery for smooth current and a resistor (Figure 3.30). When the sensor reacts to any phenomena, its resistance changes and the current does too. This current flows through the resistor and any variation in current is converted to variation in voltage, which is then amplified and analyzed. A 100Ω 5W wire resistor was used in the measurements, as it has lower noise profile than paste or carbon ones. Resistor's value should be such that when the signal is amplified, it falls into the range of the amplifier and the analyzer. In this particular case, the amplifier was not used as it was damaged. Thus, the sample was directly connected to the instrument. There are several variables that can be controlled in this setup, but the are not elaborated in this thesis:

- Voltage over the graphene and the resistor.
- The resistor and so its noise characteristics.
- The signal path to the amplifier.
- The temperature of the system.
- The bonding material and metal interfaces.

Four proof-of-concept measurements with two gases were performed. Isopropylalcohol (IPA) and acetone were blown onto the VID sensor from a bottle with a nozzle about 10cm from the sensor. Both weak blows and strong blows were performed. They are shown in their respective figures below. Color scale is uniform across all the figures and the scale is presented in Figure 3.31.

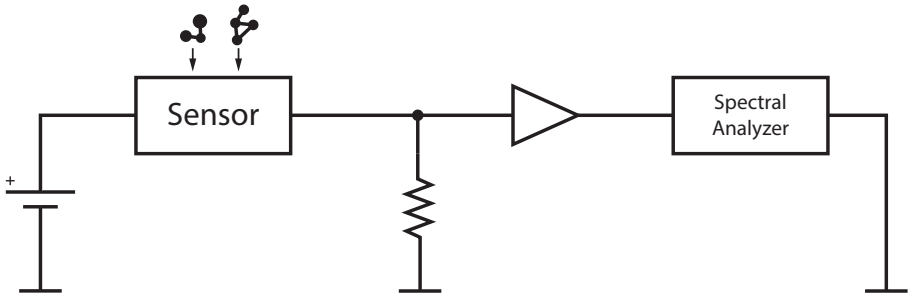

Fig. 3.30: Diagram of the connections for mesuring the grapene sensor.

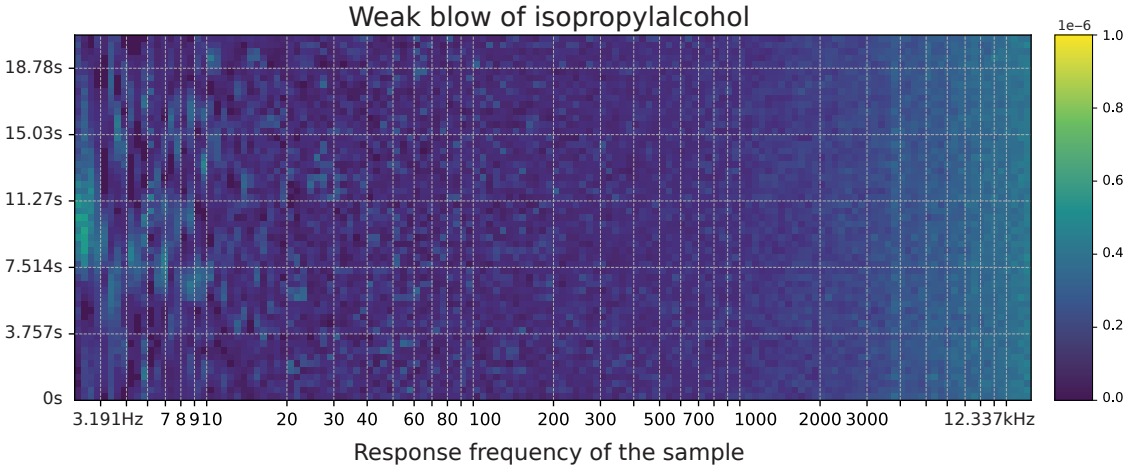

Fig. 3.31: 3D waterfall diagram of the graphene noise spectrum. The faint colored spots at low frequencies are a result of weak blow of the isopropylalcohol on a sensor from a plastic bottle. Y axis is time, with first values at the bottom and newer in the top direction, Color is the absolute intensity of the signal in $V_{RMS}/\sqrt{Hz}$.

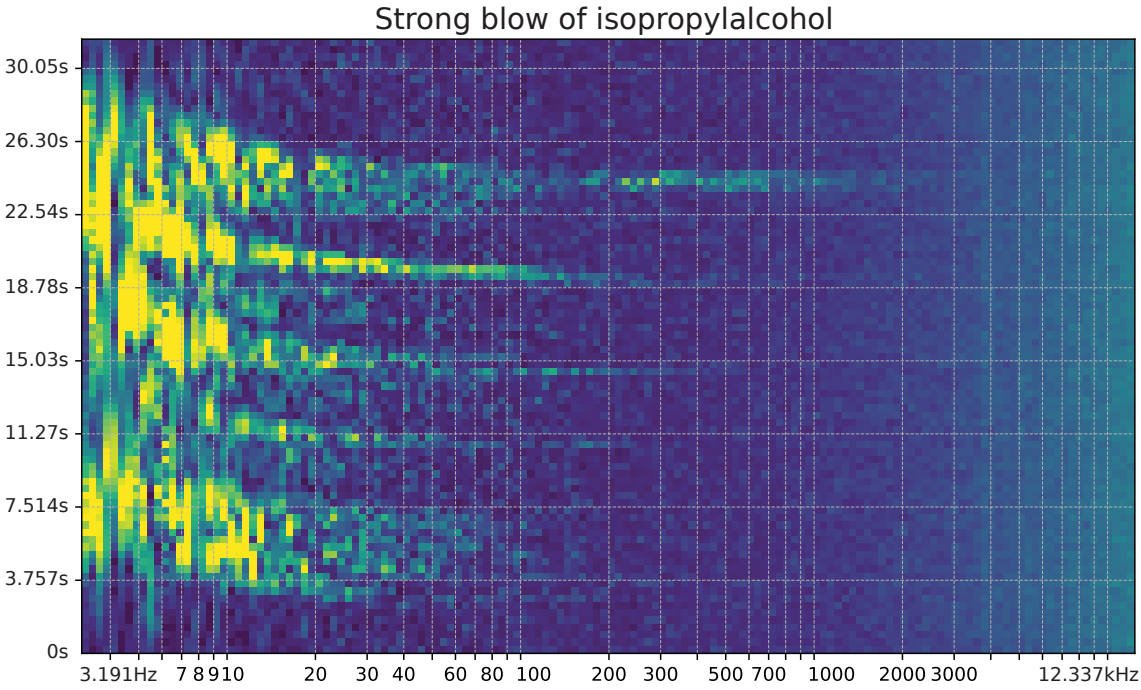

Fig. 3.32: 3D waterfall diagram of the graphene noise spectrum. The colored signal footprints are due to stronger blow of IPA from a bottle. Each higher-frequency peak represents a blowing cycle. Signal tends to turn to lower energies where it is attenuated. X-axis is the response frequency of the sample, Y axis is time, with first values at the bottom and newer in the top direction and color is the absolute intensity of the signal.

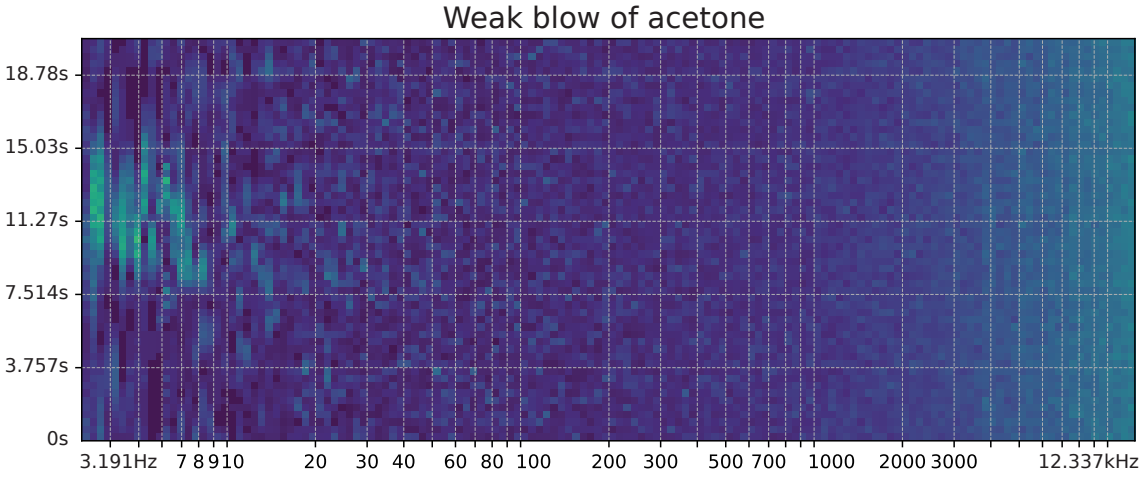

Fig. 3.33: 3D waterfall diagram of the graphene noise spectrum. Faint mark on the left is a response to weak blow of IPA from a bottle. X-axis is the response frequency of the sample, Y axis is time, with first values at the bottom and newer in the top direction and color is the absolute intensity of the signal.

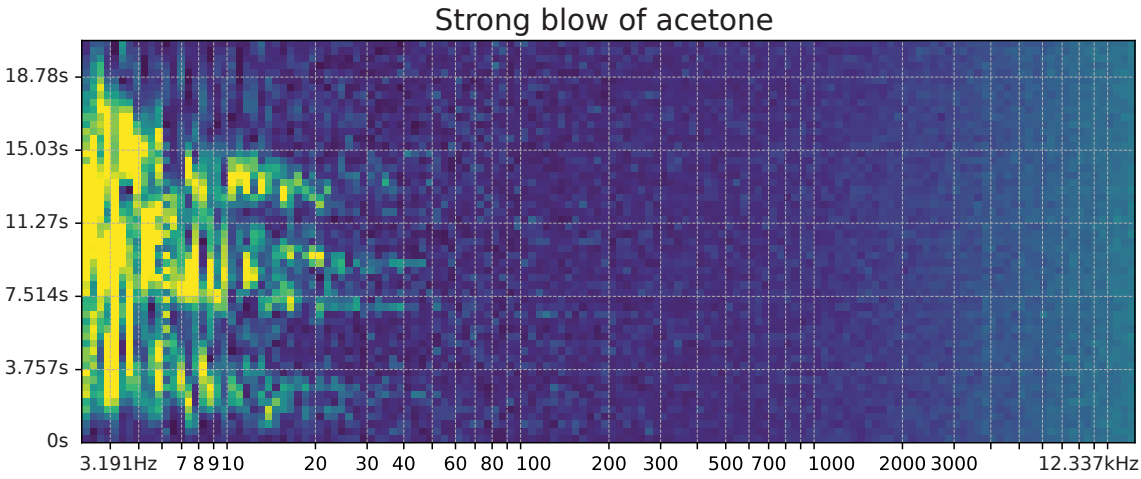

Fig. 3.34: 3D waterfall diagram of the graphene noise spectrum. Four blow cycles are sensed by the sensor and its reaction is pronounced at lower fequencies. X-axis is the response frequency of the sample, Y axis is time, with first values at the bottom and newer in the top direction and color is the absolute intensity of the signal.

Conclusion

These measurements are rather for a proof-of-concept purpose. They were performed without an amplifier, which would definitely increase the dynamic range of the noise measured. It can be seen that both isopropylalcohol and acetone react with the sensor and their spectral response can be captured. Response to the phenomena is directly proportional to the rate of change of the environmental conditions in sensor's perspective. Weak blowing (Figure 3.31, 3.33) did not have as high response as strong blowing (Figure 3.32, 3.34). From several other trials of the same experiment, the ability of detection even very weak changes (actual ambient adsorption) is promising, as well as the identification of analyte from its spectral footprint. Controlled blowing of the analyte must be achieved in further experiments and ideally, graphene should be placed directly on the silicon circuitry of extremely low noise preamplifier.

3.4.7 Response of graphene to light in the spectral domain

During previously mentioned experiments, the VID sensor was exposed to light. That's why several spectral measurements were performed for the VID sensor. Light from an iphone was slowly brought close to the sensor.

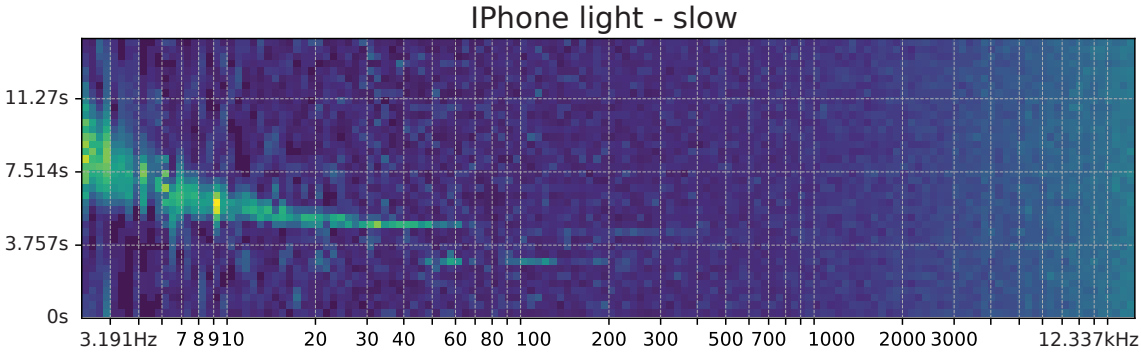

Fig. 3.35: 3D waterfall diagram of the graphene noise spectrum. As light from iphone was approaching the sensor, frequency response was detected at low frequencies. X-axis is the response frequency of the sample, Y axis is time, with first values at the bottom and newer in the top direction and color is the absolute intensity of the signal.

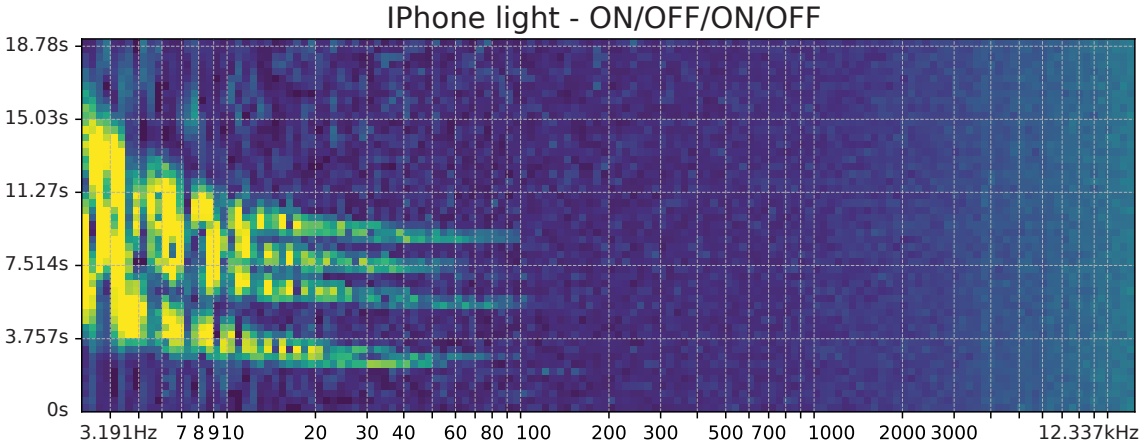

Fig. 3.36: 3D waterfall diagram of the graphene noise spectrum. Light was turned around the wall edge, so that the edge obscures the sample or not. Each higher-frequency peak corresponds to ligt passing through the wall edge so that it hit the sample. X-axis is the response frequency of the sample, Y axis is time, with first values at the bottom and newer in the top direction and color is the absolute intensity of the signal.

Conclusion

The sample definitely reacts to light. Although from subsequent experiments on the HR sample, which had very probably damaged graphene layer, it is highly probable that this effect, rather than from the response of graphene, is from a photoelectric response of the silicon-siliconoxide stack. As with the gas measurements in the spectral domain, the faster the change, the stronger the spectral reaction and the higher the frequencies the reaction is measured at. The energy then went to the lower frequencies where it got attenuated.

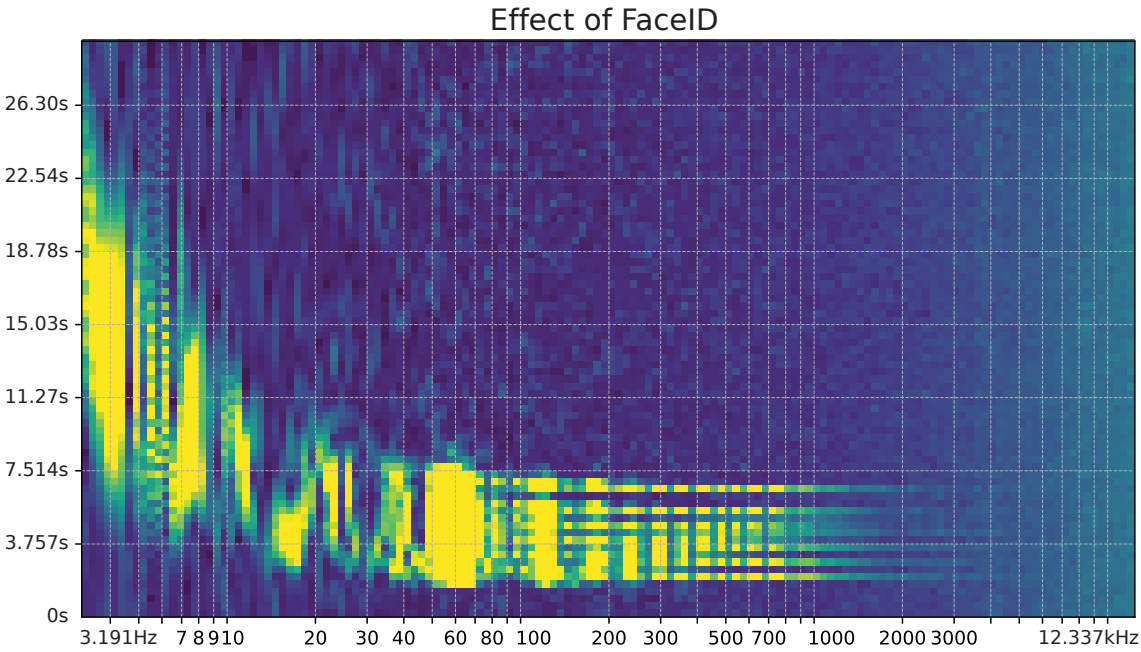

Fig. 3.37: 3D waterfall diagram of the graphene noise spectrum. Individual FaceID pulses were detected by the sensor The dieout was so fast that the reaction excited response even at higher frequencies. X-axis is the response frequency of the sample, Y axis is time, with first values at the bottom and newer in the top direction and color is the absolute intensity of the signal.

3.4.8 Conclusion on the experimental section

There were more experiments conducted than those presented in this thesis. It has been shown that when a hand is brought close to the sensor (about 12cm), 50Hz peak is measured in the response spectrum. This is due to induction of line frequency to a human body and then to a sensor. Two different people were responded by two different intensisies. This experiment was replicated, but only male and female were tested. Octave analysis with a 40dB preamplifier showed little change between open chamber and closed chamber. 50Hz peak was suppressed by about 40dB thanks to the closed chamber. A graphene array with a HR sensor connected showed response to an UV light with frequencies 365nm, 385nm and 415nm similar to those documented in subsection "Response of graphene to light in the spectral domain". HR sensor however, showed 91kΩ of resistance between the two measurement terminal. This still may be an acceptable value, but it is strongly believed that HR sensor in some way shorted through the oxide barrier to other sensors. Response on this sensor is thus not attributed to graphene itself, but rather to the silicon substrate. From the experiments presented in this thesis it is clear that graphene reacts to light from infrared to ultraviolet spectrum, it reacts strongly isopropylalcohol,

slightly more to acetone and it reacts weakly to H_2O. All these measurements are present in DC as well as spectral domain. Spectral measurements are very sensitive to the rate of change of the environment, while DC measurements show an integrator behavior. Both isopropylalcohol and acetone in all experiments had an effect of increasing the resistance. Water vapor decreased the resistance slightly and exhaled gas decreased sensor's resistance aggressively. Swept sine measurements have primarily resistance reporting character, but higher sensitivity measurement, some character of response to distinct gases could be observed. Samples tested here did not match their resistance to the theory of channel width and height. It should be noted that graphene does not conduct the same way in the X and Y direction. Cause of the channel resistance not complying with theory is attributed to poor graphene surface purity. For further sensing, it is advised to use wider channel, as it reduces resistance, increases current density. Increasing channel length is also beneficial as it increases the interaction are for gas and this helps decreasing the 1/f noise. Use of hall-bar geometry is encouraged, as it eliminates the effect of contact resistance and thanks to hall voltage, carrier concentration can be calculated. Using the sample's resistivity a carrier mobility can be computed. In this thesis this geometry was not used and these parameters were not studied. Graphene sensor sample preparation is a very important step. It is advised to use as small substrate as possible, in case of light detection, as the substrate reacts to light possibly even more than graphene, especially the doped substrate. It is better to have the cut sample even for gas sensing, to eliminate possible adsorption and condensation on the substrate. Even though it is not conductive, charge, electrostatic field and particles can accumulate on it over time. It is important to analyze the surface of graphene at least with raman spectroscopy, as graphene defects greatly influence measurement. Ideally, atomic structure should be characterized for each sensor. Most of the pristine graphene samples are not fully pristine. They containg grain boundaries and lattice defects, which to some extent influences variance across measurements with multiple samples. Graphene is a promising platform for gas sensing applications, although currently this material needs too many precise conditions for viable measurements, from production through functionalization to environmental conditions, which keeps this technology from massive production and application.

Conclusion

Graphene sensors are currently researched topic and stem concepts have been studied and summarized in this document. This thesis is broken down into two main areas. Theoretical research and sensor characterization. In the theoretical section, introduction to gas sensors is given. Afterwards, general sensor is focused to chemical sensor, chemical sensor is focused to gas sensor and gas sensor is focused to graphene-based gas sensors. General principles of operation as well as properties of these sensors are introduced.

Some focus is given to the theory of gas sensor measurements, to familiarize the reader with results shown in the experimental section. Most oftenly used measurement type is the sensor's resistivity or conductivity change in time, based on the increasing exposure to an analyte. Effects of noise in graphene are introduced and practical effects of various sources of noise on graphene are also mentioned, namely, the effect of 1/f noise to the sensitivity limit and an ability to isolate the noise from measurements.

Graphene as a material is then deeply studied and physical foundation for this material is built. Many practical effects in gas sensing are rooted in this physical model. Band structure affects the conductivity under various circumstances, such as gate-voltage introduction, which leads to electrical doping thanks to zero-band gap, unique in graphene. This leads to an increase or decrease of carrier density and this effect is used in many studies of graphene-based gas sensors. Physical phenomena that influence graphene conductance are mentioned, such as various sources of scattering, inter and intra-band conductivities, phonons, plasmons and defect. Gas sensors based on graphene belong to the category of sensors based on 2D materials. Alongside graphene, molybdenum disulfate, phosphorene, transition metals dichalcogenides and others share some unique properties and their utilization in gas sensing is introduced. Various derivatives of graphene are listed (pristine, graphene oxide, reduced graphene oxide), as many experimental sensors are built on one of these frameworks. Influence of doping on these materials is given too.

In the experimental section, sensors from graphenea company were prepared by protecting with a polymer, cutting and some were directly bonded. A PCB was designed and produced to better interface with the sensors. Cleaning process after cutting posed difficulties, as the polymer was not easy to dissolve and mechanical removal had to take place, which probably destroyed the graphene sensing layer. Other cut sensors were kept with the polymer on and these sensors did operate, although the quality of measurements was very possibly influenced by the polymer.

Many effects affecting the graphene during measurement map to the change of conductance. They were studied, but the technology available to the research

presented in this thesis was not good enough to isolate most of them. Although many of these effects such as joule heating, quantum tunneling effect and graphene plasmon resonance are too weak to have a significant impact on the measurements. DC analysis, swept-sine, resistance over time, gas in spectral domain and light in spectral domain were studied. In conclusion, derivative effects can be seen in the spectral domain and integral effects can be seen in the resistivity of graphene sensor. Isopropylalcohol and acetone showed an increase of resistance proportional to the time of exposure. An accelerated desorbing effect was seen on the samples when a mixture of analyte and air was blown onto the sensor. This was caused probably due to unevenly mixed evaporated gas that went through the nozzle to the sensor. During higher air concentration the sensor decreased resistance and during higher analyte concentration the resistance was increased. Desorption took a long time (more than 1h,11m) and heating the sample to about 60řC did not help. Graphene sensor reacts in the spectral domain to IPA and acetone proportionally to the ppm rate of exposure as well as gas speed, which attacks the sensor. Blowing pure air onto the sensor did not change any characteristics in a notable way. Light, AC radiation and various other electromagnetic spikes have an influence on the spectral measurement and these effect should be minimized. Graphene samples should use hall-bar geometry for better isolation of contact resistance and wide surface area is beneficial to the adsorption sites as well as to the smaller presence of 1/f noise.

A use of high-quality high-bandwidth ultra-low-noise preamplifier is recommended for future measurements. Deeper study on the effect of various gases to the resistance curve over time is needed. Gases such as NO_2, CO_2 and NH_3 should be tested, with known concentration in the vicinity of the graphene surface. Critical is the clean and desorbed surface before testing, which can be achieved only in very high vacuum, with the use of electron, UV or thermal energy inuput at high enough time for good statistical desorption. Argon is viable for the isolated measurement of desired analyte at variable concentration and defined pressure. Knowledge of the number of defects and atomic arrangement throughout the surface is great to study slight statistical deviations in the adsorption-desorption process.

Bibliography

[1] P. Bergveld. The impact of mosfet-based sensors. *Sensors and Actuators*, 8(2):109–127, 1985. URL: https://www.sciencedirect.com/science/article/pii/0250687485870098, doi:10.1016/0250-6874(85)87009-8.

[2] George L. Kerr. *Practical Coal Mining: A Manual for Managers, Under-Managers, Colliery Engineers, and Others*. C. Griffin & Company, Limited, London, 1900. URL: https://archive.org/details/practicalcoalmin00kerrrich/page/n13/mode/2up.

[3] National Research Council (US) Committee on Animals as Monitors of Environmental Hazards. *Animals as Sentinels of Environmental Health Hazards*. National Academies Press (US), Washington, DC, 1991. Copyright ł National Academy of Sciences. doi:10.17226/1351.

[4] A. A. Mikhailov. Ozone layer and the formation of the ozone hole, 2004. URL: https://arxiv.org/abs/physics/0401135, arXiv:physics/0401135.

[5] Florinel-Gabriel Bnic. *Chemical Sensors and Biosensors: Fundamentals and Applications*, chapter 1, pages 1–20. John Wiley & Sons, Ltd, 2012. URL: https://onlinelibrary.wiley.com/doi/abs/10.1002/9781118354162.ch1, arXiv:https://onlinelibrary.wiley.com/doi/pdf/10.1002/9781118354162.ch1, doi:10.1002/9781118354162.ch1.

[6] Peter Gründler. *Chemical Sensors - An Introduction for Scientists and Engineers*. Springer, 2007. doi:10.1007/978-3-540-45743-5.

[7] Shilpa Jain, Mohammad Khalid, Jolina Rodrigues, Tanushree Sen, Akshara Paresh Shah, Navinchandra Gopal Shimpi, and Golnoush Zamiri. Carbon-based nanomaterials and nanocomposites for gas sensing. In Navinchandra Gopal Shimpi and Shilpa Jain, editors, *Carbon-Based Nanomaterials and Nanocomposites for Gas Sensing*, Micro and Nano Technologies. Elsevier, 2023. URL: https://www.sciencedirect.com/book/9780128213452/carbon-based-nanomaterials-and-nanocomposites-for-gas-sensing, doi:10.1016/C2018-0-05031-8.

[8] M. Andersson, N. Bârsan, D. Briand, Pierrick Clément, E. Comini, J. Courbat, Arnaldo D'Amico, Corrado Di Natale, Martin Eickhoff, J.W. Gardner, P.K. Guha, Andreas Helwig, M. Huebner, Raivo Jaaniso, Teerakiat Kerdcharoen, V. Kiisk, Sung Pil Lee, Eduard Llobet, A. Lloyd Spetz, Konrad Maier, R. Moos, Gerhard Müller, D. Puglisi, F. Rettig,

S. Santra, Tilman Sauerwald, Andreas Schütze, Thara Seesaard, Chowdhury Shaestagir, Kengo Shimanoe, U. Weimar, Chatchawal Wongchoosuk, Noboru Yamazoe, and D. Zappa. Semiconductor gas sensors (second edition). In Raivo Jaaniso and Ooi Kiang Tan, editors, *Semiconductor Gas Sensors (Second Edition)*, Woodhead Publishing Series in Electronic and Optical Materials. Woodhead Publishing, second edition edition, 2020. URL: https://www.sciencedirect.com/book/9780081025598/semiconductor-gas-sensors, doi:10.1016/C2017-0-00001-0.

[9] N. Rao, C.M. van den Bleek, and J. Schoonman. Taguchi-type nox gas sensors based on semiconducting mixed oxides. *Solid State Ionics*, 59(3):263–270, 1993. URL: https://www.sciencedirect.com/science/article/pii/016727389390060G, doi:10.1016/0167-2738(93)90060-G.

[10] Qiang Wu, Yubin Yuan, Xuming Wang, Xiangrui Bu, Menglong Jiao, Weihua Liu, Chuanyu Han, Long Hu, Xiaoli Wang, and Xin Li. Highly selective ionic gel-based gas sensor for halogenated volatile organic compound detection: Effect of dipoledipole interaction. *ACS Sensors*, 8(12):4566–4576, 2023. doi:10.1021/acssensors.3c01476.

[11] Xianghong Liu, Wei Zheng, Rahul Kumar, Mahesh Kumar, and Jun Zhang. Conducting polymer-based nanostructures for gas sensors. *Coordination Chemistry Reviews*, 462:214517, 2022. URL: https://www.sciencedirect.com/science/article/pii/S0010854522001126, doi:10.1016/j.ccr.2022.214517.

[12] Ingemar Lundström, Thomas Ederth, Hans Kariis, Hans Sundgren, Anita Spetz, and Fredrik Winquist. Recent developments in field-effect gas sensors. *Sensors and Actuators B: Chemical*, 23(2):127–133, 1995. The workshop on new developments in semiconducting gas sensors. URL: https://www.sciencedirect.com/science/article/pii/092540059401280U, doi:10.1016/0925-4005(94)01280-U.

[13] Zheng Meng, Robert M. Stolz, Lukasz Mendecki, and Katherine A. Mirica. Electrically-transduced chemical sensors based on two-dimensional nanomaterials. *Chemical Reviews*, 119(1):478–598, 2019. arXiv:https://doi.org/10.1021/acs.chemrev.8b00311, doi:10.1021/acs.chemrev.8b00311.

[14] J.G. Firth, Alan Jones, and T.A. Jones. The principles of the detection of flammable atmospheres by catalytic devices. *Combustion and Flame*, 20(3):303–311, 1973. URL: https://www.sciencedirect.com/science/article/pii/0010218073900217, doi:10.1016/0010-2180(73)90021-7.

[15] Zaiki Awang. Gas sensors: A review. *Sens. Transducers*, 168(4):61–75, 2014.

[16] Chunbae Lim, Wen Wang, Sangsik Yang, and Keekeun Lee. Development of saw-based multi-gas sensor for simultaneous detection of co2 and no2. *Sensors and Actuators B: Chemical*, 154(1):9–16, 2011. Transducers 2009. URL: https://www.sciencedirect.com/science/article/pii/S0925400510001784, doi:10.1016/j.snb.2010.02.057.

[17] Hea-Min Lee, Deuk-Young Han, and Hyungkeun Ahn. Design and fabrication of saw gas sensor with resonator structure. In *Proceedings of 5th International Conference on Properties and Applications of Dielectric Materials*, volume 2, pages 1058–1061 vol.2, 1997. doi:10.1109/ICPADM.1997.616629.

[18] Baicheng Yao, Yu Wu, Yang Cheng, Anqi Zhang, Yuan Gong, Yun-Jiang Rao, Zegao Wang, and Yuanfu Chen. All-optical machzehnder interferometric nh3 gas sensor based on graphene/microfiber hybrid waveguide. *Sensors and Actuators B: Chemical*, 194:142–148, 2014. URL: https://www.sciencedirect.com/science/article/pii/S0925400513015669, doi:10.1016/j.snb.2013.12.085.

[19] Byung-Su Joo, Jeung-Soo Huh, and Duk-Dong Lee. Fabrication of polymer saw sensor array to classify chemical warfare agents. *Sensors and Actuators B: Chemical*, 121(1):47–53, 2007. Special Issue: 25th Anniversary of Sensors and Actuators B: Chemical. URL: https://www.sciencedirect.com/science/article/pii/S0925400506006228, doi:10.1016/j.snb.2006.09.013.

[20] F. Schedin, A. K. Geim, S. V. Morozov, E. W. Hill, P. Blake, M. I. Katsnelson, and K. S. Novoselov. Detection of individual gas molecules adsorbed on graphene. *Nature Materials*, 6(9):652–655, 2007. doi:10.1038/nmat1967.

[21] Sergey Rumyantsev, Guanxiong Liu, Michael S. Shur, Radislav A. Potyrailo, and Alexander A. Balandin. Selective gas sensing with a single pristine graphene transistor. *Nano Letters*, 12(5):2294–2298, 2012. PMID: 22506589. arXiv:https://doi.org/10.1021/nl3001293, doi:10.1021/nl3001293.

[22] Hai Hu, Xiaoxia Yang, Xiangdong Guo, Kaveh Khaliji, Sudipta Romen Biswas, F. Javier García de Abajo, Tony Low, Zhipei Sun, and Qing Dai. Gas identification with graphene plasmons. *Nature Communications*, 10(1):1131, 2019. doi:10.1038/s41467-019-09008-0.

[23] Xiaohui Tang, Nathalie Mager, Beatrice Vanhorenbeke, Sophie Hermans, and Jean-Pierre Raskin. Defect-free functionalized graphene sensor for formaldehyde detection. *Nanotechnology*, 28(5):055501, dec 2016. URL: https://

dx.doi.org/10.1088/1361-6528/28/5/055501, doi:10.1088/1361-6528/28/5/055501.

[24] Byungjin Cho, Jongwon Yoon, Sung Kwan Lim, Ah Ra Kim, Dong-Ho Kim, Sung-Gyu Park, Jung-Dae Kwon, Young-Joo Lee, Kyu-Hwan Lee, Byoung Hun Lee, Heung Cho Ko, and Myung Gwan Hahm. Chemical sensing of 2d graphene/mos heterostructure device. *ACS Applied Materials & Interfaces*, 7(30):16775–16780, 2015. doi:10.1021/acsami.5b04541.

[25] Ahmad N. Abbas, Bilu Liu, Liang Chen, Yuqiang Ma, Sen Cong, Noppadol Aroonyadet, Marianne Köpf, Tom Nilges, and Chongwu Zhou. Black phosphorus gas sensors. *ACS Nano*, 9(5):5618–5624, 2015. PMID: 25945545. arXiv:https://doi.org/10.1021/acsnano.5b01961, doi:10.1021/acsnano.5b01961.

[26] Rajat Kanti Paul, Sushmee Badhulika, Nuvia M. Saucedo, and Ashok Mulchandani. Graphene nanomesh as highly sensitive chemiresistor gas sensor. *Analytical Chemistry*, 84(19):8171–8178, 2012. doi:10.1021/ac3012895.

[27] Jian Lin, Jiebin Zhong, Jennifer Reiber Kyle, Miroslav Penchev, Mihri Ozkan, and Cengiz S. Ozkan. Molecular absorption and photodesorption in pristine and functionalized large-area graphene layers. *Nanotechnology*, 22(35):355701, 2011. doi:10.1088/0957-4484/22/35/355701.

[28] Jeremy T. Robinson, F. Keith Perkins, Eric S. Snow, Zhongqing Wei, and Paul E. Sheehan. Reduced graphene oxide molecular sensors. *Nano Letters*, 8(10):3137–3140, 2008. doi:10.1021/nl8013007.

[29] Mana Sriyudthsak, Arporn Teeramongkolrasasmee, and Toyosaka Moriizumi. Radial basis neural networks for identification of volatile organic compounds. *Sensors and Actuators B: Chemical*, 65(1):358–360, 2000. URL: https://www.sciencedirect.com/science/article/pii/S0925400599004001, doi:10.1016/S0925-4005(99)00400-1.

[30] Sergey Rumyantsev, G Liu, W Stillman, Michael Shur, and Alexander Balandin. Electrical and noise characteristics of graphene field-effect transistors: Ambient effects and noise sources. *Journal of physics. Condensed matter : an Institute of Physics journal*, 22:395302, 10 2010. doi:10.1088/0953-8984/22/39/395302.

[31] Valeriy Sokolov, V. Kochelap, and K. Kim. Generation-recombination noise in bipolar graphene. *Journal of Applied Physics*, 110:044327–044327, 08 2011. doi:10.1063/1.3626820.

[32] Alexander A. Balandin. Review of the low-frequency 1/f noise in graphene devices. *Nature Nanotechnology*, 8(8):549–555, 2013. doi:10.1038/nnano.2013.144.

[33] Qinghui Shao, Guanxiong Liu, Desalegne Teweldebrhan, Alexander Balandin, Sergey Rumyantsev, Michael Shur, and Dong Yan. Flicker noise in bilayer graphene transistors. *Electron Device Letters, IEEE*, 30:288 – 290, 04 2009. doi:10.1109/LED.2008.2011929.

[34] Wonjun Shin, Seongbin Hong, Yujeong Jeong, Gyuweon Jung, Jinwoo Park, Donghee Kim, Kangwook Choi, Hunhee Shin, Ryun-Han Koo, Jae-Joon Kim, and Jong-Ho Lee. Low-frequency noise in gas sensors: A review. *Sensors and Actuators B: Chemical*, 383:133551, 2023. URL: https://www.sciencedirect.com/science/article/pii/S0925400523002666, doi:10.1016/j.snb.2023.133551.

[35] Cosimo Anichini, Wlodzimierz Czepa, Dawid Pakulski, Alessandro Aliprandi, Artur Ciesielski, and Paolo Samorì. Chemical sensing with 2D materials. *Chemical Society Reviews*, 47(13):4860–4908, June 2018. URL: https://hal.science/hal-04577124, doi:10.1039/c8cs00417j.

[36] Kazi Rafsanjani Amin and Aveek Bid. Graphene as a sensor. *Current Science*, 107(3):430–436, 2014. URL: http://www.jstor.org/stable/24103495.

[37] Md. Zahid Hossain, Sergey Rumyantsev, Michael S. Shur, and Alexander A. Balandin. Reduction of 1/f noise in graphene after electron-beam irradiation. *Applied Physics Letters*, 102(15), April 2013. URL: http://dx.doi.org/10.1063/1.4802759, doi:10.1063/1.4802759.

[38] L. DiCarlo, J. R. Williams, Yiming Zhang, D. T. McClure, and C. M. Marcus. Shot noise in graphene. *Phys. Rev. Lett.*, 100:156801, Apr 2008. URL: https://link.aps.org/doi/10.1103/PhysRevLett.100.156801, doi:10.1103/PhysRevLett.100.156801.

[39] P. R. Wallace. The band theory of graphite. *Phys. Rev.*, 71:622–634, May 1947. URL: https://link.aps.org/doi/10.1103/PhysRev.71.622, doi:10.1103/PhysRev.71.622.

[40] Santosh Tiwari, Raghvendra Mishra, Sung ha, and Andrzej Huczko. Evolution of graphene oxide and graphene: From imagination to industrialization (history of graphene 1845 to 2010). *ChemNanoMat*, 4, 04 2018. doi:10.1002/cnma.201800089.

[41] K. S. Novoselov, A. K. Geim, S. V. Morozov, D. Jiang, Y. Zhang, S. V. Dubonos, I. V. Grigorieva, and A. A. Firsov. Electric field effect in atomically thin carbon films. *Science*, 306(5696):666–669, 2004. URL: https://www.science.org/doi/abs/10.1126/science.1102896, arXiv:https://www.science.org/doi/pdf/10.1126/science.1102896, doi:10.1126/science.1102896.

[42] A. K. Geim and K. S. Novoselov. The rise of graphene. *Nature Materials*, 6(3):183–191, 2007. doi:10.1038/nmat1849.

[43] Minghui Yang and Shaoqin Gong. Immunosensor for the detection of cancer biomarker based on percolated graphene thin film. *Chemical Communications*, 46(31):5796–5798, 2010. doi:10.1039/c0cc00675k.

[44] Huamin Chen, Yun Xu, Jiushuang Zhang, Weitong Wu, and Guofeng Song. Enhanced stretchable graphene-based triboelectric nanogenerator via control of surface nanostructure. *Nano Energy*, 58:304–311, 2019. URL: https://www.sciencedirect.com/science/article/pii/S2211285519300382, doi:10.1016/j.nanoen.2019.01.029.

[45] Y. Zheng, X. Zhou, H. Luo, H. Ling, W. Mo, H. Fang, C. Shen, J. Lei, M. Sun, and J. Li. Efficient removal of congo red with graphene aerogel derived from recycled anode of lithium-ion battery. *International Journal of Environmental Science and Technology*, 18(12):3995–4006, 2021. doi:10.1007/s13762-020-03114-z.

[46] Yu Shang and Dong Zhang. Preparation and thermal properties of graphene oxidemicroencapsulated phase change materials. *Nanoscale and Microscale Thermophysical Engineering*, 20(3-4):147–157, 2016. arXiv:https://doi.org/10.1080/15567265.2016.1236865, doi:10.1080/15567265.2016.1236865.

[47] Popi Karaolia, Irene Michael-Kordatou, Evroula Hapeshi, Catherine Drosou, Yannis Bertakis, Dimitris Christofilos, Gerasimos S. Armatas, Labrini Sygellou, Thomas Schwartz, Nikolaos P. Xekoukoulotakis, and Despo Fatta-Kassinos. Removal of antibiotics, antibiotic-resistant bacteria and their associated genes by graphene-based tio2 composite photocatalysts under solar radiation in urban wastewaters. *Applied Catalysis B: Environmental*, 224:810–824, 2018. URL: https://www.sciencedirect.com/science/article/pii/S0926337317310755, doi:10.1016/j.apcatb.2017.11.020.

[48] Dong Hee Shin, Chan Wook Jang, Ha Seung Lee, Sang Woo Seo, and Suk-Ho Choi. Semitransparent flexible organic solar cells employing doped-graphene layers as anode and cathode electrodes. *ACS Applied Materials & Interfaces*, 10(4):3596–3601, 2018. doi:10.1021/acsami.7b16730.

[49] Fang Ye, Qiang Song, Zhenchuang Zhang, Wei Li, Shouyang Zhang, Xiaowei Yin, Yuzhao Zhou, Huiwen Tao, Yongsheng Liu, Laifei Cheng, et al. Direct growth of edge-rich graphene with tunable dielectric properties in porous si3n4 ceramic for broadband high-performance microwave absorption. *Advanced Functional Materials*, 28(17):1707205, 2018.

[50] Ming Liu, Xiaobo Yin, Erick Ulin-Avila, Baisong Geng, Thomas Zentgraf, Long Ju, Feng Wang, and Xiang Zhang. A graphene-based broadband optical modulator. *Nature*, 474(7349):64–67, 2011. doi:10.1038/nature10067.

[51] Matthew J. Allen, Vincent C. Tung, and Richard B. Kaner. Honeycomb carbon: A review of graphene. *Chemical Reviews*, 110(1):132–145, 2010. PMID: 19610631. arXiv:https://doi.org/10.1021/cr900070d, doi:10.1021/cr900070d.

[52] Rajesh Ghosh, Mohammed Aslam, and Hemen Kalita. Graphene derivatives for chemiresistive gas sensors: A review. *Materials Today Communications*, 30:103182, 2022. URL: https://www.sciencedirect.com/science/article/pii/S2352492822000599, doi:10.1016/j.mtcomm.2022.103182.

[53] Filiberto Ricciardella, Sten Vollebregt, Tiziana Polichetti, Mario Miscuglio, Brigida Alfano, Maria L. Miglietta, Ettore Massera, Girolamo Di Francia, and Pasqualina M. Sarro. Effects of graphene defects on gas sensing properties towards no_2 detection. *Nanoscale*, 9(18):6085–6093, 2017. doi:10.1039/c7nr01120b.

[54] Jae-Hyoung Lee, Akash Katoch, Sun-Woo Choi, Jae-Hun Kim, Hyoun Woo Kim, and Sang Sub Kim. Extraordinary improvement of gas-sensing performances in sno_2 nanofibers due to creation of local pn heterojunctions by loading reduced graphene oxide nanosheets. *ACS Applied Materials & Interfaces*, 7(5):3101–3109, 2015. doi:10.1021/am5071656.

[55] , Jeong Hu Young, Dae-Sik Lee, Choi Choon-Gi, and . Flexible no_2 gas sensor using multilayer graphene films by chemical vapor deposition. *Carbon Letters*, 14:186–189, Jul 2013. doi:10.5714/CL.2013.14.3.186.

[56] Zuquan Wu, Xiangdong Chen, Shibu Zhu, Zuowan Zhou, Yao Yao, Wei Quan, and Bin Liu. Room temperature methane sensor based on graphene nanosheets/polyaniline nanocomposite thin film. *IEEE Sensors Journal*, 13(2):777–782, 2013. doi:10.1109/JSEN.2012.2227597.

[57] Tran Thanh Tung, Md J Nine, Melinda Krebsz, Tibor Pasinszki, Campbell J Coghlan, Diana NH Tran, and Dusan Losic. Recent advances in sensing applications of graphene assemblies and their composites. *Advanced Functional Materials*, 27(46):1702891, 2017.

[58] K. S. Novoselov, A. K. Geim, S. V. Morozov, D. Jiang, M. I. Katsnelson, I. V. Grigorieva, S. V. Dubonos, and A. A. Firsov. Two-dimensional gas of massless dirac fermions in graphene. *Nature*, 438(7065):197–200, 2005. doi:10.1038/nature04233.

[59] L. Pauling. *The Nature of the Chemical Bond and the Structure of Molecules and Crystals: An Introduction to Modern Structural Chemistry*. George Fisher Baker non-resident lectureship in chemistry at Cornell University. Cornell University Press, 1960. URL: https://books.google.sk/books?id=L-1K9HmKmUUC.

[60] Maha Rhouma. *Modeling and simulation of composite plasmonic structures based on graphene and metals*. PhD thesis, 02 2021.

[61] A. H. Castro Neto, F. Guinea, N. M. R. Peres, K. S. Novoselov, and A. K. Geim. The electronic properties of graphene. *Rev. Mod. Phys.*, 81:109–162, Jan 2009. URL: https://link.aps.org/doi/10.1103/RevModPhys.81.109, doi:10.1103/RevModPhys.81.109.

[62] Daniel R. Cooper, Benjamin D'Anjou, Nageswara Ghattamaneni, Benjamin Harack, Michael Hilke, Alexandre Horth, Norberto Majlis, Mathieu Massicotte, Leron Vandsburger, Eric Whiteway, and Victor Yu. Experimental review of graphene, 2011. URL: https://arxiv.org/abs/1110.6557, arXiv:1110.6557.

[63] Mark S. Oliver. Introduction to the physical properties of graphene. In *Pissofpiss*, 2008. URL: https://api.semanticscholar.org/CorpusID:46437115.

[64] Bing-Sui Lu. The casimir effect in topological matter, 05 2021. doi:10.3390/universe7070237.

[65] E. Andrei. Tight-binding model notes. https://www.physics.rutgers.edu/~eandrei/chengdu/reading/tight-binding.pdf. Accessed: 2024-12-19.

[66] Nima Chamanara and Christophe Caloz. Graphene magnetoplasmonic principles, structures and devices. In *2015 9th European Conference on Antennas and Propagation (EuCAP)*, pages 1–2, 2015. URL: https://ia801809.us.archive.org/14/items/articles_fermat/Chamanara-ART-2015-Vol10-Jul_Aug-002.pdf.

[67] Antonio Maffucci and Giovanni Miano. Electrical properties of graphene for interconnect applications. *Applied Sciences*, 4(2):305–317, 2014. URL: https://www.mdpi.com/2076-3417/4/2/305, doi:10.3390/app4020305.

[68] Sergey Mikhailov. *Frequency Mixing Effects in Graphene*, pages 519–534. InTech, 03 2011. doi:10.5772/13832.

[69] Anthony Gerges Geha, Yago aguado, and Modou B. Nadiaye. Graphene, a material with exceptional electronic properties, 2024. URL: https://arxiv.org/abs/2402.00599, arXiv:2402.00599.

[70] Carsten Winter and Luca Bignardi. Time-resolved electron spectroscopy in graphene with high harmonic radiation. https://www.uni-muenster.de/Physik.PI/Zacharias/en/research/graphene/graphene.html. Accessed: 2024-12-19.

[71] Asmahan Anan, Sulaiman Tiryaki, Mohammad El-Said, and Ayham Shaer. *The Electronic Band pStructure of Graphene and Carbon Nanotubes*. PhD thesis, An-Najah National University, 2013. URL: https://api.semanticscholar.org/CorpusID:29107347.

[72] Gao Yang, Lihua Li, Lee W.B., and Man Ng. Structure of graphene and its disorders: a review. *Science and Technology of Advanced Materials*, 19:613–648, 08 2018. doi:10.1080/14686996.2018.1494493.

[73] S. V. Morozov, K. S. Novoselov, M. I. Katsnelson, F. Schedin, D. C. Elias, J. A. Jaszczak, and A. K. Geim. Giant intrinsic carrier mobilities in graphene and its bilayer. *Phys. Rev. Lett.*, 100:016602, Jan 2008. URL: https://link.aps.org/doi/10.1103/PhysRevLett.100.016602, doi:10.1103/PhysRevLett.100.016602.

[74] B. Shubha, Praveen B M, and V. Bhat. Graphene - calculation of specific surface area. *International Journal of Applied Engineering and Management Letters*, pages 91–97, 02 2023. doi:10.47992/IJAEML.2581.7000.0168.

[75] Alexander A. Balandin, Suchismita Ghosh, Wenzhong Bao, Irene Calizo, Desalegne Teweldebrhan, Feng Miao, and Chun Ning Lau. Superior thermal conductivity of single-layer graphene. *Nano Letters*, 8(3):902–907, 2008.

PMID: 18284217. arXiv:https://doi.org/10.1021/nl0731872, doi:10.1021/nl0731872.

[76] D. S. L. Abergel, A. Russell, and Vladimir I. Falko. Visibility of graphene flakes on a dielectric substrate. *Applied Physics Letters*, 91(6), August 2007. URL: http://dx.doi.org/10.1063/1.2768625, doi:10.1063/1.2768625.

[77] Hongtao Liu, Yunqi Liu, and Daoben Zhu. Chemical doping of graphene. *J. Mater. Chem.*, 21:3335–3345, 2011. URL: http://dx.doi.org/10.1039/C0JM02922J, doi:10.1039/C0JM02922J.

[78] Chowdhury Al-Amin, phani kiran Vabbina, Mustafa Karabiyik, Raju Sinha, Chunlei Wang, and Nezih Pala. Bandgap engineering of single layer graphene by randomly distributed nanoparticles. *Journal of Materials Science: Materials in Electronics*, 27, 07 2016. doi:10.1007/s10854-016-4722-z.

[79] Katsnelson, M. I. Zitterbewegung, chirality, and minimal conductivity in graphene. *Eur. Phys. J. B*, 51(2):157–160, 2006. doi:10.1140/epjb/e2006-00203-1.

[80] V. P. Gusynin and S. G. Sharapov. Unconventional integer quantum hall effect in graphene. *Phys. Rev. Lett.*, 95:146801, Sep 2005. URL: https://link.aps.org/doi/10.1103/PhysRevLett.95.146801, doi:10.1103/PhysRevLett.95.146801.

[81] M. V. Bashevoy, F. Jonsson, A. V. Krasavin, N. I. Zheludev, Y. Chen, and M. I. Stockman. Generation of traveling surface plasmon waves by free-electron impact. *Nano Letters*, 6(6):1113–1115, 2006. doi:10.1021/nl060941v.

[82] Alexander Zhu and Ertugrul Cubukcu. Graphene nanophotonic sensors. *2D Materials*, 2:032005, 09 2015. doi:10.1088/2053-1583/2/3/032005.

[83] Qingbin Zheng, Jeng hun Lee, Xi Shen, Xiaodong Chen, and Jang-Kyo Kim. Graphene-based wearable piezoresistive physical sensors. *Materials Today*, 36:158–179, 2020. URL: https://www.sciencedirect.com/science/article/pii/S1369702119308776, doi:10.1016/j.mattod.2019.12.004.

[84] Nacir Tit, Khadija Said, Nadin M. Mahmoud, Summayya Kouser, and Zain H. Yamani. Ab-initio investigation of adsorption of co and co2 molecules on graphene: Role of intrinsic defects on gas sensing. *Applied Surface Science*, 394:219–230, 2017. URL: https://www.sciencedirect.com/science/article/pii/S0169433216321687, doi:10.1016/j.apsusc.2016.10.052.

[85] Khurram Shehzad, Tianjin Shi, Akeel Qadir, Xia Wan, Hongwei Guo, Ayaz Ali, Weipeng Xuan, Hua Xu, Zhongze Gu, Xinsheng Peng, Jin Xie, Litao Sun, Qiyuan He, Zhen Xu, Chao Gao, You Seung Rim, Yaping Dan, Tawfique Hasan, Pingheng Tan, Erping Li, Wenyan Yin, Zhiyuan Cheng, Bin Yu, Yang Xu, Jikui Luo, and Xiangfeng Duan. Designing an efficient multimode environmental sensor based on graphenesilicon heterojunction. *Advanced Materials Technologies*, 2(4), April 2017. Publisher Copyright: © 2017 WILEY-VCH Verlag GmbH & Co. KGaA, Weinheim. doi:10.1002/admt.201600262.

[86] Anderson D. Smith, Karim Elgammal, Frank Niklaus, Anna Delin, Andreas C. Fischer, Sam Vaziri, Fredrik Forsberg, Mikael Råsander, Håkan Hugosson, Lars Bergqvist, Stephan Schröder, Satender Kataria, Mikael Östling, and Max C. Lemme. Resistive graphene humidity sensors with rapid and direct electrical readout. *Nanoscale*, 7:19099–19109, 2015. URL: http://dx.doi.org/10.1039/C5NR06038A, doi:10.1039/C5NR06038A.

[87] Manu S. Mannoor, Hu Tao, Jefferson D. Clayton, Amartya Sengupta, David L. Kaplan, Rajesh R. Naik, Naveen Verma, Fiorenzo G. Omenetto, and Michael C. McAlpine. Graphene-based wireless bacteria detection on tooth enamel. *Nature Communications*, 3(1):763, 2012. doi:10.1038/ncomms1767.

[88] Alexander Sinitskii, Ayrat Dimiev, David A. Corley, Alexandra A. Fursina, Dmitry V. Kosynkin, and James M. Tour. Kinetics of diazonium functionalization of chemically converted graphene nanoribbons. *ACS Nano*, 4(4):1949–1954, 2010. doi:10.1021/nn901899j.

[89] Richa Sharma, Joon Hyun Baik, Chrisantha J. Perera, and Michael S. Strano. Anomalously large reactivity of single graphene layers and edges toward electron transfer chemistries. *Nano Letters*, 10(2):398–405, 2010. PMID: 20055430. arXiv:https://doi.org/10.1021/nl902741x, doi:10.1021/nl902741x.

[90] Usman Latif and Franz L. Dickert. Graphene hybrid materials in gas sensing applications. *Sensors*, 15(12):30504–30524, 2015. URL: https://www.mdpi.com/1424-8220/15/12/29814, doi:10.3390/s151229814.

[91] Xinxing Zhan, Xin Tong, Manqi Gu, Juan Tian, Zijian Gao, Liying Ma, Yadian Xie, Zhangsen Chen, Hariprasad Ranganathan, Gaixia Zhang, and Shuhui Sun. Phosphorus-doped graphene electrocatalysts for oxygen reduction reaction. *Nanomaterials*, 12:1141, 03 2022. doi:10.3390/nano12071141.

[92] Qiyuan He, Zhiyuan Zeng, Zongyou Yin, Hai Li, Shixin Wu, Xiao Huang, and Hua Zhang. Fabrication of flexible mos 2 thin-film transistor arrays for practical gas-sensing applications. *Small (Weinheim an der Bergstrasse, Germany)*, 8:2994–9, 10 2012. doi:10.1002/smll.201201224.

[93] Sake Wang, Jyh-Pin Chou, Chongdan Ren, Hongyu Tian, Jin Yu, Changlong Sun, Yujing Xu, and Minglei Sun. Tunable schottky barrier in graphene/graphene-like germanium carbide van der waals heterostructure. *Scientific Reports*, 9(1):5208, 2019. doi:10.1038/s41598-019-40877-z.

[94] Tomá Blecha, Zuzana Vlková ivcová, Farjana J. Sonia, Martin Mergl, Oleksandr Volochanskyi, Michal Bodnár, Pavel Rous, Kenichiro Mizohata, Martin Kalbá, and Otakar Frank. Electrical contact resistance of large-area graphene on pre-patterned cu and au electrodes. *Nanomaterials*, 12(24), 2022. URL: https://www.mdpi.com/2079-4991/12/24/4444, doi:10.3390/nano12244444.

[95] Honglin Sun, Ting Huang, Md Masruck Alam, Jingwei Li, Dong Wook Jang, Tianle Wang, Haohan Chen, Yi-Ping Ho, and Zhaoli Gao. Minimizing contact resistance and flicker noise in micro graphene hall sensors using persistent carbene modified gold electrodes. *ACS Applied Materials & Interfaces*, 16(24):31473–31479, 2024. doi:10.1021/acsami.4c05451.

[96] G. Giovannetti, P. A. Khomyakov, G. Brocks, V. M. Karpan, J. van den Brink, and P. J. Kelly. Doping graphene with metal contacts. *Physical Review Letters*, 101(2), July 2008. URL: http://dx.doi.org/10.1103/PhysRevLett.101.026803, doi:10.1103/physrevlett.101.026803.

[97] Alexandra Carvalho, Min Wang, Xi Zhu, Aleksandr S. Rodin, Haibin Su, and Antonio H. Castro Neto. Phosphorene: from theory to applications. *Nature Reviews Materials*, 1(11):16061, 2016. doi:10.1038/natrevmats.2016.61.

[98] Péter Vancsó, Gábor Zsolt Magda, János Pet, Ji-Young Noh, Yong-Sung Kim, Chanyong Hwang, László P. Biró, and Levente Tapasztó. The intrinsic defect structure of exfoliated mos single layers revealed by scanning tunneling microscopy. *Scientific Reports*, 6:29726, 2016. doi:10.1038/srep29726.

[99] Hao Qiu, Tao Xu, Zilu Wang, Wei Ren, Haiyan Nan, Zhenhua Ni, Qian Chen, Shijun Yuan, Feng Miao, Fengqi Song, Gen Long, Yi Shi, Litao Sun, Jinlan Wang, and Xinran Wang. Hopping transport through defect-induced localized states in molybdenum disulphide. *Nature Communications*, 4:2642, 2013. doi:10.1038/ncomms3642.

[100] Hai Li, Zongyou Yin, Qiyuan He, (Colin) Hong Li, Xiao Huang, Gang Lu, Derrick Fam, Alfred Tok, Qing Zhang, and Hua Zhang. Fabrication of single- and multilayer mos2 film-based field-effect transistors for sensing no at room temperature. *Small (Weinheim an der Bergstrasse, Germany)*, 8:63–7, 01 2012. doi:10.1002/smll.201101016.

[101] Soo-Yeon Cho, Seon Joon Kim, Youhan Lee, Jong-Seon Kim, Woo-Bin Jung, Hae-Wook Yoo, Jihan Kim, and Hee-Tae Jung. Highly enhanced gas adsorption properties in vertically aligned mos layers. *ACS Nano*, 9(9):9314–9321, 2015. doi:10.1021/acsnano.5b04504.

[102] J. B. Johnson. Thermal agitation of electricity in conductors. *Phys. Rev.*, 32:97–109, Jul 1928. URL: https://link.aps.org/doi/10.1103/PhysRev.32.97, doi:10.1103/PhysRev.32.97.

[103] Yotsarayuth Seekaew, Anurat Wisitsoraat, Ditsayut Phokharatkul, and Chatchawal Wongchoosuk. Room temperature toluene gas sensor based on tio2 nanoparticles decorated 3d graphene-carbon nanotube nanostructures. *Sensors and Actuators B: Chemical*, 279:69–78, 2019. URL: https://www.sciencedirect.com/science/article/pii/S0925400518317301, doi:10.1016/j.snb.2018.09.095.

[104] Vasilios Georgakilas, Michal Otyepka, Athanasios B. Bourlinos, Vimlesh Chandra, Namdong Kim, K. Christian Kemp, Pavel Hobza, Radek Zboril, and Kwang S. Kim. Functionalization of graphene: Covalent and non-covalent approaches, derivatives and applications. *Chemical Reviews*, 112(11):6156–6214, 2012. doi:10.1021/cr3000412.

[105] Caterina Soldano, Ather Mahmood, and Erik Dujardin. Production, properties and potential of graphene. *Carbon*, 48(8):2127–2150, 2010. URL: https://www.sciencedirect.com/science/article/pii/S0008622310000928, doi:10.1016/j.carbon.2010.01.058.

[106] Yong-Hui Zhang, Yabin Chen, Kai-Ge Zhou, Caihong Liu, Jing Zeng, Hao-Li Zhang, and Yong Peng. Improving gas sensing properties of graphene by introducing dopants and defects: A first-principles study. *Nanotechnology*, 20:185504, 06 2009. doi:10.1088/0957-4484/20/18/185504.

[107] Gugang Chen, Tereza Paronyan, and Avetik Harutyunyan. Sub-ppt gas detection with pristine graphene. *Applied Physics Letters*, 101, 08 2012. doi:10.1063/1.4742327.

[108] R. Pearce, T. Iakimov, M. Andersson, L. Hultman, A. Lloyd Spetz, and R. Yakimova. Epitaxially grown graphene based gas sensors for ultra sensitive no2 detection. *Sensors and Actuators B: Chemical*, 155(2):451–455, 2011. URL: https://www.sciencedirect.com/science/article/pii/S0925400510009767, doi:10.1016/j.snb.2010.12.046.

[109] Aamir Ahmed, Anoop Chib, Sheng-Joue Young, Vinay Gupta, Maheshwary Singh, and Sandeep Arya. Synthesis techniques and advances in sensing applications of reduced graphene oxide (rgo) composites: A review. *Composites Part A Applied Science and Manufacturing*, 165:107373, 12 2022. doi:10.1016/j.compositesa.2022.107373.

[110] Maurizio Donarelli and L. Ottaviano. 2d materials for gas sensing applications: A review on graphene oxide, mos2, ws2 and phosphorene. *Sensors*, 18:3638, 10 2018. doi:10.3390/s18113638.

[111] Safae Sali, Hamish R. Mackey, and Ahmed A. Abdala. Effect of graphene oxide synthesis method on properties and performance of polysulfone-graphene oxide mixed matrix membranes. *Nanomaterials (Basel)*, 9(5):769, 2019. doi:10.3390/nano9050769.

[112] Adéla Jiíková, Ondej Jankovský, Zdenk Sofer, and David Sedmidubský. Synthesis and applications of graphene oxide. *Materials (Basel)*, 15(3):920, 2022. doi:10.3390/ma15030920.

[113] Jae Hong Choi, Junghyun Lee, Mirang Byeon, Tae Eun Hong, Hyesung Park, and Chang Young Lee. Graphene-based gas sensors with high sensitivity and minimal sensor-to-sensor variation. *ACS Applied Nano Materials*, 3(3):2257–2265, 2020. doi:10.1021/acsanm.9b02378.

[114] Jun Ma, Miao Zhang, Linxi Dong, Yinbo Sun, Yanjie Su, Zhongying Xue, and Zengfeng Di. Gas sensor based on defective graphene/pristine graphene hybrid towards high sensitivity detection of no 2. *AIP Advances*, 9:075207, 07 2019. doi:10.1063/1.5099511.

List of appendices

A Python Code for Data Processing

This appendix contains the Python code used for data processing. It is a part of the whole code provided in the attachment.

Code Listing

Listing A.1: Python script for data processing

```
def Agilent_run1FNoise(inst):
# TRACE COORDINATE SETTINGS
inst.write("DISPlay:TRACe:X:SPACing␣LOGarithmic")  # Magnitude: LOG

# INSTRUMENT MODE CONFIGURATION
Agilent_35670A_measurement_mode(inst_spectr_analyzer, "Octave")  # Octave analysis
inst.write("INPut2:STATe␣OFF")  # Channels: 1 (disable second channel)
# TIME CAPTURE subwindow
inst.write("SENSe:FEED␣INPut")  # Measure from: Input
inst.write("DISPlay:TCAPture:ENVelope␣OFF")  # Envelope: OFF

Agilent_35670A_TraceCoordType(inst, "Log")
Agilent_35670A_set_Y_units_amplitude_type(inst, "RMS")
Agilent_35670A_set_Y_units(inst, "V/rthz")

# AVERAGING CONFIGURATION
Agilent_35670A_setAvgType(inst,"Exponential") # Type: Linear
inst.write("SENSe:AVERage:TIME␣2.0")  # Time: 2s
Agilent_35670A_setAvgRepeat(inst, True)  # Repeat ON
Agilent_35670A_setAvgImpulse(inst, False)
Agilent_35670A_setConfidence(inst, 0.5)
inst.write("SENSe:AVERage:HOLD␣OFF")  # OFF|0|MAXimum|MINimum

# FREQUENCY CONFIGURATION
inst.write("SENSe:FREQuency:STARt␣3.1912")  # Start: 3.1912 Hz
inst.write("SENSe:FREQuency:STOP␣6168.8")  # Stop: 6.1688 kHz
Agilent_35670A_octave(inst, 1/12)

```

```
Agilent_35670A_Supply(inst, 1, 3.9858, "VPK")
Agilent_35670A_Range(inst, "Autorange", "UpDown")
Agilent_35670A_gnd_or_float(inst, 1, "GND") #Input LOW: GND
Agilent_35670A_coupling(inst, 1, "AC") #Coupling: AC
Agilent_35670A_antialias(inst, 1, False) #Antialias: OFF
Agilent_35670A_a_wt_fltr(inst, 1, False) #A WT FLTR: OFF
Agilent_35670A_ICP_Supply(inst, 1, False) #ICP Supply: OFF

# TRACE AND DISPLAY SETTINGS
inst.write("CALCulate1:ACTive␣A")  # Active trace: A
inst.write("DISPlay:FORMat␣SINGle")  # Display format: Single
inst.write("DISPlay:TRACe:GRATicule:GRID␣ON")  # GRID: ON
inst.write("DISPlay:TRACe:BPOWer␣OFF")  # Overall: OFF
inst.write("DISPlay:TRACe:APOWer␣OFF")  # Weighted: OFF
# Phase lag: OFF
inst.write("DISPlay:TRACe:LABel␣'1f␣Sum'")  # TRACE TITLE
inst.write("DISPlay:TRACe:LABel:DEFault␣OFF")  # DFLT TITL:
    OFF

# SCALE SETTINGS
inst.write("DISPlay:TRACe:Y:SCALe:PDIV␣3")  # Y PER DIV (
    Decades)
inst.write("DISPlay:TRACe:X:SCALe:AUTO␣ONCE")  # FULL SCALE
inst.write("DISPlay:TRACe:Y:SCALe:AUTO␣ON")  # Autoscale: OFF
```

B Content of the electronic attachment

The electronic attachment archive is published at the Brno University of Technology website along with this thesis. This archive contains all the automated software used to produce the measurements. You can use and modify this software if you like to reproduce the measurements or if you want to modernize or automate your own measurement pipeline. You need to pre-install the packages required in the code, but that is easy. Also, *sweptsine_capture.py* contains a registry module, which is relevant only for windows. I hope it will be useful to you, but these programs have their own data structures, into which they store the measurements. These programs are to work together as a pipeline. First capture and see the data and later visualize the data. If you change the capture program's measurements data structure, you also need to modify the visualizer accordingly.

```
/ ..... root of the attached archive
├── DC_capture.py ..... Automated DC sweep
├── resistance_curve_capture.py ..... Live resistance capture
├── resistances_in_time_viewer.py ..... Capture section viewer
├── spotplots_capture.py ..... Press to save capture
├── spotplots_viewer.py ..... Visualizes many plots in one figure
├── sweptsine_capture.py ..... Capture and show a swept sine
├── sweptsine_splitter.py ..... Split swept sine data file
├── sweptsine_visualizer.py ..... show the swept sine data in a figure
├── waterfall_capture.py ..... Capture the waterfall
├── waterfalls_to_png.py ..... Produces PNG images from from the data file
└── waterfalls_to_svg.py ..... Produces SVG images from from the data file
```

C Conference paper: Noise Characterization of Graphene Sensors

Noise Characterization of Graphene Sensors

Patrik Staroň[1], Robert Macků[1], Petr Sedlák[1], Nikola Papež[1], Ramazanov Shihkgasan[1], Farid Orudzhev[1], Mohammed A. Al-Anber[2], Dinara Sobola[1*]

[1]*Department of Physics, Faculty of Electrical Engineering and Communication, Brno University of Technology, Brno, Czech Republic*

[2]*Laboratory of Inorganic Materials and Polymers, Department of Chemistry, Faculty of Sciences, Mutah University, Al-Karak, Jordan*

*Corresponding author: sobola@vut.cz

***Abstract*—This study investigates the operational dynamics and challenges of graphene-based sensors, focusing on refining data measurement and processing techniques to ensure accurate identification of chemical compounds in different gas atmospheres. The research highlights the importance of sensor cleanliness and the use of analytes with physical properties matching the measurement environment. The cleaning process involves using isopropyl alcohol and heating the sensor to 70°C, with cooling facilitated by the sensor's low thermal mass. This study also explores injecting saturated liquid onto the sensor to eliminate issues related to pressure and gas composition variations. Experimental methods include measuring the graphene sensor in the spectral domain using a setup that minimizes resistive noise and optimizes sensor response. Key variables such as voltage, resistor noise characteristics, signal path to the amplifier, system temperature, and bonding materials are fine-tuned to achieve the lowest parasitic noise. Time-domain and frequency-domain measurement techniques are employed to correlate resistance and impedance changes with gas concentrations, respectively.**

Keywords— graphene, noise, spectrum, gas, detection

I. Introduction

A wide range of sectors, including manufacturing, healthcare, and the automotive industry, require accurate assessment of gas mixtures within certain environments. Workspaces handling hazardous materials must adhere to strict safety standards. The only way to identify and measure volatile compounds in the atmosphere is through the use of gas detection technology. Particularly in places prone to fire risks or with poor ventilation, such as mines, there is a critical demand for gas detection systems. Despite the proliferation of gas sensors in the market, they often fall short in terms of precision, accuracy, sensitivity to specific molecules, affordability, among other issues. Graphene, known for its extraordinary characteristics, exhibits exceptional electrical and thermal conductance, superior mechanical robustness, and offers unique optical and structural benefits unmatched by any other substance[1], [2]. These traits suggest graphene's potential in gas detection technology, aiming for unparalleled sensitivity in identifying various gas molecules. However, practical applications reveal graphene's limitations in detecting certain gases and in processing the data obtained from sensors[3], [4].

As sensor resolution increases, the quality of the signal deteriorates. This study delves into the operational dynamics of graphene-based sensors and their associated challenges. The primary objective is to refine the data measurement and processing techniques for a specific graphene sensor across different gas atmospheres, ensuring the output precisely identifies the chemical compounds detected. The interference of noise, particularly at high resolutions, is a significant concern addressed in this thesis, alongside strategies for its mitigation.

Data can be gathered from sensors through various techniques. Some sensors adjust their capacitance in response to gas levels, while most alter their resistance. Theoretically, changes in the sensor's optical state or variations in acoustic wave propagation could also signal the presence of gases. Typically, sensors are equipped with electrodes that connect to the sensing material, facilitating the measurement of its physical attributes. These assessments range in complexity. The focus of this chapter is on the analysis of chemoreceptive gas sensors, including those based on graphene, which pose unique challenges due to their potential sensitivity. Measurements can be conducted across time and frequency domains.

Time-domain measurements involve recording resistance at a specific moment, requiring data analysis to correlate resistance changes with gas concentrations. Frequency-domain measurements, on the other hand, involve assessing the sensing material's impedance at certain frequencies, exploiting predictable shifts in resonance frequencies for gas detection. Noise significantly affects sensor performance; slow reaction times in the sensing material can allow system noise to dominate, potentially skewing results. This low-frequency noise, or 1/f noise, is a known issue in semiconductor sensors and is relevant to graphene-based sensors due to their inherent noise characteristics. In laboratories, gas sensors are often tested with instruments like the 8753ES, which can evaluate resonant frequencies by measuring a resonator's return loss. Alternatively, resistance measurements with a stable current supply are sufficient. Sensor noise primarily arises from two sources: thermal noise and low-frequency noise, with thermal noise being inherent to all devices. In thermal sensors, this noise results from atomic vibrations leading to inconsistent current flow[5].

II. Experimental

The actual schematic proposed for measuring the graphene sensor in spectral domain is shown in Figure 1. This is a setup that allows to push current through the sensor and a resistor, while measuring the voltage on the resistor. The resistor contributes to the noise, but the tweaking the voltage from the battery should decrease the influence of the resistive noise so that the dominant noise is the one from the sensor.

2024 37th International Vacuum Nanoelectronics Conference (IVNC) | 979-8-3503-7976-1/24/$31.00 ©2024 IEEE | DOI: 10.1109/IVNC63480.2024.10652510

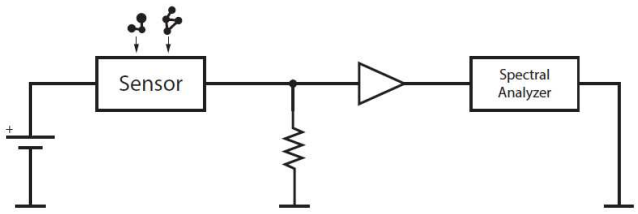

Fig. 1. Diagram of the connections for mesuring the grapene sensor.

By measuring the spectral response of the system while injecting various substances onto the sensor, it is possible to detect the response of the graphene sensing layer to the chemicals it is exposed to. The measurement equipment is very sensitive and it is possible that the resulting information will not be making sense. There are several variables that can be controlled:

- Voltage over the graphene and the resistor.
- The resistor and so its noise characteristics.
- The signal path to the amplifier.
- The temperature of the system.
- The bonding material and metal interfaces.

These variables are need to be fine-tuned in order to achieve lowest parasitic noise for the measurement. Voltage over the graphene will be chosen experimentally. Resistor and its noise should be chosen after setting the voltage threshold[6].

III. CONCLUSIONS

The gas composition, pressure, and temperature have a significant impact on the accuracy of the measurement. To ensure reliable results, it is essential that the sensor be thoroughly cleaned at the beginning of the measurement process. Furthermore, the analyte used should have the same physical properties as the measurement environment for the best possible outcome. The cleaning process involves using isopropyl alcohol to remove any contaminants and raising the sensor's temperature to 70°C. This elevated temperature helps in thoroughly cleaning the sensor. After cleaning, the sensor needs to cool down. However, due to its low thermal mass, this cooling process is relatively quick, minimizing the risk of significant re-contamination. It is important to note that the suggested cleaning temperature of 70°C is not fixed and may be adjusted based on the results obtained from initial measurements.

To address potential issues related to pressure and gas composition, injecting a liquid onto the sensor is an effective method. This approach ensures that the liquid is saturated, thereby eliminating variations in pressure and composition that could otherwise affect the measurement accuracy. This saturation helps maintain consistent conditions, leading to more reliable and accurate measurements.

ACKNOWLEDGMENT

The research described in the paper was financially supported by the Internal Grant Agency of the Brno University of Technology, grant No. FEKT-S-20-6352 and the GACR 23-07384S.

REFERENCES

[1] A. Knápek, J. Sýkora, J. Chlumská, and D. Sobola, "Programmable set-up for electrochemical preparation of STM tips and ultra-sharp field emission cathodes," Microelectron Eng, vol. 173, pp. 42–47, Apr. 2017, doi: 10.1016/J.MEE.2017.04.002.

[2] A. Knápek, D. Sobola, P. Tománek, Z. Pokorná, and M. Urbánek, "Field emission from the surface of highly ordered pyrolytic graphite," Appl Surf Sci, vol. 395, pp. 157–161, Feb. 2017, doi: 10.1016/J.APSUSC.2016.05.002.

[3] D. Sobola, N. Papež, R. Dallaev, S. Ramazanov, D. Hemzal, and V. Holcman, "Characterization of nanoblisters on HOPG surface," Journal of Electrical Engineering, vol. 70, no. 7, pp. 132–136, Dec. 2019, doi: 10.2478/JEE-2019-0055.

[4] A. AlSoud et al., "Electrical properties of epoxy/graphite flakes microcomposite at the percolation threshold concentration," Phys Scr, vol. 99, no. 5, p. 055955, Apr. 2024, doi: 10.1088/1402-4896/AD3B50.

[5] A. Knápek, M. M. Allaham, D. Burda, D. Sobola, M. Drozd, and M. Horáček, "Explanation of the quasi-harmonic field emission behaviour observed on epoxy-coated polymer graphite cathodes," Mater Today Commun, vol. 34, p. 105270, Mar. 2023, doi: 10.1016/J.MTCOMM.2022.105270.

[6] K. Ronoh, S. H. Fawaeer, V. Holcman, A. Knápek, and D. Sobola, "Comprehensive characterization of different metallic thin films on highly oriented pyrolytic graphite substrate," Vacuum, vol. 215, p. 112345, Sep. 2023, doi: 10.1016/J.VACUUM.2023.112345.

D Conference paper: Contact Interface of Graphene Sensors

Contact Interface of Graphene Sensors

Patrik Staroň[1], Robert Macků[1], Petr Sedlák[1], Nikola Papež[1], Ramazanov Shihkgasan[1], Farid Orudzhev[1], Mohammed A. Al-Anber[2], Dinara Sobola[1*]

[1]*Department of Physics, Faculty of Electrical Engineering and Communication, Brno University of Technology, Brno, Czech Republic*
[2]*Laboratory of Inorganic Materials and Polymers, Department of Chemistry, Faculty of Sciences, Mutah University, Al-Karak, Jordan*

*Corresponding author: sobola@vut.cz

***Abstract*—Gas sensors come in various types, including chemiresistive, infrared, photoionization, and semiconductor sensors. Each type leverages a distinct physical phenomenon. For carbon-based sensors, they can function under two primary categories. Graphene-metal contacts are crucial because they significantly impact the performance of carbon-based sensors. The geometry of these contacts plays a vital role in determining the sensor's effectiveness. The contact geometry affects how charge carriers are transferred between the graphene and the metal, which in turn influences the sensor's sensitivity, response time, and overall efficiency. Optimal contact geometry can minimize resistance and maximize the active sensing area, thereby enhancing the detection capabilities and reliability of the sensors.**

Keywords— graphene, contact, geometry, metal, interface

I. Introduction

The performance of graphene-based gas sensors is heavily influenced by the characteristics of the metal contacts. The geometry, material, thickness, and cleanliness of these contacts are all critical factors that determine the sensor's sensitivity, response time, and overall efficiency. Optimizing these parameters is essential for enhancing the performance and reliability of graphene-based sensors, making them more suitable for a wide range of applications [1, 2].

The geometry of metal contacts is vital for sensor performance. Optimal contact geometry ensures efficient charge carrier transfer between the graphene and the metal, which is crucial for high sensitivity and rapid response times. Inadequate contact geometry can lead to increased resistance and reduced sensor efficiency. Different geometrical configurations, such as edge contacts or surface contacts, provide various benefits in terms of conductivity and signal integrity.

Choosing the right material for the metal contacts is equally important. Different metals offer varying levels of conductivity, stability, and compatibility with graphene. Common materials include gold (Au), platinum (Pt), and palladium (Pd). Gold is often chosen for its excellent conductivity and resistance to oxidation. Platinum is known for its high stability and durability, making it suitable for harsh environments. Palladium is recognized for its good hydrogen sensitivity, which can be advantageous in specific sensing applications. The contact material impacts contact resistance and overall sensor performance, making it a critical consideration in sensor design.

The thickness of metal contacts also plays a significant role in the performance of graphene-based sensors. Thicker contacts can provide better durability and mechanical stability, essential for maintaining consistent performance over time. However, excessively thick contacts can increase resistance at the interface, negatively affecting the sensor's sensitivity. Conversely, thinner contacts may reduce resistance but be more susceptible to wear and damage. Therefore, finding the right balance in the thickness of the contacts is crucial for optimizing sensor performance [3-6].

Cleanliness of the metal contacts is another crucial factor that significantly affects sensor efficiency. Any contamination at the contact interface can increase resistance, noise, and reduce sensitivity. Ensuring that contacts are free from impurities and residues during fabrication is essential for maintaining sensor integrity and performance. Techniques such as thorough cleaning of the substrate and using cleanroom environments during assembly help achieve the necessary level of cleanliness.

The methods used to integrate and fabricate contacts with the graphene layer are also significant. Techniques such as electron beam lithography, chemical vapor deposition, and thermal evaporation are commonly used to create high-quality contacts. Each method has its advantages and limitations regarding precision, scalability, and cost. High-quality fabrication processes can help mitigate contact resistance issues and improve sensor reliability.

II. Experimental

We explored the capabilities of pristine graphene sensors, as depicted in figures 1 and 2. To test these sensors effectively, we developed a method in which the sensor is affixed to an FR4 PCB and connected to the circuit traces. Figures 3 illustrates the specific trace layout required for sensor interfacing. Additionally, to facilitate various test configurations, we designed a matrix connection PCB. This design allows for the flexible connection of any connector pin to any sensor pad, enabling the simultaneous measurement of two sensors. This configuration is not only portable but also ensures the sensor is securely mounted on the PCB. Consequently, connecting and disconnecting the sensors for testing in an environment with reduced noise is straightforward. The circuit traces were gold-plated to minimize material transition effects from the pads to the amplifier. However, we are aware that the intermetallic phase of CU-NI-AU might introduce more noise compared to a direct AU to CU transition. Therefore, this setup may not be optimal for experiments requiring ultra-high sensitivity.

2024 37th International Vacuum Nanoelectronics Conference (IVNC) | 979-8-3503-7976-1/24/$31.00 ©2024 IEEE | DOI: 10.1109/IVNC63480.2024.10652488

Fig. 1. Star electrode arrangement

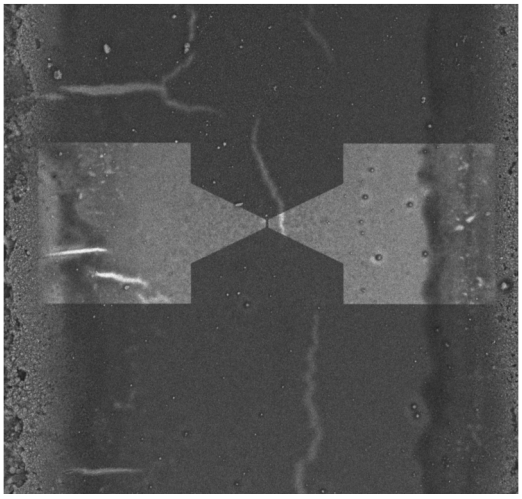

Fig. 2. Two-electrode arrangement

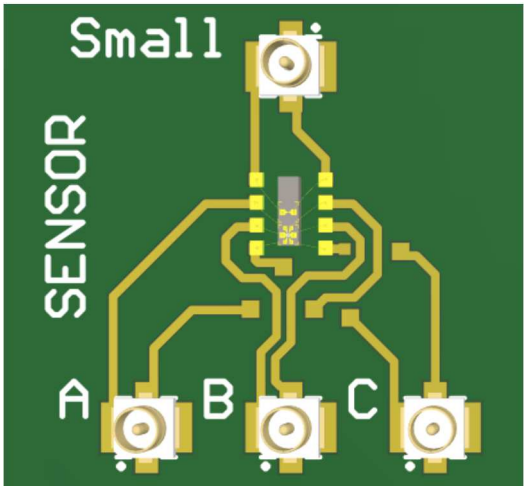

Fig. 3. PCB for the sensor interface with direct connections.

The actual schematic proposed for measuring the graphene sensor in spectral domain is shown in Figure 1. This is a setup that allows to push current through the sensor and a resistor, while measuring the voltage on the resistor. The resistor contributes to the noise, but the tweaking the voltage from the battery should decrease the influence of the resistive noise so that the dominant noise is the one from the sensor.

III. CONCLUSIONS

The performance of graphene-based gas sensors is significantly influenced by the metal contacts used. The geometry, material, thickness, and cleanliness of these contacts are crucial factors in determining the sensor's overall efficiency and effectiveness.

ACKNOWLEDGMENT

The research described in the paper was financially supported by the Internal Grant Agency of the Brno University of Technology, grant No. FEKT-S-20-6352 and the GACR 23-07384S.

REFERENCES

[1] A. Knápek, J. Sýkora, J. Chlumská, and D. Sobola, “Programmable set-up for electrochemical preparation of STM tips and ultra-sharp field emission cathodes,” Microelectron Eng, vol. 173, pp. 42–47, Apr. 2017, doi: 10.1016/J.MEE.2017.04.002.

[2] A. Knápek, D. Sobola, P. Tománek, Z. Pokorná, and M. Urbánek, “Field emission from the surface of highly ordered pyrolytic graphite,” Appl Surf Sci, vol. 395, pp. 157–161, Feb. 2017, doi: 10.1016/J.APSUSC.2016.05.002.

[3] D. Sobola, N. Papež, R. Dallaev, S. Ramazanov, D. Hemzal, and V. Holcman, “Characterization of nanoblisters on HOPG surface,” Journal of Electrical Engineering, vol. 70, no. 7, pp. 132–136, Dec. 2019, doi: 10.2478/JEE-2019-0055.

[4] A. AlSoud et al., “Electrical properties of epoxy/graphite flakes microcomposite at the percolation threshold concentration,” Phys Scr, vol. 99, no. 5, p. 055955, Apr. 2024, doi: 10.1088/1402-4896/AD3B50.

[5] A. Knápek, M. M. Allaham, D. Burda, D. Sobola, M. Drozd, and M. Horáček, “Explanation of the quasi-harmonic field emission behaviour observed on epoxy-coated polymer graphite cathodes,” Mater Today Commun, vol. 34, p. 105270, Mar. 2023, doi: 10.1016/J.MTCOMM.2022.105270.

[6] K. Ronoh, S. H. Fawaeer, V. Holcman, A. Knápek, and D. Sobola, “Comprehensive characterization of different metallic thin films on highly oriented pyrolytic graphite substrate,” Vacuum, vol. 215, p. 112345, Sep. 2023, doi: 10.1016/J.VACUUM.2023.112345.

E Conference paper: Electrical characterization of graphene sensors

Electrical characterization of graphene sensors

1st Patrik Staroň
Department of Physics
Brno University of Technology
Brno, Czech Republic
patrikstaron@vutbr.cz

***Abstract*—Graphene has shown to have great electrical, thermal and chemical properties. These qualities are suitable for construction of a chemical sensor with graphene as its sensing material. These graphene-based sensors are currently in the field of research and they are not yet viable for mass commercial application. Studies in graphene-based sensors span its very high sensitivity, selectivity, functionalization, manufacturability, stability and material configuration. We focus on the noise characterization in pristine graphene sensors, with different active channel size and layout of the electrodes. We study noise in the spectral domain, while exposing the sensor to different chemicals. We analyze and descripe the studied sensors in their geometry and graphene configuration.**

***Index Terms*—graphene, 2D sensor, measurement, geometry**

I. Introduction

Multiple industries such as manufacturing, healthcare and automotive, have need for reliable measurement of the gas composition in selected environment. Environments where people work with dangerous substances need to comply with safety requirements. Measurement and detection of volatile substances in the air can be achieved only by gas sensing devices. Areas with fire hazard or low air circulation such as mines have also a great need for gas sensors.

While there are many commertial implementations of gas sensors, they have problems with accuracy, measurement precision, selectivity to certain molecule, cost and so on.

Graphene is a material with spectacular properties. It has great electrical and thermal conductivity, has high mechanical strength and provides various optical and geometrical advantages over all other materials.

This is a premise that lead to the research of how well this material can be used to detect various gas molecules. It has been found, that graphene might be a suitable material to detect various gases at extreme resolution.

In reality, as it is a common case, graphene has problems not only with detection of certain gases, but also with interpreting the measured information from the sensor. As the resolution of the sensor goes up, the signal to noise ratio goes down.

This thesis introduces analysis and summarization of graphene sensor working principles, along problems connected with them. Primary goal is to develop a way to measure and process the data from a concrete graphene sensor in different gas environments. Result of the measurement should be informative on what kind of chemical substance is attached to the sensor. During measurement, especially with very high resolution, noise plays a significant role and this thesis addresses this noise, along with ways to reduce it.

II. Sensor measurement

Generally there are multiple methods of data acquisition from sensors. Some sensors change their capacitance based on the gas concentration. Most of the sensors change their resistance. Theoretically, even optical state of the sensor and acoustic wave propagation differences can be used to detect gas on the sensing material. Most of the sensors contain electrodes that interface the sensing material and the electrodes provide means for measurement of the sensing material physical properties. These measurements may be more or less straight forward. Chemiresistive gas sensor measurement is discussed in this chapter. Graphene sensors fall into this category and measurement of the sensors brings its own challanges. Especially with graphene sensors, which have potential to be very sensitive. Measurement can be performed using time and frequency domain. Time domain measurement is simple detection of resistance at particular time. Data processing is many times required to interpret the resistance as a concentration of particular gas. Frequency domain measurement consists of measuring the impedance of the sensing material at particular frequency and a range of frequencies is chosen. This can be benefitial, as some sensing materials have predictable resonance frequency and its shift is used to detect the concentration of the gas. Noise is a factor that influences the sensing performance too. Reaction process at the sensing material can be so slow, that the noise of the system may overtake and measurement can be compromised. This kind of noise is low-frequency noise (also known as 1/f noise). It is discussed in semiconductor based sensors but it may be also applicable to graphene sensors, as graphene provides its own source of noise. In research facilites, gas sensors are measured with devices such as 8753ES [1]. Network analyzer can measure resonant frequency by measuring resonator's return loss. Otherwise, resistance measurement with a good supply of current suffices. Sensors contain multiple sources

of noise. Most dominant are two. Thermal noise and low-frequency noise. Thermal noise is present in all devices. In thermal sensors the thermal noise is caused by vibration of the atomic structures that produce current inonsistencies. This noise has spectral density

$$S = 4 \cdot k \cdot T \cdot R \tag{1}$$

where k is Boltzmann constant, T is temperature of the material in kelvin and R is the resistance of the material. This noise is constant at all measurement frequencies and this means it can be isolated. The other source of noise is the low-frequency noise and this noise is dominant at frequencies usually up to 100kHz [2]. The spectral density of this noise is roughly 1/f. This noise decreases with increasing frequeancy forming a knee called $f0$. At this knee the noise decreased to the point where it equals the thermal noise [2]. Another source of noise is noise from material inconsistencies. These inconsistencies come from metalic interfaces for example. Within graphene sensors, the grain boundaries contribute to noise. Grain boundary noise of graphene contributes to 1/f noise [3]. After the data from the sensor is acquired, the data can be post processed to increase the accuracy of the detected gas type and concentration. It is known that sensors tend to have long detection and recovery time and this poses problem when sensor is continously measuring gas concentration. That is why advanced methods of gas sensor data processing have been developed, such as back propagation neural networks [4].

III. Measurement setup

We have several pristine graphene sensors available with geometry 1 and 2. To efficiently test these sensors, we came with a solution where the sensor is glued onto a FR4 PCB and it it bonded to the traces. The figures 4 and 5 show the layout of the traces needed to interface the sensor. To enable various configurations during testing, a matrix connection PCB was also created, to enable a connection of any connector pin to any sensor pad. These structures enable to measure two sensors at the same time. This setup is portable and the sensor is well-fixed onto the PCB. Connecting and disconnecting the sensors for measuring in a noise-reduced environment is therefore easy. The traces have been gold-plated to minimize changes of the material from the pads to the amplifier, although there is a concern that the intermetallic phase of CU-NI-AU will contribute to the noise more, than a single hard transition between AU and CU. This means that ultra-high sensitivity experiments may not be suitable with this solution.

Acknowledgment

First of all, I thank Lord Most High for creating such an interasting universe that we study until now and humbly still don't understand a lot, and I thank Him for giving me the ability to gain wisdom, learn and understand concepts I write about in this paper. I thank to my great supervisor doc. Mgr. Dinara Sobola PhD. for her help in overcoming obstacles that occured while progressing in this research. Thanks to Brno Universtity of Technology for providing the necessary

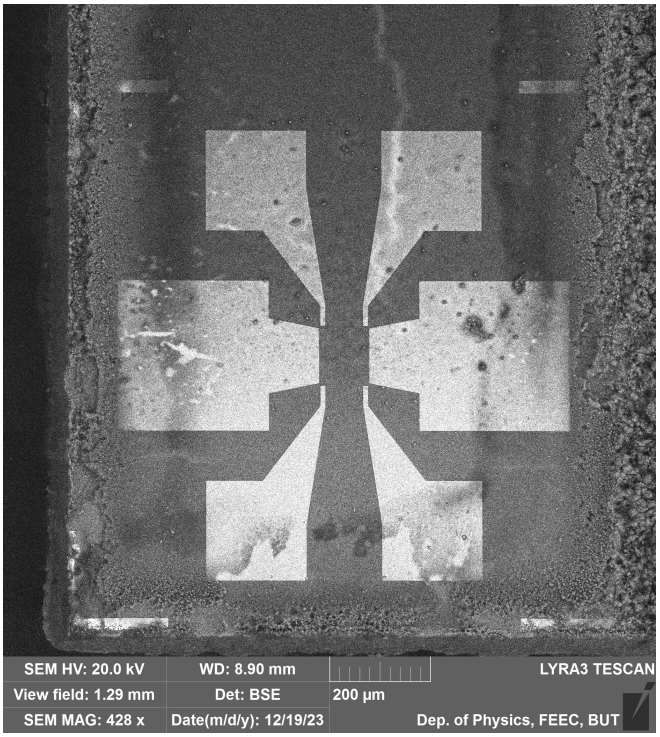

Fig. 1. Star electrode arrangement

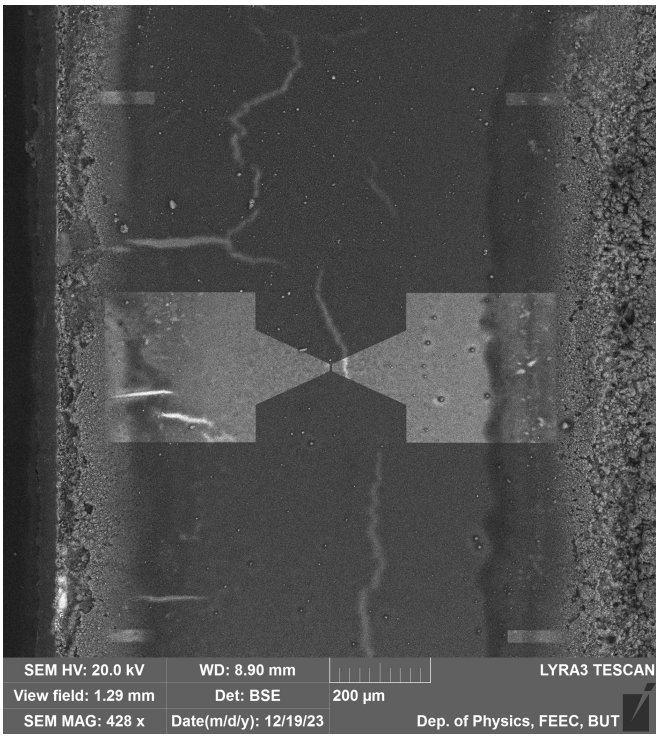

Fig. 2. Two-electrode arrangement

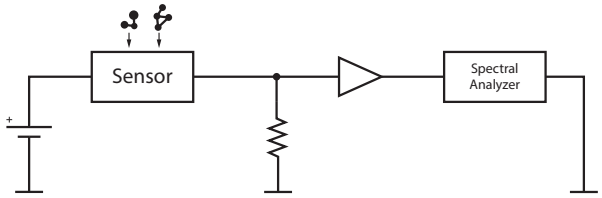

Fig. 3. Electrical diagram for mesuring the grapene sensor.

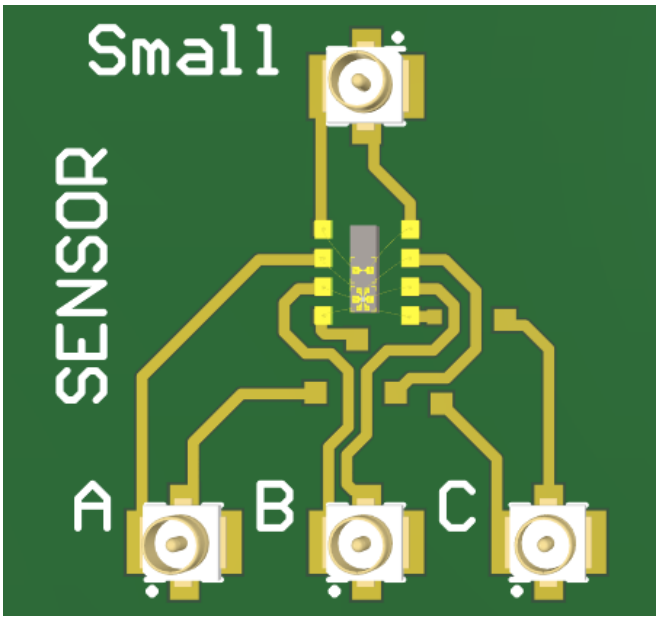

Fig. 4. PCB for the sensor interface with direct connections.

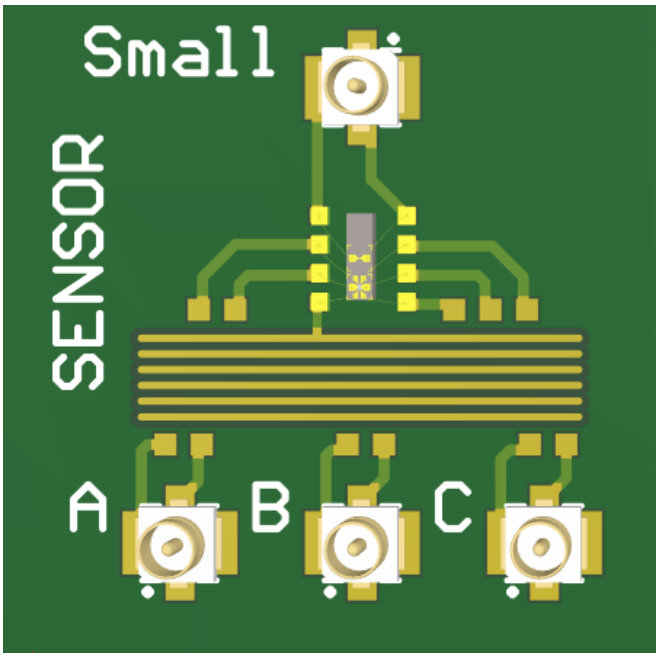

Fig. 5. PCB for the sensor interface with matrix interconnection capability

equipment for the research, Gatema company for the help in manufacturing of necessary PCB parts, and several colleagues for their advices and practical help.

REFERENCES

[1] S. CHOPRA, A. PHAM, J. GAILLARD, A. PARKER, A.M. RAO, *Carbon-nanotube-based resonant-circuit sensor for ammonia*, Appl. Phys. Lett. Vol. 80, pages 4632-4636, June 2002.

[2] A. A. BALANDIN *Low-frequency 1/f noise in graphene devices* Nature Nanotechnology, pages 549-555, 2013.

[3] W. SHIN, S. HONG, Y. JEONG, G. JUNG, J. PARK, D. KIM, K. CHOI, H. SHIN, R. KOO, J. KIM, J. LEE, *Low-frequency noise in gas sensors: A review*, Sensors and Actuators B: Chemical, Volume 383, 2023, ISSN 0925-4005.

[4] M. SRIYUDTHSAK, A. TEERAMONGKOLRASASMEE, T. MORI-IZUMI:*Radial basis neural networks for identification of volatile organic compounds*, Sensors and Actuators B: Chemical, vol. 65, no. 1, pages 358-360, 2005.